U.PORTO
FEUP FACULDADE DE ENGENHARIA
UNIVERSIDADE DO PORTO

U.PORTO
INSTITUTO DE CIÊNCIAS
BIOMÉDICAS ABEL SALAZAR
UNIVERSIDADE DO PORTO

Molecular Bioengineering of siRNA Nanoarchitectures: Towards Neurotargeted siRNA Nanocages

João Pedro Leal Cortinhas

Masters Dissertation

MIB - Integrated Masters in Bioengineering

Supervisor: Dr. Pedro Moreno (i3S)

Co-supervisor: Dr. Ana Paula Pêgo (i3S)

16-Setember-2019

The work described in this thesis was conducted at:

I3S/INEB - Instituto de Investigação e Inovação em Saúde; Universidade do Porto

The work described in this thesis was financially supported by:

This work was supported by Fundação para a Ciência e a Tecnologia (FCT, Portugal) in the framework of the project PTDC/NAN-MAT/30898/2017; Projects NORTE-01-0145-FEDER-000008 and NORTE-01-0145-FEDER-000012, supported by Norte Portugal Regional Operational Program (NORTE 2020), under the PORTUGAL 2020 Partnership Agreement, through the European Regional Development Fund (ERDF), Fundo Europeu de Desenvolvimento Regional funds through the COMPETE 2020—Operacional Program for Competitiveness and Internationalization (POCI), Portugal 2020; by Portuguese funds through FCT/Ministério da Ciência, Tecnologia e Ensino Superior in the framework of the project "Institute for Research and Innovation in Health Sciences" (POCI-01-0145-FEDER-007274); Santa Casa da Misericordia de Lisboa—Prémio Neurociências Mello e Castro (MC-1068-2015).

The authors acknowledge the support of the Bioimaging and the Histology and Electron Microscopy i3S Scientific Platforms, member of the national infrastructure PPBI - Portuguese Platform of Bioimaging (PPBI-POCI-01-0145-FEDER-022122).

Permissions to all reproduced figures were granted from their rightful owners. Figures 2 and 14 were created with BioRender software (biorender.com).

Abstract

siRNAs are a class of small oligonucleotide molecules that possess the ability to target and silence virtually any gene through a sequence-specific mechanism. As such, they show promising features for therapeutic applications, offering the possibility to treat many diseases that had previously been deemed undruggable through other therapies. However, this potential is hindered by a very poor pharmacological profile *in vivo*, as they are rapidly degraded, cleared from the circulation and exhibit very poor tissue penetration.

Molecular bioconjugate systems for siRNA delivery have emerged as an auspicious strategy to overcome some of these issues, since they can greatly promote siRNA targeted delivery and cellular uptake. Indeed, after some promising years of development, several liver-targeting siRNA conjugates are now waiting for FDA approval. Nonetheless, bioconjugates have thus far failed to translate into meaningful extra-hepatic therapies, as their current success is greatly influenced by specific characteristics of the liver and its target receptors. Their reduced size still does not allow them to evade renal clearance, and the delivery of one siRNA molecule per ligand might prove inefficient when targeting less-expressed receptors.

As such, in this work we developed a novel branched siRNA architecture, named siRNA nanocages, that allow for easy conjugation with functional biomolecules through a hybridization-driven process, while also promoting a multivalent delivery of 3 siRNAs per structure.

Their production was optimized and accomplished through a simple 2-step self-assembly process, and they were characterized through gel electrophoresis and through preliminary TEM studies. siRNA nanocages also presented the capacity to be functionalized by several different ligands, provided these were only conjugated with a specific DNA sequence. Most importantly, siRNA nanocages exhibited significant gene silencing properties in two different models after transfection, proving their applicability for RNAi-mediated gene silencing. Exploring its modular and reconfigurable nature, further optimizations of their activity were conducted.

In addition, with the goal of developing a novel bioconjugate for neuronal cell targeting, siRNA nanocages were successfully functionalized with the neuron-targeting peptide Tet1, and several internalization and uptake tests, albeit preliminary, were carried out.

Overall, siRNA nanocages displayed efficient gene modulation properties that, allied with its ease of functionalization and versatile structure, could serve as a starting point for the development of a novel bioconjugate for targeting of the nervous system, but also of other extra-hepatic targets.

Acknowledgements

I would like to express my gratitude to my supervisor, Pedro Moreno, who welcomed me in his team and allowed me to conduct this study. Without his guidance, help and valuable suggestions this work would not be possible. Thank you being so understanding and patient, and for the enormous availability displayed since the first time we met.

To Ana Paula Pêgo and the NanoBiomaterials for Targeted Therapies group for being so welcoming and for making my stay in i3S so happy and joyful. I learned a lot from you all. A special thanks to Ana Martins for her help in the lab.

To my colleagues in ABC and Núcleo de Estudantes de Bioengenharia, for the all the rewarding work we have accomplished, and for amazing time spent together.

To all my friends who, in a way or another, contributed to make these last years remarkable. All Julianas, for the continued support and jovial companionship. Filipe, Inês, Renato, Licínio, Margarida and so many other fantastic people I met during this journey. My fellow master's students, for lightening all the stress we shared. Rafaela, Romano and Luís, for remaining at my side for so many years. My friends from Marco, for all our joyful gatherings. To Bia, always able to bring a smile to my face.

To my family, who are my cornerstone and always showed unconditional support. My mother and her encouragement 24/7, my father and his invaluable help, my sister and our lighthearted moments, and my uncle and all our captivating talks. All of you were of paramount importance, and for that I am profoundly grateful.

Table of Contents

List of Figures

List of Tables

Acronyms

2’-O-Me	2’-O-methyl
2’-O-MOE	2’-O-methoxyethyl
2'-F	2’-fluoro
AD	Alzheimer’s disease
aiRNA	Asymmetric Interfering RNA
ALS	Amyotrophic Lateral Sclerosis
ASGPR	Asialoglycoprotein Receptor
ASO	Anti-Sense Oligonucleotides
ATP	Adenosine Triphosphate
BBB	Blood Brain Barrier
CNS	Central Nervous System
CPPs	Cell-penetrating Peptides and Polymers
cRGD	Cyclic Arg-Gly-Asp
CSF	Cerebrospinal fluid
DARPins	Designed Ankyrin Repeat Proteins
DHA	Docosahexaenoic Acid
DNA	Deoxyribonucleic Acid
dsDNA	double-stranded DNA
DsiGFP	Atni-GFP Dicer Substrate siRNA
DsiPTEN	Anti-PTEN Dicer-substrate siRNA
DsiRNAs	Dicer-substrate siRNAs
dsRNA	Double-stranded RNA
fsiRNA	Fork-like siRNA
GADPH	Glyceraldehyde 3-phosphate dehydrogenase
GalNAc	N-acetylgalactosamine
GFP	Green Fluorescent Protein
HDL	High Density Lipoprotein
His	Histidine
LDL	Low Density Lipoprotein
LNA	Locked nucleic acids
miRNA	microRNA
mRNA	messenger RNA
PAGE	Polyacrilamide Gel Electrophoresis
PBVAE	Poly Butyl and Amino Vinyl Ether
PD	Parkinson’s disease
PEG	polyethylene glycol
P-gp	P-glycoprotein
PKR	Protein Kinase R
PLGA	Polylactic-co-glycolic acid
PRRs	Pattern Recognizing Receptors
PS	Phosphorothioate

PTEN	Phosphatase and Tensin Homolog
RISC	RNA Induced Silencing Complex
RNA	Ribonucleic Acid
RNAi	RNA interference
RT-qPCR	Reverse-Transcription Quantitative Polymerase Chain Reaction
RVG	Rabies Virus Glycoprotein
SERT	Serotonin Transporter
shRNAs	Short Hairpin RNAs
siPTEN	Atni-PTEN small interfering RNA
siRNA	small-interfering RNAs
sisiRNA	small internally segmented interfering RNA
SPACE	Skin-penetrating and cell-entering
ssDNA	single-stranded DNA
TEM	Transmission Electron Microscopy
TLR	Toll-Like Receptors
tsiRNA	Trimer siRNA
T-tiRNA	tripodal interfering RNA
VEGF	Vascular Endothelial Growth Factor

Chapter 1: **Introduction**

1.1 Therapeutic Drug Delivery for Neurological Disorders

Neurological disorders and its resulting sequelae are one of the major threats to human health in the 21st century. Globally, these diseases were the second leading cause of death in 2016 [1], and are currently estimated to affect over 1 billion people worldwide [2]. The disorders affecting the central nervous system (CNS) are very diversified, ranging from brain tumors, spinal cord injury or ischemic strokes, and can often cause severe impairment. Due the low endogenous regenerative capacity of the adult human brain, it is vulnerable to chronic neurodegenerative diseases like Alzheimer's disease (AD), Parkinson's disease (PD) or amyotrophic lateral sclerosis (ALS), all characterized by gradual loss of neurons resulting of diverse factors like abnormal protein accumulation, neuroinflammation or oxidative stress [3]. These degenerative diseases are deeply related to ageing, what foresees an increase of overall prevalence and economic burden in the following years as a result of population growth and ageing.

Despite the considerable impact these types of disorders pose to public health, there are still very few safe and effective therapies and diagnostic tools available. Instrumental to this lack of options is the unique and complex environment of the CNS. Firstly, the anatomical access to the CNS is greatly restricted, rendering surgery-based approaches very difficult to perform [4]. Additionally, this prevents the direct study of the disease-affected site, hindering the development of new therapies by preventing objective measurements of degeneration during clinical trials [5]. Another contributing factor is the highly heterogenous and complex cellular and molecular environment of the brain, as well as the anatomical and functional complexities associated with its role of information integration and processing [6], that can hamper the gathering of precise knowledge about these conditions and their causes. In fact, although recent years have brought new insights about their pathophysiology, the underlying mechanisms and causes of neurodegenerative diseases like AD, PD or ALS are still not fully understood [7–9].

Nonetheless, one of the major barriers to therapies targeting the CNS lies in the blood brain barrier (BBB). This dynamic barrier plays an important role in regulating brain homeostasis and

isolates it from the circulatory system. It is mainly formed by a tightly packed layer of brain endothelial cells that only allows some low molecular weight, lipophilic molecules to cross to the brain parenchyma, inhibiting the transport of over 98% of the small molecules (<400 Da) and of nearly 100% of the large molecules like proteins [10]. The BBB accomplishes this through a complex system of pathways including tight junctions and adherent junctions, ATP-dependent efflux pumps like P-glycoprotein (P-gp) [11] that prevent the uptake of lipophilic xenobiotics, and various transporters that confer selective access to the CNS to some macromolecules and nutrients [12,13]. Taking all this into account, when considering systemic administration through the vascular route, the majority of drugs with pharmacological potential to treat neurological disorders are rendered ineffective due to poor BBB permeability.

However, several strategies are employed to surpass the BBB and deliver therapeutic compounds to the CNS. There has been a focus in the development of drug-delivery systems that can penetrate the BBB and selectively target the brain through the vascular route, and the field of nanomedicine emerged as a promising area of research, with several colloidal systems such as polymeric [14] and lipid nanoparticles [15,16], nanogels [17], dendrimers [18] and many others [19] being studied. Reversible disruption of the BBB through biochemical agents or ultrasounds has also been examined with a certain degree of success [19], although some concerns still arise regarding the neurotoxicity these techniques can cause to the brain, as the protective capacity of the BBB might be compromised.

Local administration can also be explored, such as intracerebroventricular or intrathecal injection. These procedures provide specific delivery to the cerebrospinal fluid (CSF) that circulates through the CNS, and can lead to immediate high drug concentrations in the CSF and, subsequently, therapeutic concentrations in the brain [20]. Despite being a highly invasive procedure, posing more safety concerns to the patient than systemic administration, intrathecal injections have been successfully applied in the clinic for the treatment of several neurological disorders [21–23]. Additionally, intranasal administration has also emerged as a viable alternative to target the CNS. While currently being employed as an alternative for many drugs to reach the systemic circulation [24], it has also been studied for drug transport to the CNS since the delivery of larger compounds such as proteins to the brain was reported more than a decade ago [25]. In fact, the human nasal cavity is the only place where the nervous system is directly contacting with the outside environment, and through the olfactory sensory neurons and the trigeminal nerve pathway, drugs can be transported to the olfactory bulb and to the CSF, and from there disperse to the rest of the CNS [26]. Being a non-invasive route of administration, it poses significantly fewer safety risks to the patient, while many studies suggest it leads to increased brain uptake and bioavailability, as well as higher drug efficacy for a variety of drugs, making it a promising approach for future therapies [27].

Despite all the advances regarding drug delivery to the brain, more challenges arise when considering the complex cellular environment of the CNS. The brain is constituted by several heterogeneous cell types like astrocytes, oligodendrocytes and different functional types of neurons, each with specific roles associated with the brain's physiological functions and contributing to maintaining homeostasis. This complexity of cell types presents a serious obstacle in the specific delivery of therapeutic compounds to the appropriate cell type and subcellular or synaptic location [5], limiting their efficacy and increasing the risk of unwanted side effects and overall toxicity and disruption of the system. As such, the development of new therapies for the treatment of CNS disorders must also address cellular targeting if an efficient treatment is to be achieved. Again, the field of nanomedicine has been the focus of many studies to achieve specific targeting [28], taking advantage of intrinsic properties of drug delivery systems like lipid nanoparticles [29] and exosomes [30], or through the use of targeting ligands like Tet-1 [31] or dopamine [32], for example.

Although many considerable challenges arise when dealing with the treatment of neurological disorders, progressive efforts are being made to develop suitable therapies. Nonetheless, most of this work has yet to translate into significant clinical options to address this issue, hence the need to find new efficient therapies for treatment of CNS diseases.

1.2 Small Interfering RNA

The inhibition of protein expression by double-stranded RNA (dsRNA) was first reported in the nematode *Caenorthabditis elegans* in 1998 [33], although this phenomenon had been observed earlier in plants [34]. This led to the discovery of the RNA interference (RNAi) mechanism, an endogenous pathway through which eukaryotic cells are able to target messenger RNA (mRNA) in a sequence-specific way, and subsequently downregulate gene expression by mRNA cleavage and degradation or translation arrest [35]. Several effectors of RNAi have since been described, such as microRNA (miRNA), 22-nucleotide RNAs that are naturally encoded in the genome, serving as post-transcription regulators of endogenous genes, and thought to act on roughly 30% of human genes [36,37]; and small-interfering RNAs (siRNA), 21-23 base pair dsRNA that are the result of endogenous or exogenous long dsRNA processing, and can naturally act as defense mechanism against invasive nucleic acids such as viral infections [35,38].

Initially, processing of the dsRNA takes place in the cytosol by an RNAse III-type endonuclease called Dicer. This dsRNA-specific enzyme recognizes and cleaves the dsRNA into shorter siRNAs with 3' overhangs of 2 nucleotides. After this reaction, resulting siRNAs assemble into the RNA Induced-Silencing Complex (RISC), with the sense strand (the passenger strand) being cleaved, and the antisense strand (guide strand) serving as a guide to the cleavage of complementary mRNA strands by the Ago2 protein of the Argonaute family, leading to

subsequent degradation of the cleaved mRNA and, thus, an efficient gene silencing [35,39] (Figure 1).

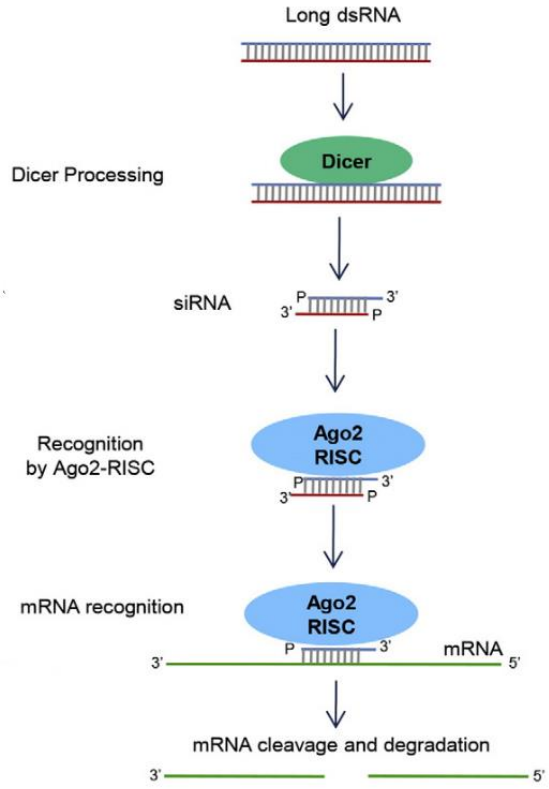

Fig.1 - Simplified scheme of the RNAi mechanism triggered by dsRNA. Adapted from Ozcan et al., 2015 [40]

Despite the fact that dsRNA, the natural trigger of RNAi mechanism, induces a strong innate immune interferon response when over 30 base pairs, possibly limiting potential therapeutic applications [41], the use of synthetic 21 base-pair siRNAs to successfully mediate gene silencing in several mammalian cell lines (including the human-derived HeLa line) was reported in 2001 [42]. These results brought promising perspectives to the utilization of RNAi in research and gene therapy.

Altogether, siRNA's ability to target specific sequences and genes with high specificity and achieve potent (albeit transient) gene silencing offers the possibility to modulate protein expression and thus influence cellular cues, promoting favorable conditions for tissue regeneration, as well as treating several diseases and genetic disorders that cannot be treated by traditional drugs. In addition, due to their adjustable nature, RNA-based therapeutics are able to keep up with new cancer mutations, novel viruses or newly discovered disease mechanisms and associated genes while maintaining an efficient treatment. Furthermore, they can pose as an invaluable tool for research, serving as a simpler and cheaper alternative to study gene function when compared to other methods such as gene knockout.

Concretely, siRNA-based therapies present several properties that are very compelling for their use in treatment of CNS disorders. As many neurological disorders lack treatment options

using more traditional strategies like surgery or chemotherapy, rational sequence design of siRNA to induce effective silencing of disease-related genes [43] can greatly contribute to the development of new drugs and formulations that might be able to address otherwise untreatable diseases. In fact, with the employment of bioinformatic tools and algorithms, the process of therapeutic siRNAs design can be greatly improved [44], making this type of drug candidates very straightforward and fast to develop. This makes them extremely attractive for the treatment of many neurological orphan or orphan-like diseases like AD, ALS or Huntington's disease, that, due to their low prevalence, lack a large enough market to attract resources for the researching and discovery of new therapies. Moreover, due to the catalytic nature of siRNA-mediated gene downregulation, one siRNA strand has the ability to degrade multiple mRNAs, making it a highly efficient process and meaning that, theoretically, low-dose and infrequent administrations could be effective. Considering that the CNS is a very sensitive and complex system, this is a very important feature, since high-dose or frequent drug administrations could cause cytotoxicity and other adverse side effects.

However, several considerable barriers arise when considering efficient *in vivo* delivery of exogenous siRNA for therapeutic purposes.

1.3 Barriers for siRNA Delivery

First of all, naked siRNAs are very unstable in vivo when administered systemically, displaying very poor pharmacokinetic properties. Their half-life in serum is reported to be as low as several minutes [45], mainly due to their susceptibility to endonuclease and exonuclease degradation [46,47]. Also, due to their small size and the fact that they do not bind extensively to plasma proteins, they show high accumulation in the kidneys and suffer from high renal clearance, being excreted into urine within 1 hour [48]. Additionally, these molecules also need to surpass inherent tissue-related barriers in order to reach their intended target, such as the vascular endothelial barrier, BBB or the reticuloendothelial system and its phagocytic cells, such as the Kupffer cells in the liver, or splenic macrophages [49]. Indeed, siRNAs show very limited biodistribution and low accumulation levels in tissues. The kidneys and the liver were shown to be the major sites of siRNA accumulation [50], mainly due to the liver's highly fenestrated endothelium and the high siRNA renal clearance. Albeit these characteristics favor passive targeting to these two organs, when it comes to extra-hepatic delivery, siRNAs do not present any active targeting delivery capability, hence the need to find ways to direct their activity to specific cell types, tissues or organs in order to increase gene silencing efficiency and avoid possible unwanted effects on unintended targets [51].

In addition, the introduction of exogenous siRNA in the organism is capable of triggering a strong innate immune response (Figure 2), as siRNA is recognized as a hallmark of viral infections by our immune system. Pattern recognizing receptors (PRRs), namely toll-like

receptors (TLR), are activated in the presence of siRNAs and start an immune signaling cascade that culminates in the expression of interferons and other inflammatory cytokines [52]. These receptors can be located in the cellular membrane, like TL3 [53], or in the endosomes and lysosomes, like TLR7 [54]. There are also cytoplasmic proteins such as PKR and RIG-1 that react to exogenous siRNA in a sequence-dependent fashion [55,56].

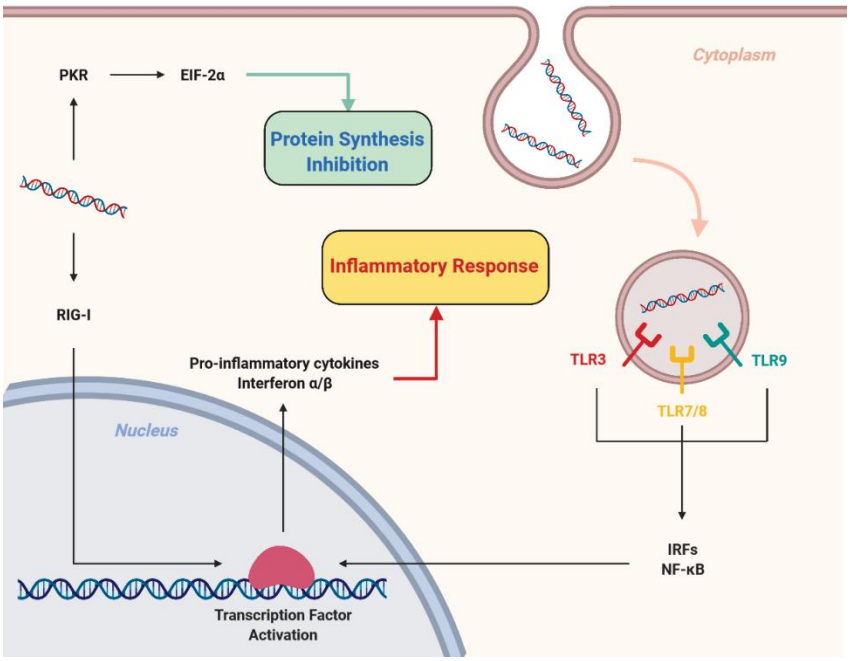

Fig. 2 – Activation of immune response by pathogen recognizing receptors in the presence of exogenous siRNA.

Nevertheless, maybe the most significant problem with the therapeutic use of siRNA's is related to their cellular uptake and endosomal escape mechanisms [49,57]. The lipid bilayer only allows small (<1 kDa) hydrophobic molecules to traverse it [58], and since siRNAs are negatively charged and around 14 kDa, they require some sort of delivery agent to reach the cytosol, where they can exert their effect. When these macromolecules are internalized by endocytosis, they traverse through multiple membrane-bound intracellular compartments [59]. However, these vesicles and endosomes also encompass a lipid bilayer, resulting in the arrest of siRNAs outside of the cytosol. Therefore, a strategy that allows successful crossing through the lipid bilayer, including endosomal escape after endocytosis, is needed before we can unlock the therapeutic potential of siRNA and other RNA-based molecules [57].

Taking all these issues into account, systemically and locally administration, of free siRNA molecules, clearly presents some serious limitations for therapeutic use. However, several strategies have already been adopted, and others are in development, in order to overcome these problems, leading to promising prospects in this field.

1.4 Chemical Modifications

One of the first and most straightforward approaches to overcome the limitations of siRNAs was their direct chemical modification, influencing their intrinsic properties like hydrophobicity, nuclease resistance, immune system activation or target binding affinity while maintaining their core ability of gene silencing. There is a vast number of specific oligonucleotide modifications that can broadly be split into backbone modifications and sugar modifications, and are also being employed on other nucleic-acid based drugs, like anti-sense oligonucleotides (ASO) [60,61].

However, due to siRNA's action being dependent on recognition and processing by RNAi intracellular enzymes, the number of modifications that can be employed are limited when compared to other oligonucleotides. Ago2 binding to the guide siRNA strand is made through multiple contacts to the phosphate charged backbone, and to 2'-OH in the central groove [62], and as such, all modifications must maintain or mimic an A-form RNA structure to be functional.

1.4.1 Ribose Modifications

Ribose modifications mainly impact binding affinity toward complementary strands, duplex conformation and nuclease resistance, as well as decrease immunogenicity and toxicity, therefore acting as a valid strategy for increasing in-vivo stability [60]. These are mainly focused on the 2'-OH group, as this group participates in the cleavage of siRNA by endonucleases [63,64]. Currently, there are two main modified RNA nucleotides used extensively in almost all therapeutic siRNAs [57]: 2'-O-methyl (2'-O-Me), a natural occurring modification in ribosomal RNA [65], and 2'-fluoro (2'-F) [49], depicted in Figure 3. Both modifications help stabilize the 3'-endo ribose conformation, ensuring the A-form RNA helix and increasing resistance to nuclease degradation [66,67]. Furthermore, 2'-O-Me modifications can also contribute to reducing the immune response caused by siRNA [68], making it the most attractive modification for siRNA-based therapeutics. Since it has been observed that the size of the modification may correlate with nuclease resistance [69], several bulky groups have also been tested, like the 2'-O-methoxyethyl (2'-O-MOE), which can increase the melting temperature of the duplex more effectively than 2'-O-Me [70], although it significantly impairs RNAi activity [71].

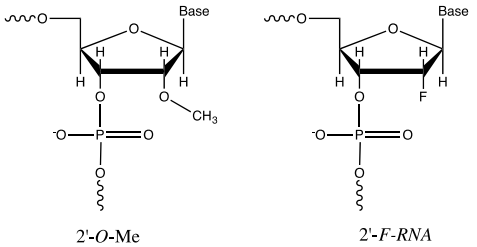

Fig.3 - Main 2' altered nucleotides utilized in therapeutic siRNAs.

Despite the fact that modifications can be applied to other positions in the ribose besides the 2'-OH group (for example, the 4' carbon), they have little usage currently due to the significant impairment of RNAi activity [61]. However, structural modifications of the furanose ring can also be employed. Locked nucleic acids (LNA), also referred to as "inaccessible RNA", are nucleic acid analogues where the 2' oxygen is connected to the 4' carbon of the ribose ring, locking the RNA into a 3'-endo conformation (Figure 4), and display high hybridization affinity towards complementary RNA [72].

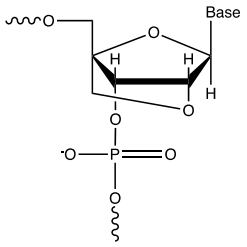

Fig.4 – Chemical structure of the locked nucleic acid analogue

When incorporated into siRNA strands, these analogues were shown to be compatible with RNAi machinery, as well as increasing siRNA serum half-life by stabilizing the RNA duplex when added as LNA overhangs on the 3' end of both sense and anti-sense strands [73]. It was also reported that LNA modifications on both the 3' and 5' end of the sense strand diminished their immunostimulatory activity. Nonetheless, these modifications can also impair siRNA gene silencing capacity when used to a large extent [74].

One should nonetheless be cautious when employing these analogues, as an extensive modification pattern can alter siRNA processing and impair the silencing potency. For example, it has been shown that the complete modification of siRNA with 2'-O-Me leads to inhibition of RNAi [75], although modifications every second nucleotide are supported. 2'-F modifications have also exhibited some toxicity *in vitro* and *in vivo* when employed in ASOs [76,77], and were shown to change the subcellular location of siRNA [78]. However, another report concluded that 2'-F nucleotides could be safely used when applied in siRNA conjugates targeting the liver [79]. Nevertheless, when considering chemical modification of nucleotides, the number of modifications, their pattern and also their location are all very important criteria for the effectiveness of siRNA [80], and a balance must be maintained between the silencing efficiency, nuclease resistance and toxicity.

1.4.2 Backbone Modifications

Phosphate backbone modifications can reduce the negative charge of the phosphodiester bond, reduce nuclease susceptibility and improve pharmacokinetic characteristics [60]. One of the first reported modifications was the phosphorothioate (PS) backbone, where one oxygen of the phosphate group was substituted by a sulfur atom [81] (Figure 5). This modification has been

the keystone in ASOs therapeutic application, as it provides increased resistance against nucleases and, given the fact that it promotes binding to albumin and other serum proteins, retards oligonucleotide renal clearance, greatly improving their pharmacokinetic profile [57,82]. Additionally, this modification can induce non-specific binding of oligonucleotides to cell receptors and promote endocytosis [83].

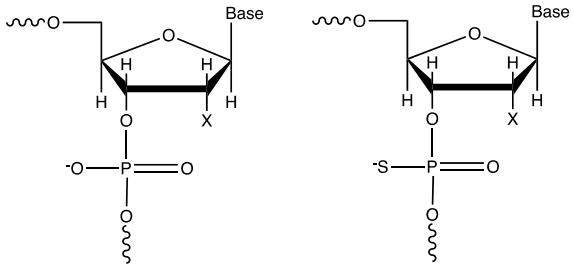

Fig.5 – Phosphodiester (left) versus phosphorothioate (right) backbone modification .

Despite the fact that a phosphorothioate backbone does not mimic the charged phosphodiester backbone, leading to interference with siRNA binding to the RISC complex, it has been shown that it is tolerated in the ends of siRNA strands, improving the stability, duration and potency of RNAi in vivo [57].

Other strategy developed was the use of a phosphotriester backbone (Figure 6), that is able to mask the negative charge of the phosphate backbone and, once inside the cell, is degraded into normal phosphodiester siRNA, inducing RNAi response. This type of modification was reported to grant serum stability and absence of immune response, as well as improved pharmacokinetic properties due to the binding of serum albumin [84].

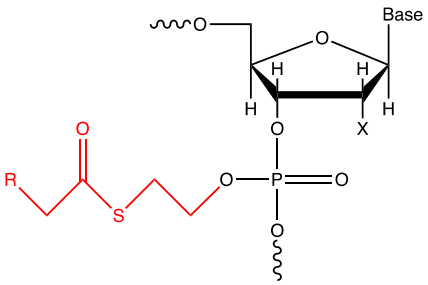

Fig.6 – Phosphotriester backbone modification. The phosphotriester group (in red) is cleaved inside the cell.

The research of stable phosphate mimics has also been one of the focus regarding siRNA. It was reported that the 5' end of the siRNA guide strand needs to be phosphorylated in order to allow adequate loading into Ago2 and the RISC complex. However, upon systemic administration, that phosphate is removed by phosphatases, requiring re-phosphorylation in order to trigger RNAi [85]. As such, chemical modifications that mimic phosphate but increase its resistance to phosphatases can improve siRNA guide strand availability to the RISC complex.

One such example is 5' E-vinylphosphonate modification, that was demonstrated to improve siRNA activity *in vitro* and *in vivo* [86].

Without a doubt, all these chemical modifications have had a crucial impact on the siRNA therapeutics field, allowing improvements on the overall stability and pharmacokinetics, and decreasing the immune response. Nonetheless, they alone are not enough to cover all the aforementioned limitations of the therapeutic use of siRNAs, still needing some sort of delivery agent to guide them to their target tissue, through the lipid bilayer and through the endosomes

1.5 Structural Modifications

In addition to chemical modifications, the manipulation of siRNA design and architecture can have a crucial effect on the efficiency of siRNA, with the ability to modulate properties like nuclease resistance and gene silencing potency through changes in the duplex structure, for example.

The canonical and most widely used siRNA structure consists of a 21-nucleotide duplex with an overhang of 2 nucleotides at the 3' end of both sense and anti-sense strands (Figure 8.A), mimicking the natural product of dsRNA processing by Dicer in the RNAi pathway. This was the first exogenous and synthetic siRNA that successfully showed sequence-specific gene silencing in mammalian cells [42], and, since then, the advances in our understanding of the RNAi mechanisms have allowed a rational-based approach in the design of RNAi inducers, with fine-tuning of the structure of the "classic" duplex bringing forth optimized alternatives.

One such example originated from the study of the effect of thermodynamic properties in the interaction between the RNA duplex and the RISC complex. It was observed that the incorporation of the guide strand into RISC was a crucial step and off-target effects can occur when the sense strand is loaded instead of the antisense strand [87]. It was reported that the thermodynamic stability at the 5' end of a strand could play a crucial role in the guide strand selection and loading into RISC complex, with functional siRNA exhibiting a thermodynamic asymmetry towards the antisense strand [88]. Nucleotide substitutions causing the destabilization of the duplex at the 3' end of the sense strand were tested in synthetic siRNA, and lead to increased gene silencing activity due to preferential loading of the antisense strand as guide strand [89]. Based on this concept, a new class of siRNA was developed: fork-like siRNAs (fsiRNAs). These siRNAs were synthetized with up to four mismatches at the 3' end of the sense strand (Figure 8.F), and showed enhanced silencing compared to classical siRNAs [90], and could presumably reduce off-target effects.

More novel structures were developed with the aim of avoiding incorporation of the sense strand into RISC in order to increase RNAi efficiency and reduce off-target effects. Asymmetric interfering RNA (aiRNA), duplexes with shorter sense strands of 15 nucleotides (Figure 8.D),

were also reported to promote effective RISC integration and reduce sense strand mediated off target effects [87]. Other siRNA design denominated "small internally segmented interfering RNA" (sisiRNA) exhibited increased target specificity and diminished off-targeting. This type of duplex has a sense strand separated into 2 smaller segments of 10-12 nucleotides (Figure 8.E), possibly excluding it from being incorporated into RISC and explaining these results [91].

Another subject of research refers to the increase of gene silencing potency of siRNAs of new RNAi effectors. Dicer-substrate siRNAs (DsiRNAs), first described in 2004, consist of longer duplexes of 25-30 base pairs and have shown significantly more activity than traditional siRNAs, with up to 100-fold increase in silencing activity. In particular, DsiRNAs of 27 base pairs in length and with blunt ends (Figure 8.B) displayed the highest interfering activity, producing up to 95% of gene silencing at concentrations as low as 1 nM while traditional siRNAs were almost ineffective. Additionally, these larger 27-mer duplexes did not activate any interferon response. Such increase in potency could be explained by the contribution of Dicer to a more effective incorporation of the cleavage products in the RISC complex, as canonical siRNAs, unlike DsiRNAs, are not substrates of this endonuclease [92].

Since their discovery, this class of DsiRNAs has further been optimized, with an asymmetric design consisting of an overhang of 2 nucleotides on the 3' end of the antisense strand and a blunt end, unfavorable for Diver binding, with 2 DNA residues on the 3' end of the sense strand. These features promote the production of a single, predictable and maximally active type of 21-mer siRNA after Dicer cleavage [93]. Additionally, the introduction of chemical residues has also been studied mainly to confer protection against nucleases. Unlike canonical siRNAs, DsiRNAs do not support extensive modifications patterns, particularly at the Dicer cleavage site near the blunt end, as it could impair the functional processing of the duplex (Figure 7) [93], and as such, the most effective patterns reported limit the modifications to about 9-11 nucleotides in the antisense strand modified with 2'-O-Me, while also promoting a reduction in immune system activation [94]. Overall, DsiRNAs offer the ability to induce gene silencing with increased longevity and potency at lower concentrations when compared to traditional 21-mer siRNAs, as well as reduced toxicity due to lower dosage requirements, although with higher synthesis costs.

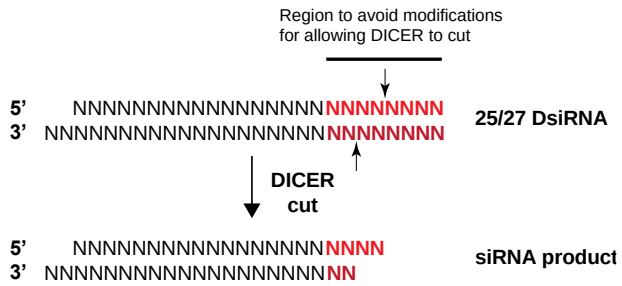

Fig.7 – Schematic showing the general rule for DsiRNA modifications [93], where the DICER cleavage site should be left unmodified for efficient processing into the 21mer siRNA product. N stands for any nucleotide.

The structural manipulation of the duplex can also serve as an alternative to chemical modifications when trying to increase stability by promoting resistance to nucleases. Short hairpin RNAs (shRNAs), consisting of a 29 base-pair RNA stem loop with a 2 nucleotide overhang at the 3' end and a loop of 4 nucleotides (Figure 8.C), were identified as potent RNAi inducers due to Dicer processing, similar to DsiRNAs [95]. Although the protection of one end might confer a small resistance to nuclease degradation, Abe et al. further optimized this design, developing a dumbbell-shaped circular RNA structure by adding an additional loop with an RNA ligase, closing the structure (Figure 8.G). With both ends protected, dumbbell RNAs exhibited more stability in biological fluids due to increased resistance to enzymatic degradation, while also showing prolonged RNAi activity as a result of slow release of RNA from the structure due to Dicer inefficient recognition [96].

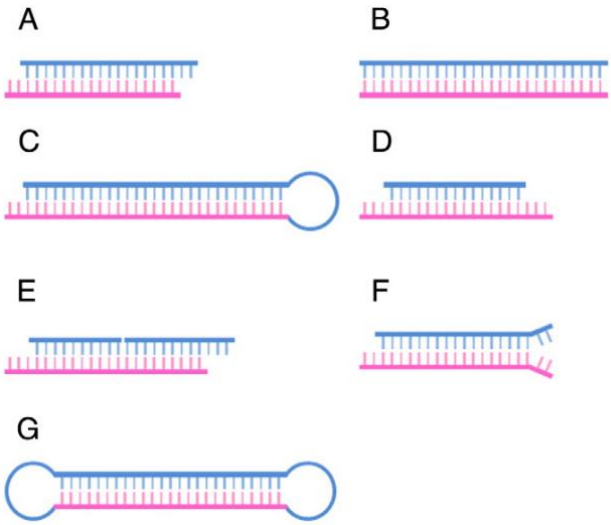

Fig.8 – Representation of several synthetic RNAi inducers. Sense strand in blue, antisense in pink. **A)** Canonical siRNA. **B)** 27-mer, blunt-ended Dicer-substrate siRNA (DsiRNA). **C)** short hairpin RNA (shRNA). **D)** asymmetric interfering RNA (aiRNA). **E)** small internally segmented interfering RNA (sisiRNA). **F)** fork-like siRNA (fsiRNA). **G)** dumbbell siRNA. Reproduced from Ku et al., 2016 [97]

Although dsRNA longer than 30 base pairs induce an interferon response [41], the employment of chemical modifications can contribute to attenuate this effect. As a result, longer linear duplexes that contain the canonical siRNA sequence repeated several times can also be designed. Such examples are dimer and trimer siRNAs, that contain the same siRNA sequence repeated 2 and 3 times respectively. 2'-O-Me modifications were selectively introduced in these structures, successfully inhibiting the interferon response, while trimer siRNAs (tsiRNA) exhibited significantly more activity than their canonical counterparts [98]. Further work with tsiRNA has led to efficient silencing of 3 different genes simultaneously by incorporating 3 different siRNA sequences in the same trimer, validating their use as a potential multi-target drug [99].

Indeed, the presence of mutations in the target gene or the involvement of more than a single gene in a disease-associated mechanism could hamper the therapeutic effectiveness of siRNA. Therefore, variations in siRNA architecture that confer the ability to silence several genes simultaneously could be an effective strategy to boost treatment effectiveness. Another distinct approach regarding this subject is the use of branched siRNA structures instead of linear dsRNA. Due to the precise self-assembly nature of nucleic acids through Watson-Crick base pairing, several well-defined architectonic variations can be created with the help of rational sequence design. The development, through direct annealing, of trimeric (Figure 9.A) or tetrameric (Figure 9.B) siRNA structures, with 3 and 4 branches respectively, is such an example. These structures provided prolonged silencing using 3 or 4 different target sequences for the same gene simultaneously, and the tetramer RNA structure was reported to be much more resistant to exonuclease degradation [100]. In fact, the sterically crowded environment around the siRNA plays a key role in the structure resistance against nucleases but also in the prolonged RNAi activity, as the processing by Dicer is hindered and the siRNA molecules are more slowly released. Subsequent studies conducted with the trimeric siRNA structure successfully led to the silencing of 3 different genes involved in a ß-catenin degradation pathway, suggesting their potential for multi-targeted therapies [101].

An additional way to assemble branched RNA structures is through the use of chemical linkers. Several oligonucleotide dendrimers based on phosphoramidite synthons have long been developed and proposed for various applications [102–104], with this technology also being applied to new RNA architectures for RNAi activation. Aviño et al. employed symmetric doubler phosphoramidites to synthetize structures with two and four branches of siRNAs (Figure 9.C) that performed similarly to unmodified siRNA duplexes in the silencing of tumor necrosis factor-α [105]. In another example, a branched RNA structure named tripodal interfering RNA (T-tiRNA) was produced, consisting of 3 branches containing siRNA duplexes and held together by a trebler phosphoramidite core extended with short DNA linker sequences (Figure 9.D). This structure was able to mediate silencing of up to three different mRNAs and also exhibited higher transfection efficiency due to the more compact structure and higher negative-charge density, promoting the interaction with cationic transfection reagents [106]. The modular nature of T-tiRNA allows for a variety of functional RNAs to be incorporated into its structure, provided they have a complementary sequence for the DNA linker of the phosphoramidite core, making it a very versatile tool for the building of multi-functional RNA structures.

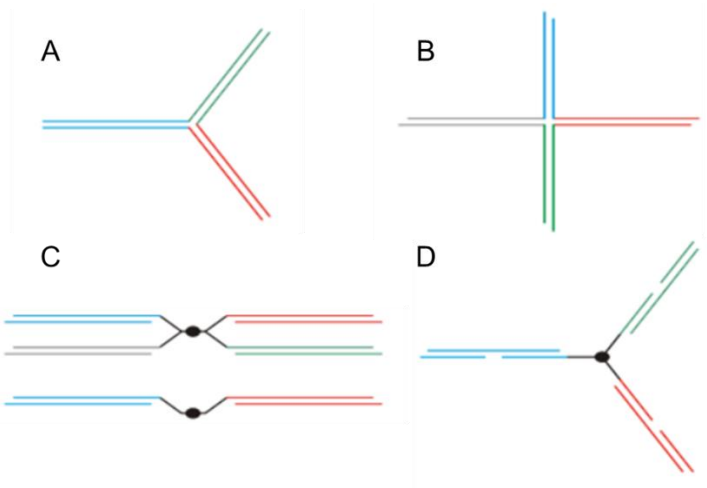

Fig.9 – Representation of various multi-target siRNA with branched architectures. A) Trimeric siRNA. B) Tetrameric siRNA. C) Four-stranded (top) and two-stranded (bottom) siRNAs. D) Tripodal interfering RNA (T-tiRNA). Adapted from Gvozdeva et al., 2016 [107]

To this day, a wide range of structural variations of siRNA has been reported, bringing forth many improved features such as increased stability and nuclease resistance, higher potency and reduced off-target effects. In addition, the development of multi-target siRNAs opens new possibilities for the treatment of complex diseases and, as our understanding of disease mechanisms improves, the use of this kind of RNAi inducers may enhance treatment efficacy by allowing the targeting of multiple pathological agents. For now, the cost of synthesis and complexity of some of these structures may restrict their use in the clinic, albeit the structural flexibility shown by RNAi mediators foresees further advancements and optimizations in this area.

1.6 Nanocarriers

Nanoparticles have been employed for siRNA delivery, as they show great potential to facilitate their uptake and improve siRNA pharmacokinetic profile [40]. In addition, they can be loaded with multiple siRNA molecules, allowing for significant uptake without overloading the target receptors, and are also able to protect siRNAs from degradation.

The most widely used and developed approach is to use lipid nanoparticles as a delivery agent. They are usually about 100-200nm and require coating with a neutral polymer such as polyethylene glycol (PEG) to prevent interactions with opsonic proteins in blood, which would lead to clearance by the reticuloendothelial system. One problem is that, due to their size, these particles may have trouble with tissues where the vascular endothelial barrier is not fenestrated, limiting their applications to organs like the liver and the kidneys [49].

Given their positive charge, cationic lipid nanoparticles easily interact with negative-charged siRNA, leading to efficient encapsulation. They are internalized through endocytosis

and, once inside an endosome, they disrupt its membrane by interacting with anionic lipids from the lipid bilayer, and allow the release of oligonucleotides into the cytosol [108]. Another type of lipids being studied for siRNA delivery are ionizable lipids, that can be protonated and deprotonated according to the environment pH, and have been shown to be more efficacious than net-charge cationic lipids [109]. Overall, lipid nanoparticles as carriers for siRNAs show great promise specifically when targeting the liver, with some systems already in clinical trials [110]. In fact, the first ever approved RNAi drug by the FDA, Patisiran, is formulated with hepatotropic lipid nanoparticles for the treatment of polyneuropathy of hereditary transthyretin-mediated amyloidosis [111].

Polymeric nanoparticles are also widely used for the delivery of oligonucleotides, with several different types of carriers [112]. Polylactic-co-glycolic acid (PLGA), one of the most well-known biocompatible polymers, was among the first used *in vivo* [113], and polymeric micelles have also been employed, showing improved pharmacokinetics and biocompatibility [114]. Dendrimers are hyperbranched polymeric systems with well-defined architecture that present reactive end-groups that allow for controlled branching from the core. Therefore, their size and number of reactive surface groups available for modifications can be precisely controlled by the number of "generations" produced [115] (Figure 10). Although this system shows high flexibility regarding conjugation with several ligands, there is some degree of toxicity displayed due to the strong "proton sponge" effect, leading to extensive endosome rupture [18].

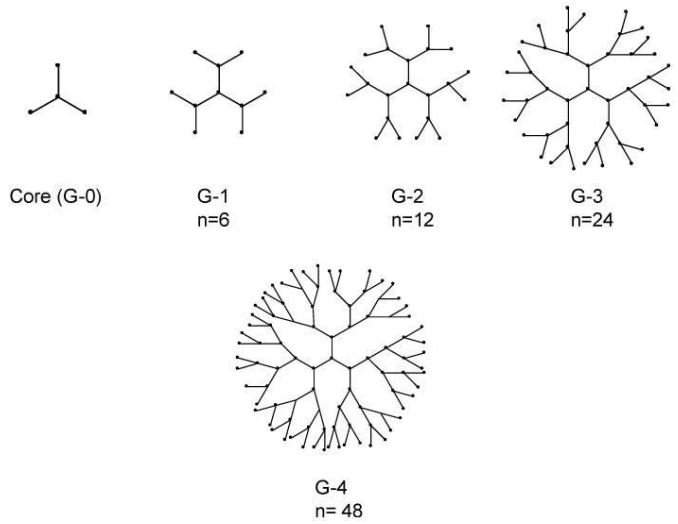

Fig.10 – Dendrimer branching with each generation. Adapted from Biswas et al., 2013 [115]

The major concerns with the utilization of nanoparticles for the delivery of siRNA are related to the toxicity of non-biodegradable carriers. While these complexes have the capacity for carrying multiple siRNA molecules, allowing for high uptake through one single internalization event, most of the exogenous material belongs to the carrier. This can lead to high levels of accumulation and possible toxicity [49]. In fact, the administration of Patisiran, the only RNAi drug in the market, has to be performed in combination with corticosteroids and

antihistamines, and it comes with various side effects like nausea, headache and breathing difficulties. Due to this fact, subsequent drugs developed by same the company have been in the form of bioconjugates [116]. Additionally, nanoparticle-based delivery is typically limited to clearance organs with fenestrated or discontinuous endothelium like the liver or the spleen [117]. As such, the paradigm of siRNA delivery has been shifting to a conjugate-mediated approach.

1.7 Bioconjugates

The concept of molecular bioconjugates encompasses a system where a biomolecule or target ligand is covalently or non-covalently conjugated with one or more siRNA molecules in order to improve the siRNA's pharmacokinetics and direct their action to a specific cell type. Bioconjugate present several advantages: they are well-defined molecular entities that can be precisely characterized; display high selectivity to their target receptors; and due to their simple composition, they are less likely to generate non-specific toxicity [49,51]. Modifications such as these should be targeted to the terminus of siRNA strands, in order to not compromise their enzymatic processing. However, this approach requires chemical stabilization of the siRNA to avoid the same issues that naked siRNA faces, like nuclease degradation and high renal clearance.

Independently of the conjugated molecule, the structure of the linker in a conjugate can also have an effect on the accumulation and activity of the siRNA. Different linkers have been employed (Figure 11), with different strategies in mind, and can usually be separated into two broader categories: cleavable and stable linkers. Cleavable linkers may prevent a decrease in silencing activity by removing the conjugated molecule and facilitate the loading of siRNA on the RISC complex, as well as facilitating endosomal escape. Examples include charge-based linkers like fusion proteins [118]; disulfide bonds that are reduced in the intracellular environment [119]; thioether bonds processed by thioesterases [120]; pH-sensible linkers like hydrazone bonds [121]; or even photo-labile bonds [122]. On the other hand, stable bonds and click-chemistry approaches like alkyne-azide bonds [123] or bonds based on phosphoramidite chemistry [124] may provide increased stability of the conjugate.

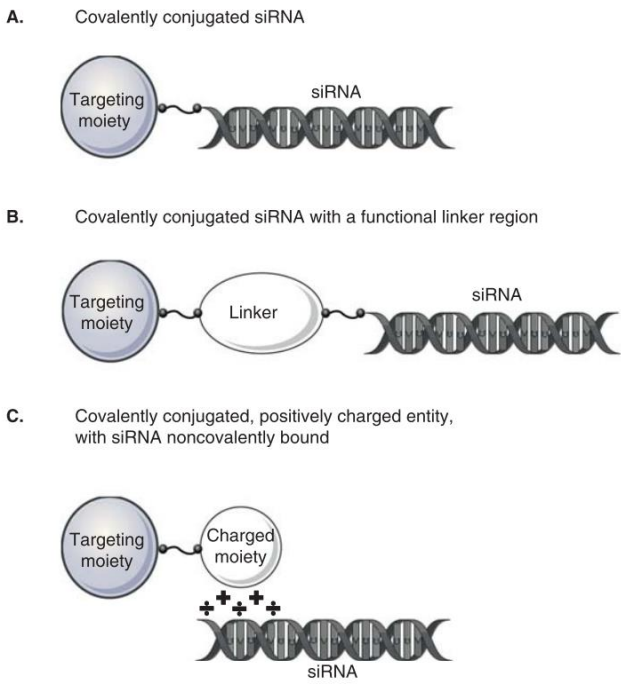

Fig.11 – Different strategies for linking molecular bioconjugates. Reproduced from Nielsen et al, 2014 [51]

1.7.1 Lipids

Lipids were the first class of molecules explored for oligonucleotide conjugation due to their lipophilic properties that could ensure interaction with the cellular membrane, and cholesterol clearly is the most well-characterized [125]. Cholesterol conjugates increase nucleic acid hydrophobicity and cellular association, forming complexes with LDL and HDL particles and promoting cellular uptake by receptor-mediated endocytosis through scavenger receptors [126] or galactose receptors [127]. One of the first reports studying the effect of cholesterol conjugation for siRNA suggested that it could significantly improve siRNA half-life in serum, as well as bioavailability [128]. These characteristics cause siRNA-cholesterol conjugates to accumulate in many organs: more effectively in the liver, adrenal glands and spleen, but also in the kidneys, pancreas, heart, lungs, thymus, ovaries and testes, as well as in muscle and fat, following subcutaneous injection in mice [129]. In fact, the conjugation of siRNA with cholesterol proved to be an effective strategy for the delivery to various tissues. Cholesterol conjugates improved siRNA uptake in a myeloma cell line without the use of transfection reagents [130]; caused increased accumulation and successful P-glycoprotein silencing in the tumoral tissue of a mice xenograft model [131]; successfully promoted neuronal uptake and silencing of huntingtin protein, attenuating neuronal pathology after a striatal injection in two mice models of Huntington disease [132,133], to name a few examples. Several siRNAs conjugated with this molecule have also shown increased silencing in the liver [134] and in the skeletal muscles of mice [135].

Because most lipid-siRNA conjugates cannot surpass the BBB following systemic administration [129], direct injection of these molecules into the CNS has been employed when targeting neuronal cells. Besides cholesterol, docosahexaenoic acid (DHA) was another lipid conjugate tested with this strategy, as it is the most common polyunsaturated fatty acid in the mammalian brain [136]. Striatal injections of a siRNA-DHA conjugate led up to 70% and 50% decrease in huntingtin mRNA levels in mouse striatum and cortex respectively, while avoiding neuronal death and immune response [137], therefore proving to be a promising approach for the treatment of neurodegenerative diseases. Other lipids have also been tested for targeting of different tissues: α-tocopherol (or vitamin E) for liver administration [138] or squalene for thyroid carcinoma [139], both achieving significant silencing.

Another factor influencing the uptake and gene silencing activity of these conjugates is the linker between the siRNA and the lipophilic group. As one study suggested, the length of the linker could play a role in the activity of siRNAs, with conjugates displaying optimal activity with linkers containing between 6-12 carbon atoms. They concluded that the shortening of the linker could reduce the efficiency of cellular uptake, and the lengthening could facilitate uptake while impairing silencing activity [140]. Taking all into account, lipid conjugation shows promising features for the delivery of siRNAs *in vivo* to a variety of organs, greatly improving their biodistribution, although it lacks cell-specific targeting.

1.7.2 Cell-Penetrating Peptides and Polymers

Cell-penetrating peptides and polymers (CPPs) are a class of short peptides or polymers that share the ability to facilitate cellular uptake due to their ability to permeate the cell membrane and translocate into the cytoplasm through various mechanisms. Additionally, they can also cause endossomolysis, disrupting the membrane in low pH endocytic vesicles and releasing their payload on the cytosol. It is currently thought that this is due to the "proton sponge" effect, where high concentrations of these cationic molecules in an acidic environment causes a change in the endosome osmolarity, resulting in swelling and leakage into the cytoplasm [141]. It has long been demonstrated that these molecules can also help deliver covalently-linked siRNAs into cells [142].

Another example of an important feature that can be present in these types of peptides is the imidazole ring, a component of the amino acid histidine (His). This weak base has the ability to acquire a cationic charge when the pH drops below 6 [141], as seen in Figure 12. As such, imidazole or histidine vectors have been widely used in conjugation with other molecules to increase transfection efficiency, like histidylated polylysine [143], histidine-rich dendrimers [144], or a Tat peptide elongated with histidine residues [145].

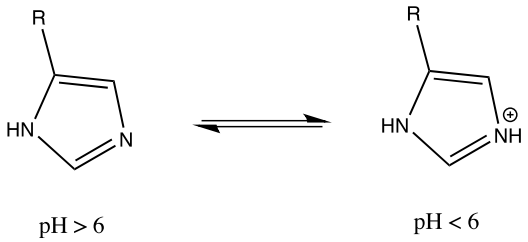

Fig.12 – Imidazole conversion into its charged form in low pH.

A further example encompassing CPPs for siRNA delivery is the amphipathic polymer of poly butyl and amino vinyl ether (PBAVE), that was extensively studied for delivery to hepatocytes. This polymer caused a 500-fold improvement in efficiency when administered in conjunction with a cholesterol-siRNA conjugate relative to the simple conjugate alone [146]. A successful case is the use of skin-penetrating and cell-entering (SPACE) peptide in conjugation with siRNAs, causing significant silencing of IL-10 and GADPH in the epidermis following direct skin administration [147].

However, despite their effectiveness, the use of this kind of compounds still has some limitations, as they can lead to toxicity [148,149] and, due to their cationic nature, can form insoluble complexes with siRNA and hamper their biologic activity by preventing their loading into RISC [150].

1.7.3 Receptor-Ligand Conjugates

As the systemic administration of naked siRNA leads mainly to accumulation in the liver and kidneys, there is the need to confer active targeting properties to the siRNA molecules if other tissues are to be addressed. This can be achieved by associating siRNA with a molecular ligand that specifically binds to certain surface markers highly expressed by the intended cell type. Obvious cell markers to target are endocytic receptors, preferably with a high number of copies expressed and with fast recycling time. Nonetheless, a targeting moiety should possess functional groups not essential for biological activity that can be altered freely for the chemical attachment of siRNA [51].

By far the most successful biomolecule to achieve this kind of targeted delivery with oligonucleotides is N-acetylgalactosamine (GalNAc). GalNAc is a ligand for the asialoglycoprotein receptor (ASGPR) which is highly expressed on the basolateral membrane of hepatocytes. It can reach more than 500,000 copies/cell and has an estimated recycling time of 15 minutes, granting high rate of internalization and cellular trafficking efficiency [151]. Pre-clinical trials showed that siRNA-GalNAc conjugates (Figure 13) can provide near-complete gene silencing with very low doses of administration [152,153] and, in spite of the failure in phase III clinical trials by the triGalNAc-siRNA conjugate Revuisiran [154], several new formulations based on GalNAC conjugates are now in clinical trials [116].

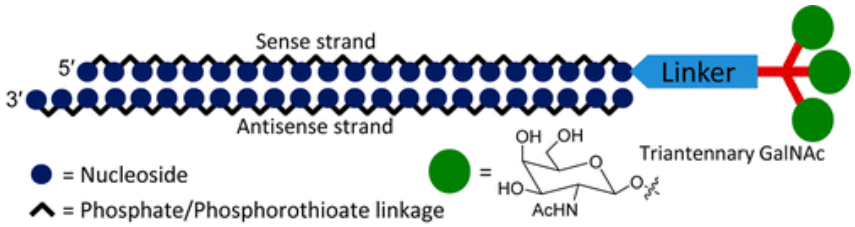

Fig.13 – siRNA molecule conjugated with three GalNAc molecules through a triantennary linker. Adapted from Matsuda et al., 2005 [155]

Another case of success is the conjugation of siRNA with peptides such as the cyclic Arg-Gly-Asp (cRGD), a ligand for αVβ3/5 integrins (highly expressed in tumor and vascular endothelial cells). A report showed moderate success in inhibiting blood vessel growth in zebrafish, as well as inhibiting tumor growth in mice following intravenous injections through the use of siRNA-cRGD conjugates against VEGF receptor [156]. Due to the reported high expression of glycoprotein folic acid receptor in tumoral cells [157], folic acid conjugation was also proposed for specific delivery to tumors. Due to receptor-mediated endocytosis, it was demonstrated that the accumulation of siRNA-folic acid conjugates in tumoral cells *in vivo* was significantly higher than unmodified siRNA [158]

The use of siRNA bioconjugates with targeting ligands can also contribute significantly to target some of the most inaccessible organs and tissues like the brain. Rabies virus glycoprotein (RVG) is a short peptide that specifically binds to acetylcholine receptors expressed by neuronal cells and, as such, was tested as targeting ligand in a siRNA conjugate. The synthesis of chimaeric RVG peptides by adding several positively charged arginine residues to its C terminal allowed siRNA binding through charge interactions and led to the production of siRNA-RVG conjugates. Following intravenous injections in mice, these conjugates were able to cross the BBB (likely through transcytosis) and achieved specific gene silencing in the brain without eliciting an immune response [159]. Thus, the conjugation with RVG peptides can be a non-invasive strategy to deliver siRNAs across the BBB. Another study demonstrated the use of sertraline-conjugated siRNAs targeting the serotonin transporter (SERT) through intranasal administration in mice. Being an inhibitor of SERT, the covalent binding of sertraline to siRNA caused the endocytosis and accumulation of this conjugate in serotonin neurons, rich in SERT receptors. Consequently, a downregulation in the expression of these receptors was reported, with short-term reversion of depressive-like behavior in corticosterone-treated mice. Sertraline-siRNA conjugates also exhibited more pronounced effects than conventional long-term anti-depressive treatments [160]. Anandamide-siRNA conjugates have also been tested for receptor-mediated endocytosis of siRNA. Anandamide targets cannabinoid receptors present in immune and neural cells, and successfully delivered siRNA into RBL-2H3 cells that model neuronal uptake. Moreover, this conjugate also displayed gene silencing levels similar to siRNA delivered through a standard transfection reagent [161].

1.7.4 Antibodies

Direct conjugation of siRNA with antibodies may be a potentially growing field, owing to their ability of highly specific recognition and high-affinity binding for biological targets. The high molecular weight of the resulting conjugates (~150 kDa) also allows for a prolonged presence in the blood. One of the first studies in this area relied on siRNA-antibody conjugation through the use of protamine, a protein with nucleic acid binding properties. A fusion protein was synthetized with protamine linked to the C terminal of the heavy chain of an antibody for the HIV-1 envelope, allowing for the conjugation with siRNA through the interaction with protamine. When using siRNAs targeting an HIV associated gene, this conjugate caused the inhibition of HIV replication specifically in infected T cells, and also displayed targeting properties against HIV envelope-expressing B16 tumor cells *in vivo*. A variation of this fusion protein with an antibody targeting ErbB2 was also able to specifically deliver siRNA into cells expressing ErbB2 [118].

A more recent report showed that the covalent attachment of an antigen-binding fragment of monomeric CD71 antibody to various siRNAs exhibited over 72% gene silencing in muscle gene targets following 4 weekly intramuscular injections, in a peripheral artery disease mice model. This was translated into a 24% increase in average running distance of these mice. In addition, a single intravenous injection of this conjugate also elicited a 90% reduction in target mRNA levels in muscle cells [162].

The use of antigen-binding fragments instead of antibodies for siRNA conjugation probably facilitates the endosomal escape of the conjugate due to the smaller size of these fragments, as well as their lower receptor-binding affinity. The resulting size of full antibody-siRNA conjugates might also hamper their tissue penetration, although a study directly comparing these two approaches is needed to further conclude on this subject.

Antibody mimetics have also emerged as viable candidates for conferring targeting properties to siRNA conjugates. These are synthetic molecules that have been engineered to mimic the specificity of antibody-antigen binding without being structurally related to antibodies, and can present several advantages like facilitated production. One example are affibodies, bundles of 3 α-helixes based on the binding domain of protein A [163]. When non-covalently conjugated to several siRNAs through a fusion protein with a RNA binding domain, affibody-siRNA conjugates formed nuclease-resistant particles that displayed selective transport into tumor cells, as well as significant gene silencing. Furthermore, intravenous injection of these conjugates into a xenograft mice model led to significant tumor suppression [164]. Other class of antibody mimics that started to be tested recently for siRNA targeted delivery were designed ankyrin repeat proteins (DARPins), that consist of at least 3 or more customizable ankyrin repeat motifs presenting high target affinity and ease of production [165]. For now, only one single study showed the employment of DARPins in siRNA delivery. In this

study, a method of synthesis and purification of DARPin-siRNA conjugates containing several labile or stable linkers was established, and the targeting capacity of these conjugates was tested in a cell line. The results showed that EpCAM-targeted DARPins successfully mediated conjugate internalization and gene silencing in EpCAM-positive cell. Moreover, the conjugates containing labile disulfide linkers were shown to induce more potent gene silencing effects when compared to conjugates with stable linkers like thiol-maleimide linkers, although showing less nuclease resistance in serum [166]. The differences in silencing potency are most likely due to facilitated endosomal escape and RISC incorporation following intracellular linker cleavage.

1.7.5 Aptamers

Aptamers are another example of promising molecules to approach siRNA targeted delivery. They are nucleic acids that form 3D structures by folding within themselves through intra-molecular base pairing, hereby allowing them to be designed to potentially bind to virtually any receptor [167]. The fact that aptamers are nucleic acids also allows for the production of RNA-DNA or RNA-RNA "chimeras", with the aptamer bound to the siRNA terminus through base-pairing. Beside their similarity to antibodies in targeting properties, these chimeras have additional advantages like low production cost, lower variation from batch to batch and longer shelf-life.

siRNA-aptamer chimeras have been studied for application in several areas such as anti-HIV therapeutics. A chimera constituted by an aptamer targeting the viral enveloping protein gp120 linked to a DsiRNA targeting *tat/rev* RNA (essential for HIV replication) was described. Although intravenous injections of the aptamer alone in a humanized HIV mice model caused significant suppression of HIV replication, treatments with the chimera showed increased suppression as well as prolonging the antiviral effect over several weeks [168]. This combined approach provides an efficient therapeutic strategy for the treatment of HIV infections. Further optimizations of this design led to the development of a modular unit consisting of the aptamer with a "sticky" bridge sequence of 16 nucleotides attached via a carbon linker. This sequence allowed for the non-covalent binding through base-pairing of different siRNAs to the same aptamer, expanding the utility of this chimera by offering the possibility to incorporate varied DsiRNAs, thus generating chimeras targeting different genes [169]. In another report, an aptamer targeting the prostate specific membrane antigen was conjugated with siRNAs targeting PLK1 and BCL2 genes, usually overexpressed in most human tumors. After 10 intratumoral injections in a xenograft mice model of prostate cancer, up to 90% silencing efficiency was observed, as well as tumor growth decrease and even tumor regression [170].

It has also been demonstrated that aptamers can be used to target the CNS. Esposito et al. reported that the aptamers Gint4.T and GL21.T targeting receptor tyrosine kinases could penetrate an *in vitro* model of the BBB while conjugated to miRNAs, and also target

glioblastoma stem-like cells [171]. This work was further expanded and chimeras of Gint4.T aptamer and STAT3-targeting siRNA were used in a *in vivo* subcutaneous xenograft model, showing efficient delivery and over 60% suppressed expression of STAT3 in the glioblastoma xenograft. Furthermore, the inhibition of tumor growth and angiogenesis was observed [172].

Although aptamer-siRNA chimeras exhibit good targeting properties, other problems still need to be addressed, like nuclease susceptibility [49] and inefficient endosome escape. While trying to overcome the issue of endosomal escape, a combinatorial approach merged the targeting and therapeutic properties of these chimeras with a small protein for the disruption of the endosomal membrane. A small protein tag was created, encompassing two functional domains: a dsRNA binding domain for the docking of the chimera through the siRNA duplex; and a pH-dependent poly-histidine to cause osmotic swelling and consequently the rupture of the endosome. This protein tag could theoretically bind to any chimera, serving as an universal platform to address endosomal escape while maintaining silencing and targeting efficiency, improving the therapeutic properties of other siRNA-aptamer conjugates [173].

1.7.6 Dynamic Polyconjugates

Dynamic polyconjugates are a type of siRNA conjugates developed by Arrowhead Pharmaceuticals that encompass several functional domains in a combinatorial approach to ensure specific cell targeting and endosomolytic properties, while also incorporating a shielding agent to avoid nonspecific interactions. The first reported polyconjugate was an amphiphilic polymer constituted by a PBAVE chain with PEG and GalNAc residues attached through an acid-cleavable linker, and a siRNA duplex attached through disulfide bonds. The rationale behind this design was that the GalNAc residues would ensure specific hepatocyte targeting and internalization through receptor-mediated endocytosis while the PEG residues provided shielding from nonspecific interactions like opsonic protein binding in circulation. After internalization, the acidic environment of the endosome would cleave the linkers between the polyconjugate and the PEG and GalNAc residues, separating them from the PBAVE-siRNA conjugate. Then, the endosomolytic properties of PBAVE would cause the rupture of the endosomal membrane and escape into the cytoplasm, where the reducing environment would cleave the disulfide bond and release the siRNA duplex to induce the RNAi mechanism [174] (Figure 14).

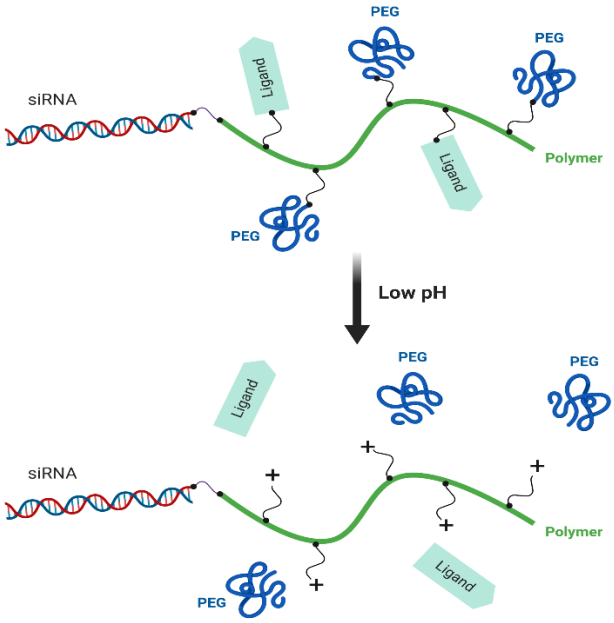

Fig. 14- Schematic representation of the mechanism of action of dynamic polyconjugates.

In fact, these polyconjugates display considerable biologic activity due to their effective internalization and endosome escape properties. When tested in mice via intravenous injection, they exhibited consistent knockdown of the apolipoprotein B endogenous gene, with phenotypic changes such as reduced serum cholesterol lasting up to 10 days with a single injection [174]. Another study demonstrated that after a single intravenous injection, these conjugates contributed to the knockdown of the F7 gene in cynomolgus monkeys with 99% efficacy, with the effect lasting up to 80 days [175].

Wong et al. also employed dynamic polyconjugates to improve the efficacy of siRNA-cholesterol conjugates. In a previously mentioned study, siRNA-cholesterol conjugates were co-injected in mice with the modified PBAVE-GalNAc-PEG polymer previously reported. This new approach led to an efficacy improvement of over 500-fold when compared to regular siRNA-cholesterol conjugate activity in mice hepatocytes; one intravenous injection caused 75% suppression of the apolipoprotein B gene in the liver of rhesus monkeys up to 30 days [146]. Another paper also reported the use of a dynamic polyconjugate targeting hepatocytes, but instead of PBAVE, the endosomolytic agent used was melittin, a peptide present in bee venom. As expected, the co-injection of this polyconjugate with siRNA-cholesterol conjugates displayed improved efficacy when compared to single siRNA-cholesterol conjugates: 99% suppression of the F7 gene was observed in mouse livers following one intravenous injection, significantly higher than the 20% gene silencing caused by siRNA-cholesterol conjugates alone [176].

These formulations were able to reach clinical trials for the treatment of Alpha-1 antitrypsin deficiency, but they were terminated early due to the toxicity displayed in a non-

human primate model [177]. Nonetheless, they served as proof of concept for combinatorial approaches to the delivery of siRNA *in vivo*.

Table 1 – Examples of several conjugates employed for siRNA delivery.

Targeted Tissue/Organ	Conjugate	Target	Clinical Stage	References
Liver	siRNA-Cholesterol	Apolipoprotein B	Pre-clinical	(Soutschek et al., 2004)
	siRNA- α-tocopherol	Apolipoprotein B	Pre-clinical	(Nishina et al., 2008)
	Triantennary GalNAc-siRNA	TTR-FAC	Phase III (discontinued)	(Nair et al., 2014) Trial Reference: NCT02319005
		PCSK9	Phase III (Active)	(Nair et al., 2014) Trial Reference: NCT03397121
		Antithrombin	Phase III (recruiting)	(Nair et al., 2014) Trial Reference: NCT03549871
		ALAS-1	Phase III (active)	(Nair et al., 2014) Trial Reference: NCT03338816
		TTR	Phase III (recruiting)	(Nair et al., 2014) Trial Reference: NCT03759379
		Complement C5	Phase II (recruiting)	(Nair et al., 2014) Trial Reference: NCT03841448
		Glycolate Oxidase	Phase II (enrolling)	(Nair et al., 2014) Trial Reference: NCT03350451
	Dynamic Polyconjugate	Apolipoprotein B	Pre-clinical	(Rozema et al., 2007)
		F7	Pre-clinical	(Rozema et al., 2015)
	PBAVE-GalNAc-PEG polymer co-injected with siRNA-cholesterol	Apolipoprotein B	Pre-clinical	(Wong et al., 2012)
	Melittin-GalNAc polymer co-injected with siRNA-cholesterol	alpha-1 antitrypsin	Phase I (withdrawn)	(Turner et al., 2018) Trial Reference: NCT02363946.
		HBV	Phase II (withdrawn)	(Wooddell et al., 2013) Trial Reference: NCT02452528

Targeted Tissue/Organ	Conjugate	Target	Clinical Stage	References
Muscle	siRNA-cholesterol	Myostatin	Pre-clinical	(Khan et al., 2016)
	siRNA-anti CD71 Fab	Apolipoprotein B HPRT	Pre-clinical	(Sugo et al., 2016)
Tumoral Cells	siRNA-cholesterol	P-glycoprotein	Pre-clinical	(Chernikov et al., 2017)
	siRNA-squalene	RET/PTC1	Pre-clinical	(Raouane et al., 2011)
	siRNA-cRGD	VEGFR2	Pre-clinical	(Liu et al., 2014)
	siRNA-folic acid	-	Pre-clinical	(Thomas et al., 2009)
	siRNA-ErbB2 affibody	AURKB HER-2	Pre-clinical	(Dar et al., 2015)
	siRNA-receptor tyrosine kinase aptamer	STAT3	Pre-clinical	(Esposito et al., 2018)
Skin	siRNA-SPACE	Il-10 GADPH	Pre-clinical	(Hsu et al., 2011)
Brain	siRNA-cholesterol	Huntingtin protein	Pre-clinical	(DiFiglia et al., 2007) (Alterman et al., 2015)
	siRNA-DHA	Huntingtin protein	Pre-clinical	(Nikan et al., 2016)
	siRNA-RVG	GFP	Pre-clinical	(Kumar et al., 2007)
	siRNA-sertraline	SERT	Pre-clinical	(Ferrés-Coy et al., 2016)
Neuronal/ Immune Cells	siRNA-anandamide	Kinase SYK	Pre-clinical	(Willibald et al., 2012)
Epithelium	siRNA-DARpin	Luciferase	Pre-clinical	(Lorenzer et al., 2019)
HIV Infection	DsiRNA-gp120 aptamer	tat/rev RNA CD4 TNPO3	Pre-clinical	(Neff et al., 2011) (Zhou et al., 2013)
	siRNA-protamine-HIV1 envelope Fab	EGFP	Pre-clinical	(Song et al., 2005)
Prostate	siRNA-PSMA aptamer	PLK1 BCL2	Pre-clinical	(McNamara et al., 2006)

Overall, the employment of molecular bioconjugates with siRNA shows very promising features, with several approaches for increasing efficiency and targeting specificity described.

In addition to the previous referred studies on siRNA conjugates, several studies developed for ASO conjugates might also be translated into siRNA therapeutics. High-throughput techniques have been employed to discover new classes of small molecules capable of improving ASOs uptake and efficiency, and several candidates have been identified and observed to improve ASOs potency and internalization efficiency. They act by increasing the permeability of endosomes, although their mechanisms differ from the usually employed endosomolytic agents like PBAVE, and could be interesting candidates for application in siRNA conjugates [178]. Another example was a report studying the use of dendritic polylysines on the delivery of ASOs. These positively charged nano-sized spherical polymers were functionalized with cRGD and evaluated as delivery agents of ASOs, showing integrin receptor-mediated uptake without causing cytotoxic effects [179]. Despite only being tested for ASOs delivery, the structural features of cRGD-dendritic polylysines also makes them theoretically viable for siRNA delivery.

However, the use of bioconjugates still presents some limitations. In most cases, their small size does not solve the rapid renal clearance issues of siRNAs, although several conjugates can help to mitigate this issue by promoting binding to serum proteins or increasing their hydrodynamic radius. One possible solution is the employment of PEG functionalization.

Iversen et al. studied this approach, conjugating PEG chains of different sizes to the 5' end of siRNAs, and observed that up to 50% of siRNAs conjugated with a 20 kD PEG chain remained in circulation 1 hour after intravenous injection, contrasting with the almost complete clearance of naked siRNAs after several minutes [180]. Additional conjugates like the previously mentioned dynamic polyconjugates also employ PEG functionalization as a strategy to improve their pharmacokinetic profile [174].

Another pressing issue is that an internalization event only leads to a single siRNA molecule being loaded onto the cytosol, requiring many other events to accumulate siRNA in sufficient concentration to achieve a pharmacological effect. The incorporation of different siRNA structural designs like branched siRNAs into these conjugates might be a solution to this challenge. Despite all these obstacles, some successes have already been accomplished, with the efficient liver targeting by GalNAc leading to several clinical trials of siRNA conjugates [125]. Although different receptors have been identified for several targets such as the BBB, endothelium, tumors, leukocytes and others [49,181], future work should focus on identifying and characterizing new target receptors apart from the liver, as well as increasing the efficacy of the existing conjugates by promoting endosomal escape, for example. This is crucial for conjugates targeting extra-hepatic systems if they are to achieve similar efficiency as GalNAc conjugates.

Chapter 2: **Aim of the Thesis**

Neurological disorders are one of the clinical unmet needs of the 21st century, lacking efficient therapies and subsequently causing considerable economic and social burden. siRNA-based therapies may present a viable solution to this issue, as they show promising features for the treatment of many diseases and conditions by being able to silence virtually any gene. However, this potential has only been clinically translated into liver-targeted therapies thus far.

One promising option for the delivery of siRNAs is through the use of siRNA molecular conjugate systems, however they have thus far only been most successful for liver targeting. In fact, these conjugates may be susceptible to high renal clearance and usually only transport one siRNA molecule, limiting their pharmacological efficiency.

Thus, the main goal of this work aimed to develop a novel molecular conjugate-type nanosystem that could be efficiently applied for neuronal cell gene silencing. Objectives of this thesis encompassed the design and development of a novel siRNA nanoarchitecture (henceforth designated siRNA nanocage) that could further allow easy conjugation with functional biomolecules, primarily targeting neuronal cells.

These siRNA nanocages will be constructed by hybridization-mediated self-assembly of two single-stranded branched RNA structures with complementary RNA arms that will form three Dicer-siRNA duplexes linked in a cryptand-like structure [103] (Figure 15). Dicer-mediated recognition and cleavage of these duplexes will allow for the release of active 21-mer siRNAs from the nanocage. Additionally, the inclusion of an overhang sequence in both branching units will allow, through site-specific hybridization, their functionalization with biomolecule-oligonucleotide conjugates such as neuronal targeting ligands.

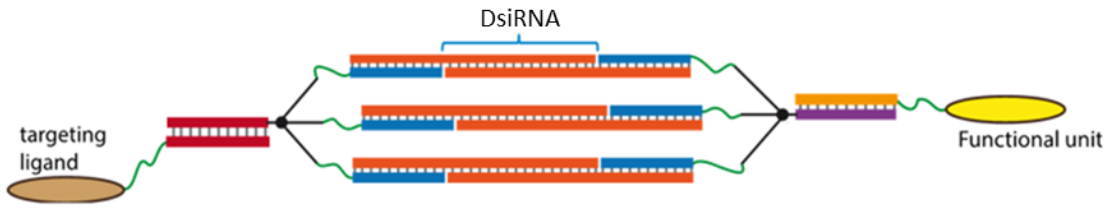

Fig.15– Schematic representation of a siRNA nanocage, functionalized with biomolecule-oligonucleotide conjugates through complementary base-pairing with the two overhang sequences

Thus, we propose siRNA nanocages as a molecular bioconjugate system with a well-defined structure, as well as easily tunable properties due to their modular functional units and precise assembly through Watson-Crick base-pairing. Furthermore, siRNA nanocages will allow the delivery of multiple siRNAs per structure (in this first generation, a number of 3 siRNAs per structure was tested), enabling effective gene silencing of therapeutic targets while displaying high biocompatibility due to their composition being mainly nucleic acids. Their compact structure could also promote increased stability and facilitate tissue penetration due to the increased size.

Specific objectives of this thesis will include:

1. Self-assembled production, purification and functionalization of siRNA nanocages, and analysis through polyacrylamide gel electrophoresis (PAGE);
2. Structural characterization through transmission electron microscopy (TEM);
3. Assessment of enzymatic (Dicer/RNAse H) processing of siRNA-nanocages *in vitro*;
4. *In vitro* transfections with siRNA nanocages in neuronal cell lines, and evaluation of gene silencing properties through quantitative reverse transcription polymerase chain reaction (RT-qPCR) and luminescence assays;
5. Evaluation of the cellular uptake of functionalized siRNA-nanocages in neuronal cell lines through fluorescence spectroscopy and confocal microscopy.

Chapter 3: **Materials and Methods**

3.1 Oligonucleotides

All oligonucleotides used were purchased from Integrated DNA Technologies, except the Tet1-DNA conjugate (Eurogentec) and the Treblers (Oligonucleotide Synthesis Facility, Yale University). Their sequences are presented in Table 2:

Table 2 – Oligonucleotide sequences utilized during this work. DNA in capital letters, RNA in capital letters preceded by an "r", 2'-O-Me RNA in capital letters preceded by an "m".

Name	Sequence (5'-3')
Trebler Sense A	TGTGCTTGTGATTGATGT-(SPACER 18)(TREBLER)-CAATAATGACTAAAAGCG
Trebler Antisense A	CTTGTCTCGTTTCTATCT-(SPACER 18)(TREBLER)-AAGACTCAGGAAAAGCGA
Trebler Sense B	CGCGCCGACATCCAGTCG -SPACER18-TREBLER- CAATAATGACTAAAAGCGACG
Trebler Antisense B	CGCGGCGCCGATACGACG -SPACER18-TREBLER-GGCAACCAATATACAATGGCG
Sense A D-R strand (GFP)	ACATCAATCACAAGCACArUrGrArCrCrCrUrGrArArGrUrUrCrArUrCrUrGrCrArCrCrArCrCrG
Antisense A D-R strand (GFP)	AGATAGAAACGAGACAAGrCrGrGrUrGrGrUrGmCrAmGrAmUrGmArAmCrUmUrCrArGrGrGrUrCrA
Sense A D-R strand (PTEN)	ACATCAATCACAAGCACArUrUrCrGrArCrUrUrArGrArCrUrUrGrArCrCrUrArUrArUrUrUrArU
Antisense A D-R strand (PTEN)	AGATAGAAACGAGACAAGrArUrArArArUrArUmArGmGrUmCrAmArGmUrCmUrArArGrUrCrGrArA
Sense B D-R strand (PTEN)	CGACTGGATGTCGGCGCGrUrUrCrGrArCrUrUrArGrArCrUrUrGrArCrCrUrArUrArUrUrUrArU
Sense B D-R strand (PTEN) – Cy5	/5Cy5/CGACTGGATGTCGGCGCGrUrUrCrGrArCrUrUrArGrArCrUrUrGrArCrCrUrArUrArUrUrUrArU
Antisense B D-R strand (PTEN)	CGTCGTATCGGCGCCGCGrArUrArArArUrArUmArGmGrUmCrAmArGmUrCmUrArArGrUrCrGrArA

Sense D-R strand version I (GFP)	CGACrUrGrGrArUrGrUrCrGrGCGCGmAmCmCrCrUmGrAmArGmUrUrCrArUrCrUrGrCrA
Antisense D-R strand version II (GFP)	CGTCrGrUrArUrCrGrGrCrGrCCGCGrUrGrCrArGrArUrGmArAmCrUmUrCmArGmGrGmUTT
Sense D-R strand version II (GFP)	CGACTGGArUrGrUrCrGrGrCrGrCrGmAmCmCrCrUmGrAmArGmUrUrCrArUrCrUrGrCrA
Antisense D-R strand version II (GFP)	CGTCGTATrCrGrGrCrGrCrCrGrCrGrUrGrCrArGrArUrGmArAmCrUmUrCmArGmGrGmUTT
DNA Arm Sense	CGCGCCGACATCCAGTCG
DNA Arm Antisense	CGCGGCGCCGATACGACG
siGFP	5'-UGCAGAUGAACUUCAGGGUCA = 3'-CCACGUCUACUUGAAGUCCCA
siPTEN	5'-CGACUUAGACUUGACCUAUAU = 3'-AAGCUGAAUCUGAACUGGAUA
Tet1-DNA Conjugate	HLNILSTLWKYRC-Spacer 18- CGTCGCTTTTAGTCATTATTG
Biotin-DNA Sense Conjugate	/5BitoinTEG/CGCTTTTAGTCATTATTG
Biotin-DNA Antisense Conjugate	/5BitoinTEG/TCGCTTTTCCTGAGTCTT
PTEN Forward Primer	CAAAGAGATCGTTAGCAGAAACA
PTEN Reverse Primer	ATGCTTTGAATCCAAAAACCTTACT
Ywhaz Forward Primer	ACGACGTACTGTCTCTTTTGG
Ywhaz Reverse Primer	GTATGCTTGCTGTGACTGGT

Concentrations were estimated by measuring absorbace at 260 nm using a NanoDrop™ 1000 Spectrophotometer (Thermo Fisher Scientific). For nanocages, the molar extinction coefficient was determined by adding up the coefficients of its composing oligonucleotides, and the double-stranded sequences were multiplied by a factor of 0,7 to account for hyperchromicity.

3.2 Nanocage *in silico* Design

The sequences for the nanocages were designed *in* silico with the help of the NUPACK software [182] (http://www.nupack.org/). The targeted secondary structure was defined using the NUPACK script language and served as the input for sequence design by the software. Briefly, the optimization performed by NUPACK minimizes the formation of secondary

structures through self-complementarity, the output being a set of sequences with the highest probability to assemble into the user-defined structure. Nucleotide tetramers were excluded from sequence design, as they are known to adopt specific secondary structures [183].

3.3 Assembly and Functionalization Reactions

All nanocage assemblies were made in an assembly buffer of 30 mM Tris-HCl + 50 mM NaCl, pH7,3.

3.3.1 Nanocages for Purification, Functionalization and Characterization

Nanocages used for the purification and functionalization tests, as well as for TEM analysis, were assembled first by mixing sense and antisense A Treblers with sense and antisense A D-R strands (GFP), in a molar ratio of trebler:D-R strand of 1:3,6, and applying the following temperature cycle: 85ºC, 5 min → 50°C, 60 min → 4°C. After this, sense and antisense branches were mixed in a molar ratio of 1:1 and the following temperature cycle was applied: 50°C, 45 min → 20°C, 5 min → 4°C; forming anti-GFP nanocages.

Biotin functionalization was achieved by mixing sense and antisense biotin-DNA conjugates with nanocages and incubating for 30 minutes at room temperature.

3.3.2 Nanocages for Dicer Digestion and PTEN Gene Silencing Experiments

Nanocages used for the *in vitro* Dicer digestion tests were assembled by assembled first by mixing sense and antisense A Treblers with sense and antisense A D-R strands (PTEN), in a molar ratio of trebler:D-R strand of 1:3,6, and applying the following temperature cycle: 85ºC, 5 min → 50°C, 60 min → 4°C. After this, sense and antisense branches were mixed in a molar ratio of 1:1 and the following temperature cycle was applied: 50°C, 45 min → 20°C, 5 min →4°C; thus forming anti-PTEN nanocages.

3.3.3 Oligonucleotides and H-Nanocages for U2OS-GFPLuc Transfections

The different versions of duplexes for U2OS-GFPLuc transfections were assembled by mixing version I or II sense/antisense D-R strands (GFP) and applying the following temperature cycle: 95°C, 2 min → slow cool for 30 min to 20ºC → 20°C, 5 min > 4ºC. Afterwards, both sense and antisense DNA arms were added, incubating for 1 hour at room temperature.

H-Nanocages for U2OS-GFPLuc transfections were assembled by mixing sense and antisense B Treblers with sense D-R strand version I (GFP) and antisense D-R strand version II (GFP) in a molar ratio of Trebler:D-R strand of 1:2,5, and applying the following temperature cycle: 90ºC, 3 min →slow cool for 30 min to 20ºC → 10 min, 20ºC → 4ºC. Afterwards, sense and antisense strands were mixed with a molar ratio of 1:1, and the following temperature cycle was applied: 60ºC, 30 min → slow cooling for 30 min to 20ºC → 4ºC; thus forming anti-GFP H-nanocages.

3.3.4 Nanocages for Cellular Uptake Assays

Nanocages used for the cellular uptake assays were assembled first by mixing sense and antisense B Treblers with sense B D-R strand (PTEN) labeled with cy5 and antisense B D-R strand (PTEN) , in a molar ratio of trebler:D-R strand of 1:3,6, and applying the following temperature cycle: 85°C, 5 min → 50 °C, 60 min → 4°C. After this, sense and antisense branches were mixed in a molar ratio of 1:1 and the following temperature cycle was applied: 50°C, 45 min → 20°C, 5 min →4°C; forming Cy5-labeled anti-PTEN nanocages.

Nanocages were then functionalized with Tet-1 by mixing Tet1-DNA conjugate with nanocages at a molar ratio of nanocage:Tet1 of 1:1,2 for 1 hour at 25ºC and with stirring of 800 rpm.

3.4 PAGE Analysis

All Page analysis were carried out using a Mini-PROTEAN Tetra Cell System (Bio-Rad). Polyacrylamide gels were made using a 30% Acrylamide/Bis Solution (Bio-Rad), 10x TBE Buffer stock solution (NZYTech); and polymerized with the use of 10% APS and TEMED.

Acrylamide percentage, voltage and run time of the presented PAGEs were represented in Table 3:

Table 3 – Running conditions of PAGEs presented during the work.

Presented PAGE	Run Conditions
Figure 18	4%+6% 1x TBE, 40 minutes at 80V
Figure 19	4%+6% 1xTBE, 60 minutes at 80V
Figure 20	4%+6% 1x TBE, 90 minutes at 80V
Figure 21	4%+6% 1x TBE + 50 mM NaCl, 50 minutes at 80V

Figure 22	4%+6% 1x TBE + 50 nM NaCl, 45 minutes at 80V
Figure 23	4%+6% 1x TBE + 50 mM NaCl, 180 minutes at 80V
Figure 27	4%+6% 1x TBE + 50 mM NaCl, 50 minutes at 70V
Figure 32	4%+6% 1x TBE + 50 mM NaCl, 50 minutes at 80V
Figure 34	4%+8%, 1xTBE + 50 mM NaCl, 14 hours and 35 minutes at 80V, 4ºC

All gels were stained with SYBR Gold (Thermo Fisher Scientific) for 8-10 minutes and were revealed in a Gel Doc™ XR+ Imaging System (Bio-Rad) and analyzed using the Image Lab 6.0 software (Bio-Rad).

3.5 Nanocage Purification

For nanocage purification, nanocages were first run through a preparatory 4%+6% polyacrylamide gel for 1 hour and 40 minutes at 80V. After, the gel was visualized under UV light and the corresponding nanocage bands were cut with a scalpel. The gel slices were then centrifuged for 8 minutes at 6000xg in 0,6 mL Eppendorf's with a hole in the bottom, made with a 19G needle (Terumo). The resulting gel slurries were transferred to 0,22 µm Corning Costar Spin-X columns (Sigma-Aldrich) with 500 µL of assembly buffer and were subjected to 3 incubations (6 hours + overnight + 6 hours) at 15ºC and with agitation at 1400 rpm in a Thermomixer® (Eppendorf). After every incubation, the columns were centrifuged for 5 minutes at 13000xg and supernatant was collected. In the end, all the gathered supernatants were joined and concentrated through an Amicon 3 kDa column (Merck), according to manufacturer instructions.

3.6 Transmission Electron Microscopy

For negative staining transmission electron microscopy Formvar/carbon film-coated mesh nickel grids (Electron Microscopy Sciences, Hatfield, PA, USA) treated with 15 seconds of glow discharge. A treatment with 5 µL poly-D-lysine (1µg/mL, Sigma) for 30 seconds, followed by draining with filter paper, was also attempted. 5 µL of anti-GFP nanocages (0,1 µM) were mounted on the grids and were left standing for 2 minutes. The liquid in excess was removed with filter paper, and 5 µL of uranyl acetate (2%) were added on to the grids and left standing for 10 seconds, after which liquid in excess was removed with filter paper. Afterwards, the

grids were washed 3 times in an inverted drop of nuclease-free water (Qiagen) for 5 seconds, without removing the excess liquid. Visualization was carried out on a JEOL JEM 1400 TEM at 80 kV (Tokyo, Japan). Images were digitally recorded using a CCD digital camera Orious 1100W Tokyo, Japan. The transmission electronic microscopy was performed at the HEMS core facility at i3S, University of Porto, Portugal, with the assistance of Rui Fernandes. Images were analyzed and measured with the help of the Image J software.

3.7 Enzymatic Digestion Assays

For *in vitro* Dicer digestion assays, Genlantis™ Recombinant Human DICER Enzyme Kit was used. Samples were incubated according to kit instructions, with 2 units of recombinant Dicer in a volume of 15 µL, at 37°C for 12 and 24 hours, After, 2 µL of Stop Solution were added.

For RNAse H cleavage assays, samples were incubated with RNAse H enzyme and 1x RNAse Buffer (New England BioLabs) in a 10 µL volume for 15 minutes at 37°C.

3.8 PTEN Gene Silencing Assays

3.8.1 HT22 Cell Culture

HT22 cells were grown in Dulbeco's Modified Eagle Medium with GlutaMax (Gibco), supplemented with 10% Fetal Bovine Serum (FBS, Gibco) and 0,1% Gentamycin (Gibco). Cells were passaged every 2-3 days at a ratio of 1:20.

3.8.2 Anti-PTEN Nanocage Transfections

Cells were plated in 96-well plates, with a density of 2500 cells/well. The following day, they were transfected with siPTEN, purified and non-purified anti-PTEN nanocages, as well as purified anti-GFP nanocages, with the help of Lipofectamine RNAiMAX reagent (Thermo Fisher Scientific). Transfection was conducted according to supplier's instructions. In brief, nanocages/siRNA-lipid complexes with a ratio of 0,25 µL of RNAiMAX per 10 µL of volume were formed by adding in a 1:1 ratio a solution of nanocages/siRNA in Opti-MEM (Gibco) to a solution of RNAiMAX in Opti-MEM and incubating for 10 minutes at room temperature. After, 10 µL of the complexes were added to each well, for a total volume of 100 µL.

3.8.3 RT-qPCR

After 72 hours medium was discarded, and cells were washed 2 times with PBS 1x. Afterwards, cells were lysed in lysis buffer (PBS 1x + 10 mM Tris-HCl + 0,25% IGEPAL CA-630 (Sigma-Aldrich) + 150 mM NaCl, pH 7,4) for 5-15 minutes at 4°C. The lysates were then transferred to 0,6 mL maximum recovery tubes (Axygen) and centrifuged for 5 minutes at 700xg, 4°C. The supernatant was trasfered to another 0,6 mL tube.

One Step SYBR R PrimeScript RT-PCR Kit II (Perfect Real Time) (Takara) kit was used to perform one-step RT-qPCR. In brief, 384-well plates were prepared in ice and according to the kit's protocol, with primers for the PTEN and Ywhaz genes and a final volume per well of 9 µL + 1 µL lysate. The temperature cycle used was as follows: 42°C, 5 min → 95°C, 10 s, followed by 40 cycles of 95°C, 10 s → 55°C, 30 s → 72°C, 30 s. RT-qPCRs were conducted in a CFX384 Touch™ Real-Time PCR Detection System (Bio-Rad) at the CCGen core facility at i3S, University of Porto, Portugal, with the help of Paula Magalhães, Tânia Meireles and Ana Marafona.

Resulting data was analyzed through the delta-delta Ct method, and relative fold gene expression of PTEN was calculated based on the expression of the Ywhaz housekeeping gene.

3.9 Luciferase Gene Silencing Assays

3.9.1 U2OS-GFPLuc Cell Culture

U2OS-GFPLuc cells were grown in Dulbeco's Modified Eagle Medium (DMEM) with GlutaMax (Gibco), supplemented with 10% Fetal Bovine Serum (FBS, Gibco) and 0,1% Gentamycin (Gibco). Cells were passaged every 3-4 days at a ratio of 1:10/15.

3.9.2 D-R strand Duplexes Transfections

Cells were plated in 96-well plates, with a density of 9000 cells/well. The following day, they were transfected with 4 different D-R strand duplexes, L_RNA and siGFP, with the help of Lipofectamine RNAiMAX reagent (Thermo Fisher Scientific). Transfection was conducted according to supplier's instructions and as explained previously, with a ratio of 0,25 µL of RNAiMAX per 10 µL of volume. Cells were analyzed after 48 hours

3.9.3 H-Nanocage Transfections

Cells were plated in 96-well plates, with a density of 8000 cells/well. The following day, they were transfected with siGFP, purified anti GFP nanocages and H-nanocages, and anti-PTEN nanocages, with the help of Lipofectamine RNAiMAX reagent (Thermo Fisher Scientific). Transfection was conducted according to supplier's instructions and as explained previously, with a ratio of 0,25 µL of RNAiMAX per 10 µL of volume. After 3 days, cells were trypsinized and moved to a 48-well plate and were analyzed the following day.

3.9.4 Luciferase Reporter Gene Assay

Cells were washed two times with PBS 1x. Afterwards, cells were lysed in lysis buffer (PBS 1x + 0,15% Triton X-100) for 30 minutes at 4°C. 10 µL of lysate and 100 µL of Luciferase Assay Reagent (Promega) were added per well to a 96-well white plate, and the luminescence was immediately read in a SynergyMx™ MultiMode Microplate Reader (BioTek).

Luminescence results were normalized with the use of Micro BCA Protein Assay Kit (Thermo Fisher Scientific). In brief, 50 µL of lysate and 100 µL of Micro BCA Working Reagent were added per well to a 96-well plate. The plate was incubated at 37°C and after 2 hours, absorbance was read at 562 nm in a SynergyMx™ MultiMode Microplate Reader (BioTek). A standard curve of Bovine Serum Albumin was used to determine the protein concentration in each sample.

3.10 Cellular Uptake Experiments

3.10.1 Primary Cortical Neurons Cell Culture

Primary cortical neurons of mouse embryos (E16.5) (kindly supplied by Marília Torrado, nBTT group, i3S) were cultured in pre-coated surfaces with 50 µg/mL Poly-D-Lysine (70-150k kDa, Sigma; overnight at 4°C) in Neurobasal Medium (Gibco) supplemented with 2% b27 (Invitrogen), 0,5 mM L-Glutamine (Gibco), 25 µM glutamate and 0,1% Gentamycin (Gibco), for 7 days.

3.10.2 Spectrofluorometer Assay

Primary cortical neurons were plated as described above in a 96-well plate and with a density of 25000 cells/well. 1 hour before treatment, cells were incubated with 50 µg/mL salmon sperm DNA (Thermo Fisher Scientific) to block the Poly-D-Lysine positive-coated surface. After that, cells were incubated for 3 hours with Cy5-labeled siGFP, functionalized and non-functionalized anti-PTEN nanocages. Following this incubation, cells were treated 3 times with 15 U/mL heparin within 1 hour, in order to remove membrane-bound oligonucleotides.

Cells were also transfected with Cy5-labeled siGFP and anti-PTEN nanocages, with the help of Lipofectamine RNAiMAX reagent (Thermo Fisher Scientific). Transfection was conducted according to supplier's instructions and as explained previously, with a ratio of 0,3 µL RNAiMAX per 10 µL of volume, and with the use of Neurobasal Medium (Gibco) instead of Opti-MEM.

Afterwards, cells were lysed in lysis buffer (0,5% SDS + 0,5% Triton-X100 in PBS 1x) for 30 minutes at 4°C, and a Fluoromax-4 Spectrofluorometer (Horiba) was used to read the fluorescence of the lysates (Excitation: 633 nm; Emission: 650-700 nm). Fluorescence intensity was obtained by calculating the numeric integral of the spectrum between 655 and 670 nm. A calibration curve made with Cy5-labeled D-R duplexes to determine the molar quantities of internalized material (Figure S.7).

Fluorescence results were normalized with the use of Micro BCA Protein Assay Kit (Thermo Fisher Scientific). In brief, 50 µL of lysate and 100 µL of Micro BCA Working Reagent were added per well to a 96-well plate. The plate was incubated at 37°C and after 2 hours, absorbance was

read at 562 nm in a SynergyMx™ MultiMode Microplate Reader (BioTek). A standard curve of Bovine Serum Albumin was used to determine the protein concentration in each sample.

3.11 Confocal Microscopy

Primary cortical neurons were plated as described above in a 12-well Ibidi well chamber, with a density of 5000 cells/well. 1 hour before treatment, cells were incubated with 50 µg/mL salmon sperm DNA (Thermo Fisher Scientific) to block the Poly-D-Lysine positive-coated surface. After that, cells were gradually cooled to 4ºC (30 minutes) and were incubated for 1 hour with Cy5-labeled functionalized and non-functionalized anti-PTEN nanocages. Following this incubation, medium was gradually changed and cells were incubated for 2 hours at 37°C.

Afterward, cells were washed 3 times with warm HBSS (without completely removing the medium) and were fixed at room temperature with Pierce 4% Formaldehyde (Thermo Fisher Scientific), firstly by adding half the well volume in formaldehyde, and by removing all the medium after 10 minutes and adding formaldehyde again, for 10 more minutes. After washing with PBS 1x, cells were permeabilized and blocked by incubating with PBS + Triton-X100 0.2% + 1% BSA (1 g/100 mL) for 30 minutes. They were then incubated with anti-βIII antibodies (BioLegend) diluted in PBS+1% BSA overnight at 4°C, and after with anti-mouse A488 (Invitrogen) for 1 hour at room temperature. Nucleus staining was done using Hoechst (Thermo Fisher Scientific) diluted in PBS for 10 minutes at room temperature. After several washes with PBS, cells were mounted in Fluoromount (SIGMA).

Images were acquired in a Spectral Confocal Laser Scanning Microscope Leica TCS-SP5 AOBS at the Bioimaging core facility at i3S, University of Porto, Portugal.

3.12 Statistical Analysis

A normal Gaussian distribution was assumed for all results. Statistical analysis are detailed in each figure.

Chapter 4: **Results and Discussions**

4.1 siRNA Nanocages Assembly

In order to develop siRNA nanocages to successfully mediate RNAi, the structure design was based on two fundamental building blocks: a trebler-phosphoramidite branching unit (Figure S.1) [103], with four short DNA linker sequences attached (one through the 5' end and the remaining three through the 3' end); and single-stranded DNA-RNA hybrid sequences (denominated D-R strands) where the DNA region is complementary to the linker sequences from the trebler. Therefore, any oligonucleotide can theoretically be incorporated into this structure by complementary base pairing with the DNA linker sequences.

The assembly of the siRNA nanocages is a two-step process. Firstly, through the annealing of three single-stranded DNA/RNA molecules to the complementary linker sequences in the trebler, an intermediary structure is formed, denominated as a branch (Figure 16).

Fig.16 – Branch annealing: intermediary step in the assembly of an siRNA nanocage by hybridization of the DNA sequence of 3 D-R strands with the 3 DNA linkers of the trebler.

By performing this reaction with two different treblers, as well as two partially complementary single stranded DNA/RNA hybrid oligonucleotides (D-R strands), the "sense" and "antisense" branches are obtained. These two structures are then assembled into a nanocage through the hybridization of the respective complementary single-stranded RNA region. The RNA duplex formed can be designed *in silico* to correspond to an active DsiRNA sequence, thus forming a gene specific siRNA nanocage (Figure. 17). Furthermore, two DNA

overhangs remain, allowing for the functionalization with oligonucleotide-biomolecule conjugates through site-specific base-pairing.

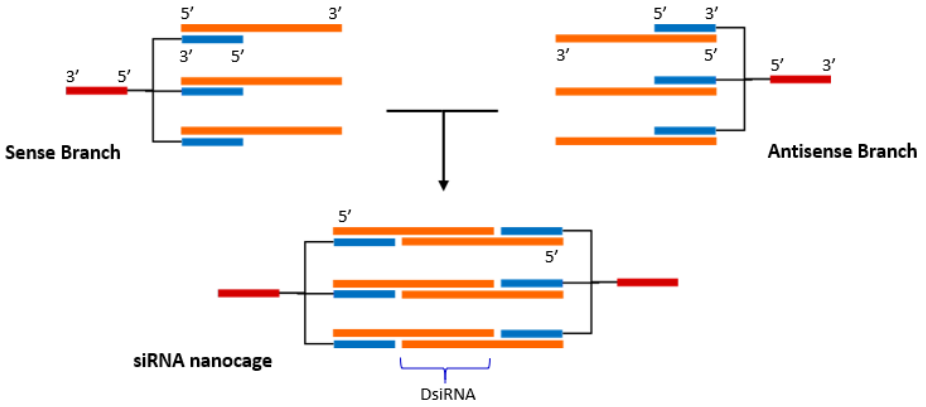

Fig.17 – siRNA nanocage self-assembly. The RNA sense and antisense strands in both branches (orange) hybridize, forming a 27 bp DsiRNA that will be recognized and cleaved into biological active siRNA. Small ligands can be conjugated with the DNA overhang sequence (red).

4.1.1 Branch Annealing

Initially, a stepwise study of the self-assembly of siRNA nanocages was performed. Firstly, branch annealing was made by mixing the treblers with several molar ratios of anti-GFP D-R strands, in an assembly buffer. A temperature cycle encompassing an initial denaturing phase (94°C, 3 min) followed by a fast (30 sec) cooling to 4°C was applied, and the resulting samples were analyzed by PAGE (Figure 18).

The presence of 3 distinct bands in the lanes corresponding to the mixture can be observed, indicating the formation of three homogeneous types of structures. As the migration of a structure in PAGE is directly influenced by its molecular weight, according to our model this data suggests that these 3 bands correspond to branches with either one, two or three single-stranded sequences. In fact, with an increasing molar excess of D-R strands, a shift from lower to higher molecular-weight bands can be observed, indicating that the three trebler linkers start to become fully hybridized as expected.

At a trebler:D-R strand molar ratio of 1:3, the band corresponding to branches with only one arm hybridized almost fully disappears, with the majority of structures corresponding to branches with two or three D-R strands hybridized. Theoretically, at this ratio only one band should be observed, corresponding to the fully hybridized branch; however, a considerable proportion of branches only has two arms annealed. This secondary band can be explained possibly due to steric hindrance caused by the flexible single-stranded D-R strands already annealed, mistakes in concentration measurement or impurities in the oligonucleotides.

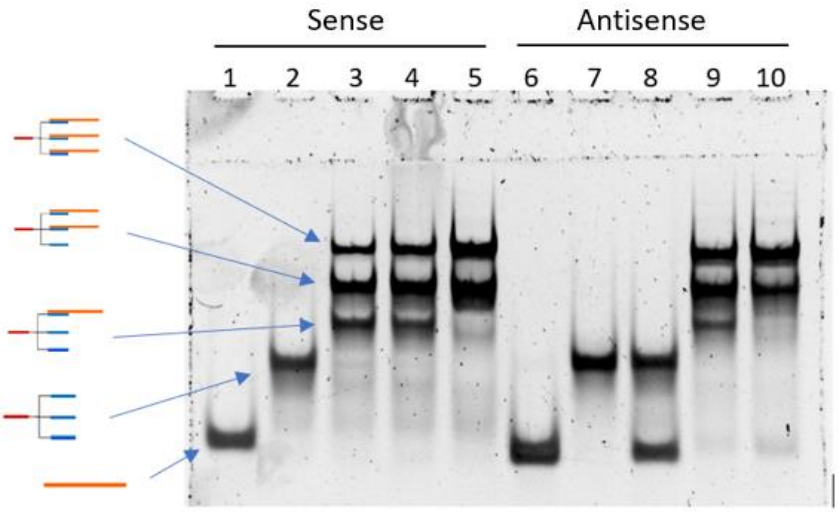

Fig.18 – PAGE analysis of branch annealing. Lanes 1 and 6 correspond to anti-GFP D-R strands; lanes 2 and 6 correspond to the treblers; lanes 3-5 and 8-10 correspond to the mixture of the two components with increasing molar ratios of trebler:D-R strand (1:1,5; 1:2,25; 1:3). An error occurred at lane 8, with the wrong trebler being used, and consequently no annealing was observed.

One further explanation for the extra band in the 1:3 ratio is the formation of secondary structures due to internal folding of the unpaired RNA sequences in annealed arms. In order to optimize the process of branch assembly and minimize the formation of these structures, several temperature cycles with increased annealing temperatures were tested. The resulting samples were analyzed by PAGE (Figure 19).

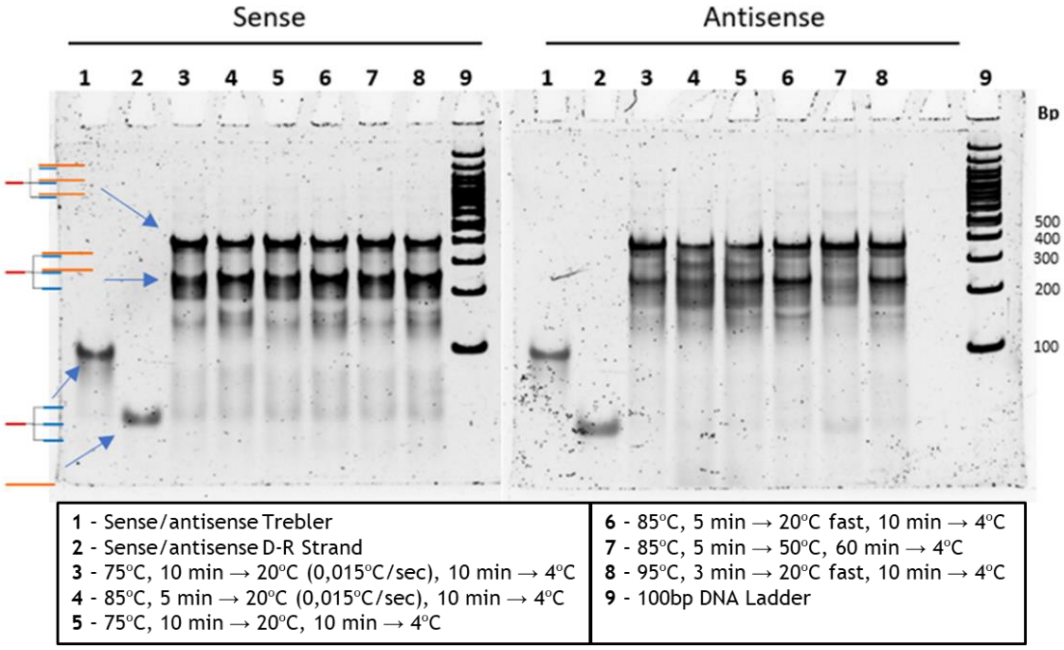

Fig.19 - PAGE analysis of several branch annealing reactions with different temperature cycles, shown inside the box. Lanes 3-8 of both gels correspond to a molar ratio of 1:3 of trebler to D-R strands. DNA ladder is presented in lane 9 with the corresponding base-pairs of each band.

When analysing the assembly of the sense branch, there are no noticeable differences between the several cycles, except for fainter bands corresponding to the trebler hybridized with only one D-R strand in lanes 3, 5 and 7. On the other side, in the PAGE of the antisense branch we can clearly see a single well-defined band in lane 7, probably corresponding to the fully hybridized branch, along with an overall fainter smear, when compared to the other lanes. Thus, this cycle (85°C, 5min → 50 °C, 60min → 4°C) was the one that showed to be more favorable to the annealing of the branch with the antisense RNA, and that showed a more efficient assembly. Following the initial heating at 85°C for the separation of all the hybridized nucleic acids, the 50°C at which the annealing reaction occurs seems to allow the hybridization between the extended D-R strands and the DNA linkers in the trebler while preventing the formation of unwanted structures with lower melting temperature. As such, the annealing of both branches started to be made with this temperature cycle, although the time of incubation at 50°C was reduced to 30 min in order to avoid RNA degradation by long exposure to high temperatures.

4.1.2 Nanocage Assembly

After optimizing the first step of branch annealing, the assembly of the nanocages was made by mixing anti-GFP sense and antisense branches in an equimolar ratio in assembly buffer. The solutions were then subjected to several heat cycles in order to assess what was the optimal temperature of assembly. The resulting solutions were analyzed by PAGE (Figure 20).

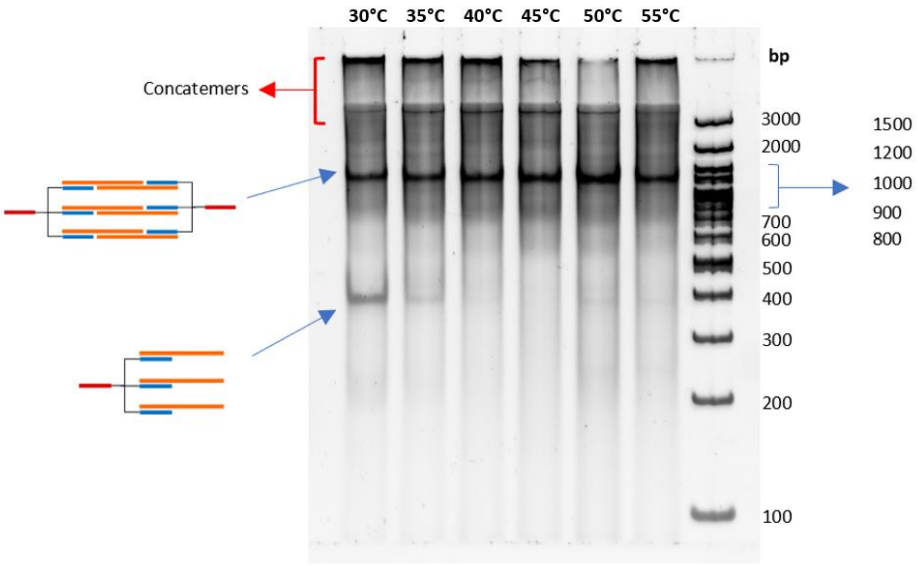

Fig.20 – PAGE analysis of siRNA nanocage self-assembly. Equimolar ratios of anti-GFP sense and antisense branches were mixed in a solution of assembly buffer with different heating cycles. The corresponding initial heating temperature is displayed above each lane; after 45 min of incubation at the corresponding temperature, samples were cooled to 20°C for 5 min, and then cooled to 4°C. DNA ladder is presented in the rightmost band, with the corresponding base-pairs of each band.

It is possible to observe a clear band with equivalent molecular weight of around 1200 base-pairs, which is believed to correspond to siRNA nanocages, according to the theoretical assembly model. A smear is also observable in all lanes. This could possibly be explained by several reasons: i) complex nucleic acids structures migrating in gels can present slightly different migration patterns due to their flexibility and possibility to assume different conformations, during the gel run; ii) structures with assembly errors will also present different migration patterns and present also the abovementioned issues which will add up to the overall smear pattern of a gel. One or two high (>3000 bp) molecular-weight bands can also be observed in each lane, indicating the presence of larger structures. These probably correspond to concatemers, misassembled structures resulting of the hybridization of many siRNA branches in succession (possibly due to the presence of incompletely assembled two-armed branches observed previously).

When comparing all the lanes, the most successful assembly seems to have occurred at 50°C, as the corresponding nanocage band seems to be most pronounced. In addition, there were clearly less concatemers formed with this temperature cycle. In fact, 50°C is closest to the theoretical melting temperature of the two DNA linker duplexes (Figure S.2). This allows for the denaturation of secondary structures formed between the single-stranded RNA of individual branches while maintaining the DNA linker duplex hybridized, leading to a more efficient hybridization between the branches.

In fact, when the assembly was performed at 30°C, an extra band can be observed with lower molecular weight. By comparing the position relative to the DNA ladder (~400bp), the band presumably corresponds to three-armed branches that did not undergo hybridization with another branch. This is possibly due to 30°C not being sufficient to undo the secondary interactions between the single stranded RNA of each branch, thus preventing them from forming an siRNA nanocage with another branch. As such, the temperature cycle considered optimal to the siRNA nanocage assembly and used from now on was 50°C, 45 min → 20°C, 5 min → 4°C.

The objective of this work is to develop siRNA nanocages that can effectively induce RNAi-mediated gene silencing of therapeutic targets. Based on that, we also produced siRNA nanocages with DsiRNA duplexes targeting the phosphatase and tensin homolog (PTEN) gene. The modulation of PTEN activity was reported to enhance the regenerative capacity of corticospinal neurons in mice, thus proving to be a potential therapeutic strategy for the treatment of neurological disorders such as spinal cord injury [184].

The assembly of anti-PTEN siRNA nanocages was also studied through PAGE after the two-step assembly in the conditions reported previously (Figure 21).

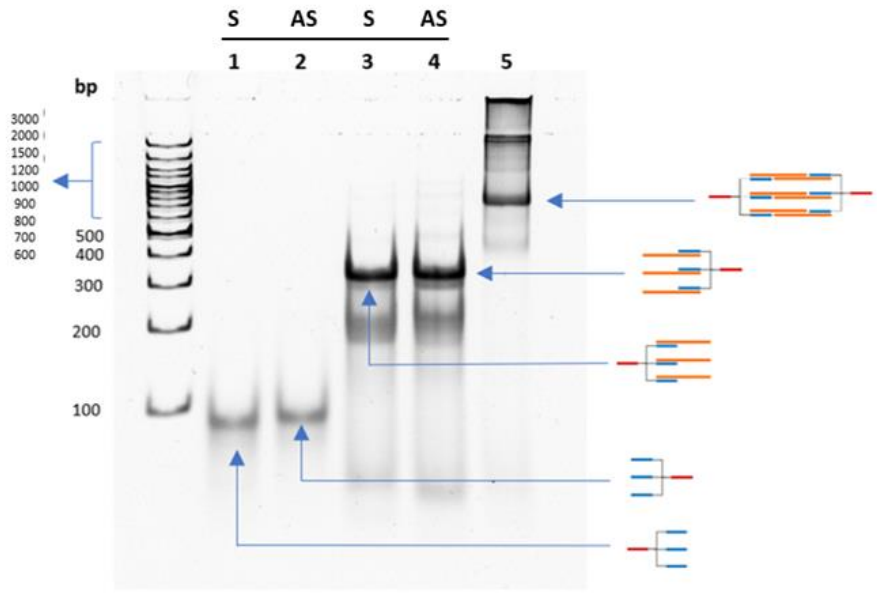

Fig.21 – PAGE analysis of the assembly process of anti-PTEN nanocages. Both reactions were performed by mixing the components in assembly buffer, with temperature cycles previously reported. Lanes 1 and 2 correspond to sense and antisense trebler; lanes 3 and 4 to the sense and antisense branch; and lane 5 to the mixture of the two branches. DNA ladder is presented in the leftmost lane, with the corresponding base-pairs of each band.

Anti-PTEN nanocages components display a similar profile to anti-GFP nanocages produced previously, with the bands corresponding to the two branches displaying an apparent molecular weight of around 400 bps when compared to the ladder. Once again, a clearly defined band of higher molecular weight can be seen in the lane corresponding to the mixture of the two branches, indicating that the desired structure, the nanocage, was homogeneously formed. Furthermore, the presence of the previously observed higher molecular weight bands, corresponding to concatemers, are also present.

Taken together, these studies of siRNA nanocage self-assembly through PAGE may suggest that a well-defined structure is formed after the two-step reaction, assumed to be the nanocages predicted by our theoretical model. However, in order to prove this hypothesis, additional characterization studies need to be performed. Ongoing work is aimed at characterizing the 3D structure formed by nanocages through TEM; furthermore, techniques like dynamic light scattering and atomic force microscopy could also help in this characterization.

In addition, the assembly of anti-GFP and anti-PTEN nanocages showed similar profiles when analysed through PAGE, indicating that the sequence of the RNA duplexes does not affect the assembly process significantly. This may indicate that, according to what was expected, siRNA nanocages targeting different genes can be produced, requiring only that the RNA arms in both sense and antisense branches are complementary to one another.

4.1.3 Nanocage Purification

An issue regarding the assembly process is the formation of concatemers. The presence of bands of higher molecular weight (<3000 bp) suggest that unwanted structures are being formed. Indeed, when looking at the model of the siRNA nanocages assembly it is plausible that, when in solution, the three RNA strands in one branch might not all hybridize with the three RNA strands of a single complementary branch. The intramolecular process of producing a closed structure is promoted, in highly diluted solutions, normally through a cooperative effect imparted by high local concentrations (due to proximity) of the complementary strands [103]. However, due to their flexible nature and rapid hybridization kinetics of nucleic acids, some of them could hybridize with a second or even a third different branch, subsequently forming an increasingly ramified structure. In addition, the presence of residual branches with only 2 RNA strands (as seen in figures 19 or 20) might also contribute to the formation of concatemers, because if they hybridize with a full complementary branch, a single RNA strand would still remain unpaired.

In order to obtain only clearly defined siRNA nanocages, a purification protocol through PAGE was tested. In short, after performing the assembly reaction for anti-GFP nanocages, the resulting samples were run through a preparative polyacrylamide gel, and the band expected to correspond to the nanocages was cut; the resulting gel fragment was then left eluting in buffer for approximately 1,5 days. The resulting solution was then concentrated and analysed through an analytical PAGE (Figure 22).

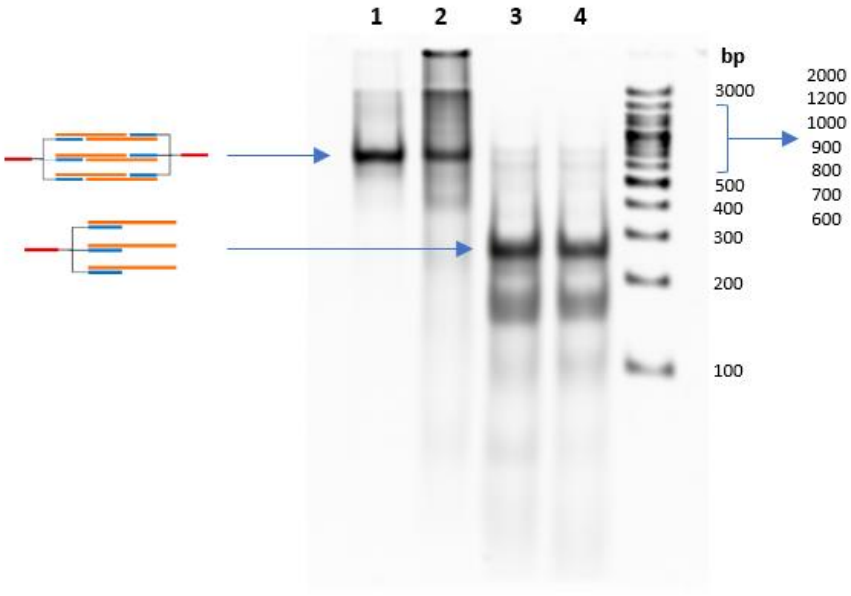

Fig.22 – PAGE analysis of the purification procedure of anti-GFP nanocages. Lane 1 corresponds to nanocages after purification; lane 2 to nanocages before purification; lanes 3 and 4 to the sense and antisense branches. DNA ladder is presented at the rightmost lane, with the corresponding base-pairs of each band.

It is clearly visible that the purified sample presents a much cleaner nanocage band in a much higher percentage in relation to other forms. A simple volume analysis of the nanocage band in the Image Lab software reveals that this band accounts for approximately 50% of lane intensity, as opposed to the unpurified sample, that yielded around 18%. When compared to the unpurified sample, there is also considerably less smearing, and the previously observed concatemer bands do not appear. This indicates that the purification was successful, as a high-purity product was obtained. Although purification by PAGE allowed to obtain a seemingly homogenous sample of correctly assembled siRNA nanocages, the molar yield of pure nanocages corresponds to only around 20% of the initial loaded product in the preparative gel.

In fact, while this method grants high purity products, the yields are reportedly low (<50%) due to the inefficiency of the elution step, and can be even lower due to the presence of modified oligonucleotides [185]. Alternatively, electroelution could be performed in a dialysis bag [186], where the application of an electric current causes the nucleic acids to migrate out of the gel, possibly increasing the yield. On the other hand, purification methods based on gel electrophoresis are time-consuming and hard to scale up. High performance liquid chromatography could be another technique to employ in the future, as it has already been used for similar branched siRNA structures with higher yields [105,187].

4.1.4 Nanocage Functionalization

The designed nanocage structure includes two single-stranded DNA overhang sequences, intended to serve as linkers, allowing for the functionalization with active moieties such as targeting ligands. Biomolecules conjugated with a single-stranded DNA (ssDNA) sequence can hybridize with the overhang, thus easily functionalizing the structure in a non-covalent way, and potentially allowing the rapid screening of different biologically active moieties as long as these can be obtained as molecule-ssDNA conjugates. In order to test this model, siRNA nanocages were incubated with two different biotin-ssDNA conjugates containing complementary sequences to the overhangs. The resulting samples were analyzed through PAGE (Figure 23).

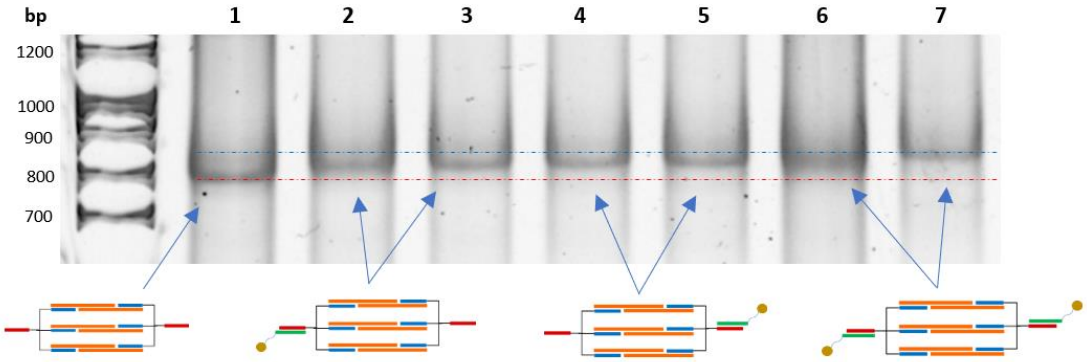

Fig.23 – PAGE analysis of the functionalization of siRNA nanocages with biotin-DNA conjugates complementary to the sense and antisense overhang. Biotin conjugates were mixed (30 min, RT) with nanocages at different molar ratios. Lane correspondence: **1)** siRNA nanocages; **2)** nanocage + sense biotin conjugate (1:1,1); **3)** nanocage + sense biotin conjugate (1:1,5); **4)** nanocage + antisense biotin conjugate (1:1,1); **5)** nanocage + antisense biotin conjugate (1:1,5); **6)** nanocage + sense and antisense biotin conjugates (1:1,1:1,1); **7)** nanocage + sense and antisense biotin conjugates (1:1,5:1,5). DNA ladder is presented in the leftmost lane, with the corresponding base pairs of each band.

In the samples where biotin conjugate was added, a small shift can be observed in relation to the nanocage band (red dotted line). The shift is more pronounced in the lanes were both sense and antisense biotin conjugates were added (blue dotted line), indicating that a structure with slightly higher molecular weight is being formed. These observations suggest that the functionalization with the biotin conjugates is occurring as expected, with both overhangs pairing with the DNA sequence from the conjugate. In fact, a small shift was expected due to the reduced size of the conjugate sequence (18 nucleotides).

As such, these results correlate with the expected observations, implying that this system is effective for the functionalization of these structures. Nevertheless, more tests need to be performed if different biomolecules are to be employed. Furthermore, these results also serve as evidence for the assembly of siRNA nanocages as predicted theoretically.

4.2 TEM Structural Characterization

PAGE analysis can yield some information about the molecular processes that are occurring by allowing to infer on structural properties of nucleic acids through the observation of specific shifts in molecular weight. However, by itself, this technique does not allow to observe the precise structural features of nucleic-acid nanostructures.

Thus, in order to further assess if the proposed model for nanocage self-assembly is working, characterization through TEM observations was attempted. Theoretical calculations for the expected size of nanocages and its components were made, based on approximate structural parameters of A and B double-helix forms [188] (Figure S.3), and the resulting estimates are depicted in Figure 24.

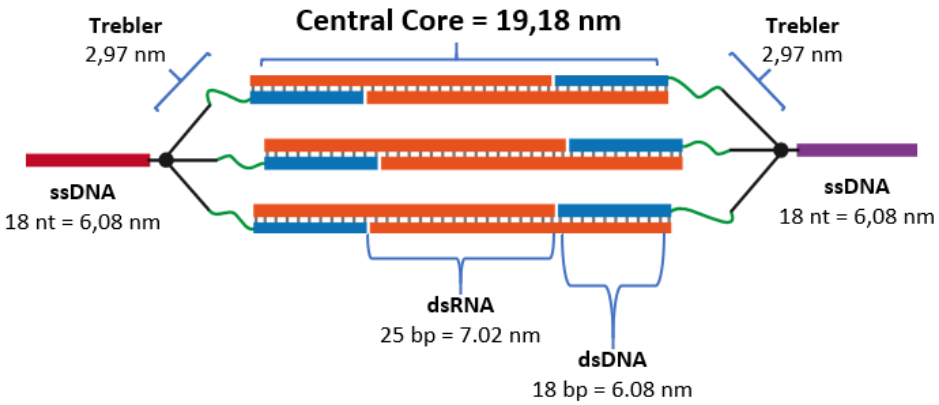

Fig.24 – Expected maximum dimensions for the different segments of nanocages assuming a fully extended conformation

These estimates were used as basis for analyzing and identifying the structures by TEM. Nevertheless, the calculations should be taken as rough approximations, as different factors can affect the apparent dimensions during TEM analysis, as will be discussed below.

Purified nanocages were adhered on grids treated by glow-discharge (to promote nucleic acid adhesion through charge interactions) and uranyl acetate was used for negative staining. After, they were observed through TEM microscopy, and several images were acquired, as exemplified in Figure 25:

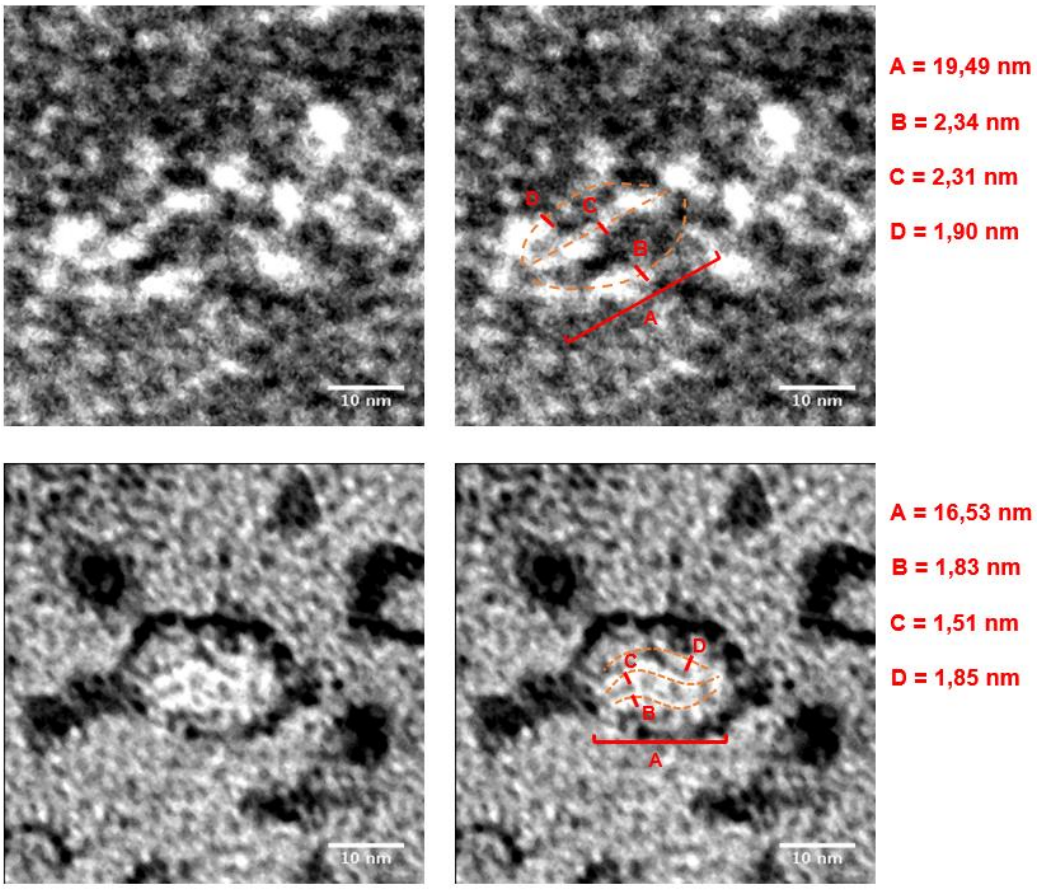

Fig.25 – Examples of images acquired through negative-stain TEM. Background shows darker staining, and biological samples show brighter staining. Specific areas were selected (left), and their sizes were analyzed to find correspondence to expected nanocage dimensions (right). Scale bar: 10 nm.

As the dimensions of the structures were very close to the resolution limit of the microscope used, fine structural data could not be obtained. It should also be stated that the deposition process of the structures onto the grids, involving drying and staining can alter the structure itself, as seen and stated by others [189]. Additionally, the nanocages present several points with increased flexibility such as the ones corresponding to the trebler molecule and hexaethylene glycol linkers used, as well as the nicks present in the central core of the structure (discontinuities of the double strand due to the inherent design of the structure, as seen in Figure 24). This flexibility makes the conformation of the structure after deposition somewhat unpredictable.

The most stable region of the nanocages deemed possible to observe was the central core region (of around 19 nm), as it involves the presence of 3 double helixes in close proximity and the possibility to exist in a close to parallel conformation when deposited in TEM grids. In fact, when the images were analyzed, some areas exhibited positive-stained patterns suggesting the presence of the structures (especially the parallel configuration of strands) with size ranges close to theoretical calculations.

It is worth noting that these were preliminary tests, and as such, the protocol has not been thoroughly optimized. Extensive aggregates were found in many samples, many times leading to analysis being impracticable, and it was found that the type of staining might have been promoting this. In fact, positive uranyl ions might interact with the negative-charged phosphate backbone of DNA and induce some degree of aggregation. The glow discharge procedure to promote nucleic acid adhesion might not be fully functional either, and as such, ongoing work is being done with poly-lysine-coated grids. Other approach could be to take advantage of nanocages inherent ability to be functionalized with oligonucleotide-conjugates through base-pairing in the overhang sequence. Electron-opaque materials like gold could be functionalized and used to promote siRNA nanocage recognition in TEM.

The reduced nanocage dimensions difficult detailed observations through TEM, thus higher resolution techniques are necessary to better characterize them. At the moment, several tests are also being conducted by AFM. In alternative, high resolution techniques like cryogenic TEM could also be employed.

Nonetheless, although TEM results are at the moment only indicative, they do go in favor of the interpretations after gel electrophoresis analysis.

4.3 Enzymatic Recognition and Cleavage

The Dicer endoribonuclease plays a key role in the RNAi mechanism, being responsible for the cleavage of longer dsRNAs into 21-mer siRNAs and aiding in their integration in the RISC complex. If siRNA nanocages are intended to be biologically active, it is important to assess if the RNA duplexes in its structure can act as Dicer substrates. As DsiRNAs are contained in the nanocage branches, there is the need for Dicer to recognize and excise them, releasing the intrinsic active siRNAs in order to induce RNAi activation.

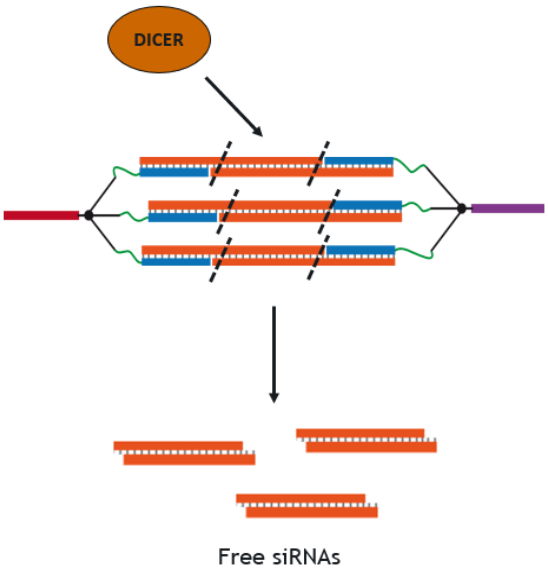

Fig.26 – Proposed mechanism for the activation of RNAi mediated by siRNA nanocages

In order to test if siRNA nanocages can be recognized and cleaved by Dicer to form active siRNAs, anti-PTEN nanocages were incubated with human recombinant Dicer for 12 and 24 hours, and then analyzed by PAGE (Figure 27).

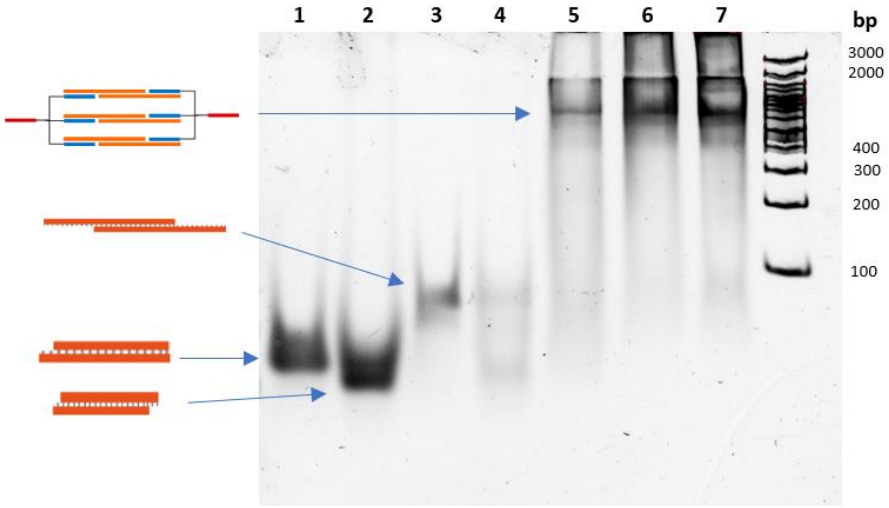

Fig.27 – PAGE analysis of the digestion of nanocages with Dicer. D-R strand duplexes, DsiPTEN and anti-PTEN nanocages were incubated with recombinant human Dicer at 37°C for 12 and 24 hours. Lane correspondence: **1)** DsiPTEN; **2)** DsiPTEN + Dicer, 12h; **3)** D-R duplex; **4)** D-R duplex + Dicer, 12h; **5)** nanocage + Dicer, 12h; **6)** nanocage + Dicer, 24h; **7)** nanocage. DNA ladder is presented at the rightmost lane, with the corresponding base pairs of some bands.

As expected, the recombinant enzyme successfully cleaved the DsiPTEN into presumably the smaller and active 21-mer siPTEN, judging by the lower band in lane 2. Additionally, it also appears to have recognized the extended DsiPTEN duplex that mimics the hybridized arms of the nanocage, although the intensity of the bands in lane 4 was very low. Nonetheless, no signs of cleavage were observed when nanocages were incubated with Dicer for 12 and 24 hours, indicating that the enzyme was unable to recognize the DsiPTEN arms when incorporated in the nanocages, or the amounts released were not detectable by the employed method. Additional experiments with different timepoints, enzyme quantity and with anti-GFP nanocages similarly did not result in a detectable amount of released active siRNA sequences.

In fact, it has been reported that Dicer shows preference for linear dsRNA, exhibiting reduced activity when processing branched RNA structures due to the sterically crowded environment [100]. Furthermore, presence of 3' overhangs of 2 nucleotides can also be a determining factor for the activity of this enzyme, as they facilitate Dicer attachment through its PAZ domain to excise the siRNA [190]. The introduction of theses overhangs in a branched octahedron structure for RNAi led to significant increases in Dicer recognition and cleavage, emphasizing their importance regarding the enzyme activity [187]. On the other hand, the presence of the overhangs might not be a crucial requirement, as Dicer has even demonstrated the capacity to recognize and cleave closed RNA duplexes such as dumbbell siRNA *in vitro*, albeit with low efficiency [96]. Overall, the fact that siRNA nanocages do not possess overhangs

in their RNA arms and the fact that their branched structure might hamper Dicer cleavage could possibly justify these results.

4.4 Biological Activity Evaluation

4.4.1 Gene Silencing Properties of Anti-PTEN Nanocages

The main goal of this work was ultimately to produce a novel structure that could induce specific gene silencing in therapeutic targets. Hence, the biological activity of siRNA nanocages as RNAi mediators was assessed by transfecting anti-PTEN nanocages into HT22 cells, a mouse hippocampal neuronal cell line. Subsequently, the PTEN expression was analyzed through RT-qPCR (Figure 28).

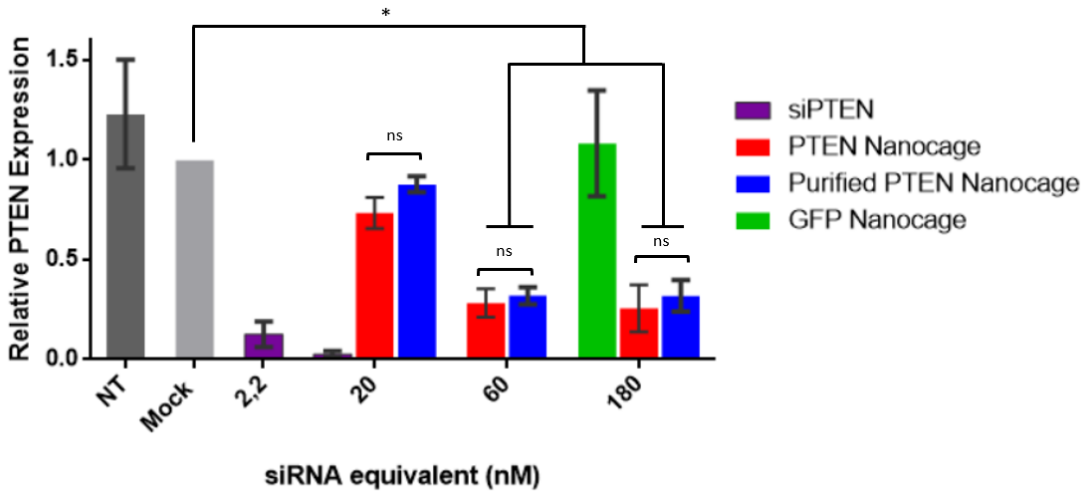

Fig.28 – Analysis of the gene silencing properties of anti-PTEN nanocages. HT22 cells were transfected with siPTEN, non-purified anti-PTEN and anti-GFP nanocages, as well as purified anti-PTEN nanocages. RNAiMAX was used as a transfection agent. After 72 hours, mRNA levels were analyzed by RT-qPCR. Concentration is expressed as siRNA equivalent (1 nanocage=3 siRNAs). Purified and non-purified nanocages were compared through a two-way Anova, with Sidak's multiple comparison tests, and were both compared to Mock through t-test. Results are expressed as mean ± standard deviation of relative PTEN expression normalized to the mock control. N=3 independent experiments. *ns=non-significant*; **p<0,0001*.

As nanocages are trivalent structures encompassing 3 siRNA duplexes, the following concentrations are expressed as siRNA concentrations, where the siRNA equivalent concentration of nanocages is 3 times their original concentration.

Significant mRNA silencing was observed for both purified and non-purified nanocages targeting the PTEN gene, with both achieving around 70% efficiency at 60 nM and 180 nM. Apparently, the use of purified nanocages did not elicit any significant difference in the biologic activity when compared to the unpurified ones. Canonical siPTEN was used as a positive control

of the transfection and, as anticipated, exhibited remarkably high RNAi activity, with a silencing efficiency of about 90% already at the lowest concentrations of 2,2 nM. In addition, anti-GFP nanocages did not display any RNAi activity against PTEN, as expected. This may suggest that the nanocages do not possess intrinsic silencing properties, and that the activity observed by anti-PTEN nanocages was due to their functional DsiRNA arms.

The similar silencing efficiency between the purified and non-purified nanocages was not expected. According to the predicted model of nanocage assembly, as well as previous characterization experiments, non-purified nanocage samples also include in its composition concatemers, misassembled structures of high molecular weight. The functional DsiRNA duplexes "trapped" in these highly branched structures would presumably be less accessible to the Dicer processing. As such, the activity of non-purified nanocages was predicted to be lower than the purified ones.

One possible explanation for this is that both nanocages and concatemers alike are subjected to non-specific degradation before or after transfection. This non-specific degradation would promote the release of a highly heterogeneous mix of RNA duplexes with widely diverse RNAi activities. Thus, this mixture could conceal the inherent silencing properties of purified and non-purified nanocages. Alternatively, the concatemers could still leave the active siRNA regions sufficiently exposed to be processed intracellularly by Dicer.

It is also worth noting that, despite Dicer not recognizing and cleaving nanocages *in vitro*, a noticeable RNAi effect was still observed. This may suggest that, in an intracellular environment, Dicer does in fact cleave the RNA arms of nanocages; or support the theory that non-specific degradation is responsible for the release of several types of active siRNA. Alternatively, nanocages could also be triggering an RNAi response through a Dicer-independent mechanism. In fact, branched siRNA structures have been reported to induce the RNAi mechanism without requiring Dicer processing [106,191].

Before drawing more precise conclusions on this matter, further concentrations between 20 and 60 nM should be tested. It seems that silencing potency reaches a threshold at 60 nM, as a 3-fold increase in nanocage concentration does not significantly alter mRNA expression. Therefore, there is the need to further study the correlation between concentration and silencing activity.

4.4.2 Optimization of siRNA Release: RNAse H Nanocages

Since it was observed that Dicer cannot recognize and cleave siRNA nanocages, a different nanocage design was proposed in order to improve their biological activity. This design intended to take advantage of RNAse H properties to facilitate the release of active siRNA from the nanocages.

RNAse H is an intracellular enzyme that has the ability to cleave and degrade the RNA of a RNA-DNA hetero-duplex [192]. Its mechanism of action is well studied, as this enzyme plays a key role in the mechanism of action of gapmers, a class of ASOs. Usually, site-specific cleavage mediated by RNAse H can be induced in gapmers by inserting a "gap" - 6 or more base-pairs of an RNA-DNA hetero-dimer – in their design [193].

Thus, by slightly modifying the 5' end of the D-R strands, a similar hetero-dimer could be inserted in the linker region. The presence of a DNA-RNA hybrid in the linking region should lead to the cleavage of the RNA sequence by RNAse H, liberating the biologically active siRNA branch from the nanocage (Figure 29).

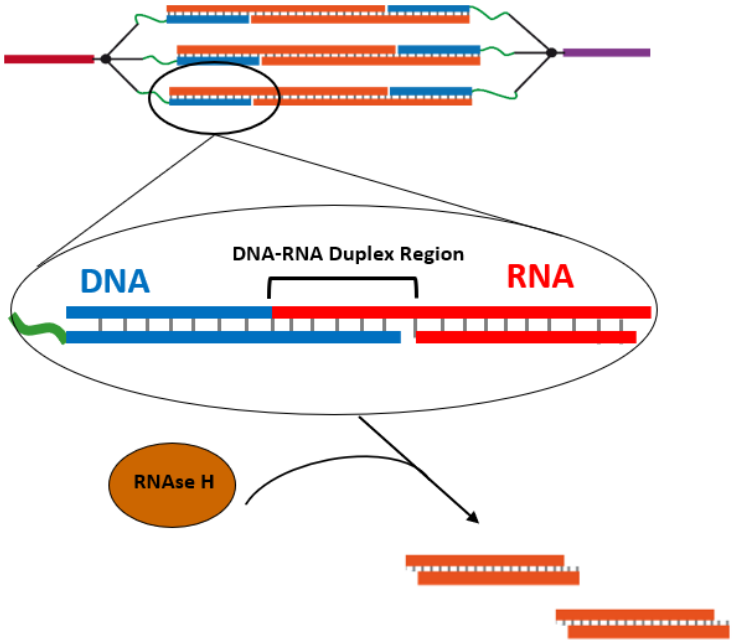

Fig. 29 – Model predicting the RNAse H-mediated release of active RNA duplexes from the nanocages. By introducing several RNA nucleotides (red) in the D-R strand sequence that hybridizes with the DNA linker section (blue), a DNA-RNA duplex is formed. This way, RNAse H will cleave the RNA sequence from the duplex, causing the separation of the siRNA arm from the trebler and thus releasing it from the nanocage.

This idea was tested for the assembly of nanocages. Firstly, two different versions of RNA/DNA patterns were designed (Figure 30) and subsequently studied to determine which one would induce the most favorable cleavage profile for the release of active siRNA.

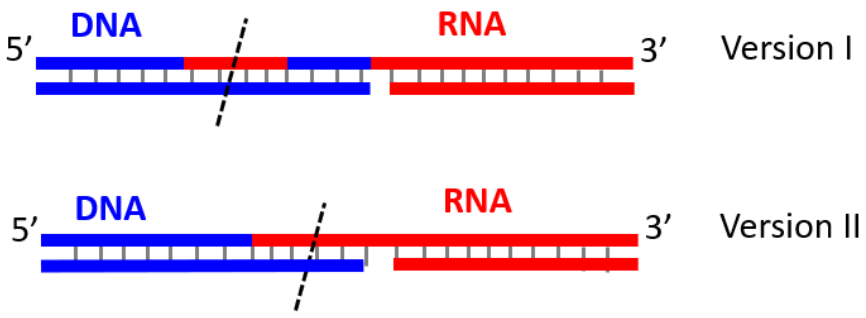

Fig.30 – Different versions of a DNA-RNA pattern that could be applied to the 5' end of sense and antisense D-R strands, thus inducing site-specific RNAse H cleavage (dotted line).

The first version is based on the pattern usually employed in gapmers, where an active "gap" sequence (DNA only sequence) is present in-between flanking sequences that promote increased binding affinity. Specifically, in our design we have introduced short 10 nucleotide RNA regions in between two DNA regions of the D-R strands to form accessible DNA-RNA heteroduplex sites for RNAse H recognition and cleavage. However, according to this model, the resulting RNA strand would possess a small DNA block on the 5' end. The presence of this DNA block could influence the recognition and loading of the resulting modified siRNA duplex by the RISC machinery. Thus, a second version was designed, without a DNA block separating the heteroduplex region from the RNA. Through PAGE analysis, both these versions displayed the ability to induce cleavage when digested with RNAse H *in* vitro (Figure S.4).

To select the optimal pattern to include in the nanocage design, the silencing potency of the different combinations of the siRNA duplex was studied. Sense and antisense D-R strands of either version I or II were annealed into a duplex. Additionally, the 5' overhangs of all duplexes were hybridized to small DNA arms to induce the formation of the DNA-RNA heteroduplex (represented in Table 4).

Table 4 – Different duplex designs for RNAse H-mediated cleavage. DNA in blue, RNA in red. Sense strands are always represented as the top strands and antisense strands are represented as the lower strands. Approximate cleavage sites indicated by dotted lines.

Name	Strands	Design
Oligo A	Sense I + Antisense I	
Oligo B	Sense II + Antisense II	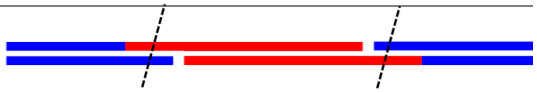
Oligo C	Sense I + Antisense II	
Oligo D	Sense II + Antisense I	

U2OS-GFPLuc, an osteosarcoma cell line overexpressing a GFP-Luciferase fusion protein, was used for transfections with these oligonucleotides. 48 hours after transfection, the luciferase expression was analyzed through a luciferase reporter gene assay (Figure 31).

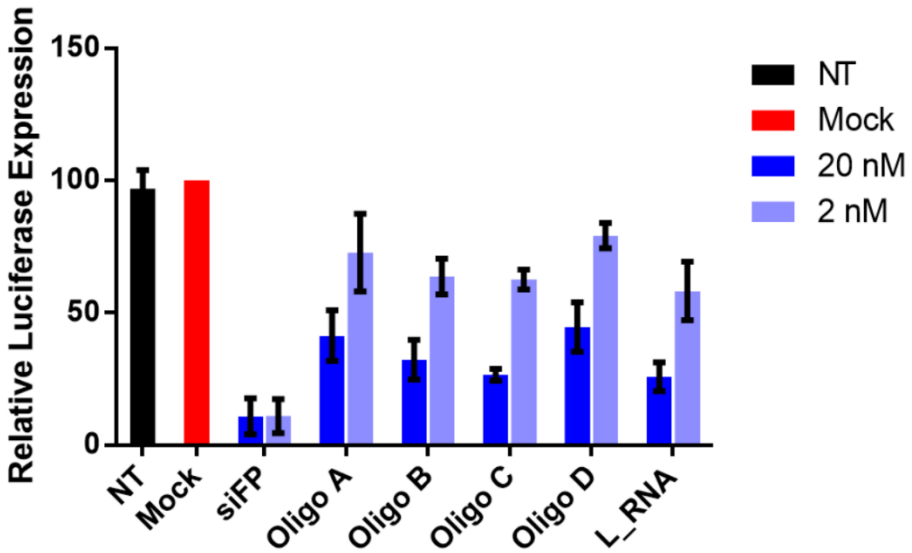

Fig.31 – Relative expression of luciferase 48 hours after transfection with multiple D-R strand duplexes. Cells were transfected with 4 different anti-GFP D-R duplexes, as well as with the original Dicer substrate design duplex (L_RNA) and canonical siGFP. 48 hours after transfection, luciferase expression was evaluated by a luciferase reporter gene assay and normalized by microBCA protein assay. Two-way Anova, with Sidak's multiple comparison tests, was used to compare all Oligos and L_RNA, and no significant differences were found. All Results are expressed as mean ± standard deviation of relative luciferase expression normalized to the mock control. N=3 independent experiments.

As anticipated, the RNAi activity was more pronounced with siGFP (≈ 90%), as they are the canonical mediators of RNAi. No significant differences were observed between the 4 oligos, although the C duplex appeared to display a tendency to elicit slightly stronger RNAi activity at both concentrations, when compared to the other 3 oligonucleotides. In fact, the C duplex includes a version II antisense strand, which means that, according to the predicted model of RNAse cleavage, it does not contain a DNA block on its 5' end following cleavage. This might facilitate the antisense strand integration into RISC, inducing a more potent RNAi response. Indeed, duplexes A and D, that included a version I antisense strand, appeared to be the two least efficient at both concentrations. However, no significant differences were observed, and thus more experiments are needed to corroborate this theory. It is also worth noting that the control Dicer sensitive duplex (L_RNA) exhibited similar silencing potency while having its 5' overhangs blocked. This can suggest that, for these simple duplexes, the RNAse H and Dicer-mediated cleavages have a similar low intracellular activity or the resulting cleavage product (an RNA duplex) has a format and sequence that, differently from the canonical siRNA sequence used, is not optimally active. In addition, as previously proposed, non-specific degradation of these duplexes might have an important role, which would produce RNA fragments that could also induce gene silencing, albeit with less potency. The kinetics associated with this non-specific degradation may be higher when compared to the proposed mechanisms of RNAse H cleavage and Dicer processing, and that could induce a bias in the observed silencing potency, masking the real differences between the intrinsic silencing activity of each duplex.

Nonetheless, the C duplex was deemed to be the one with the best pattern for inducing RNAi activity, and as such was the one used to assemble nanocages.

4.4.3 Gene Silencing Properties of Anti-GFP RNAse H Nanocages

The new duplex was then tested in fully assembled nanocages (henceforth named RNAse H nanocages or H-Nanocages). Firstly, to confirm that RNAse H cleavage is effectively induced by the new sequence design, RNAse H nanocages were incubated *in vitro* with the enzyme and subsequently analyzed by PAGE (Figure 32).

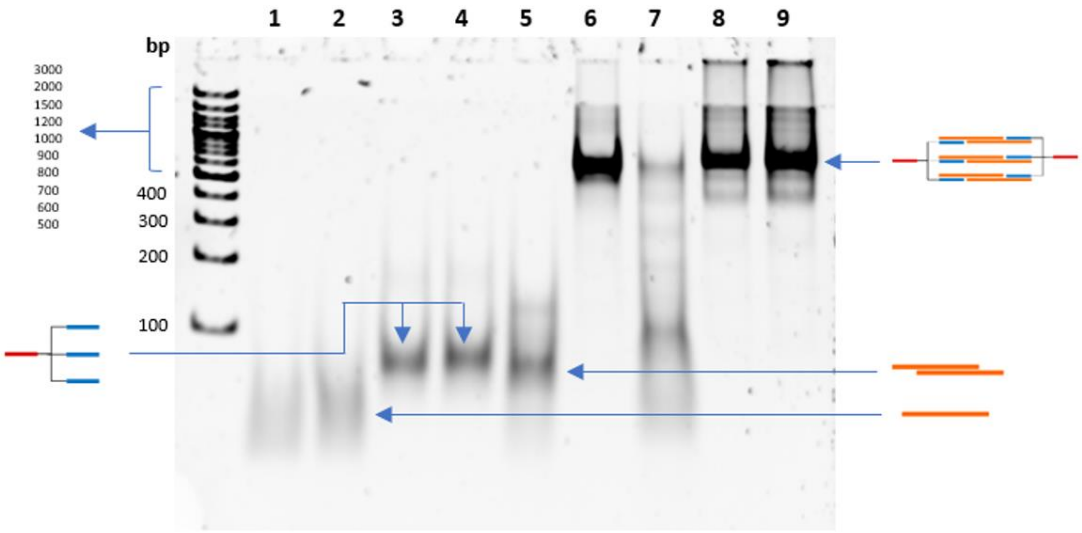

Fig.32 – PAGE analysis of RNAse H-mediated nanocage cleavage. Purified RNAse H and regular anti-GFP nanocages were incubated with RNAse H for 15 minutes at 37°C. Lane correspondence: 1) sense D-R strand; 2) antisense D-R strand; 3) sense trebler; 4) antisense trebler; 5) D-R duplex; 6) RNAse H nanocage; 7) RNAse H nanocage + RNAse H; 8) Nanocage; 9) Nanocage + RNAse H. DNA ladder is presented at the leftmost lane, with the base-pairs of the corresponding bands.

It is noticeable that the incubation of regular nanocages with RNAse H did not produce any visible changes in their band profile, as seen in lane 8. This seems to indicate that the enzyme did not recognize the structure. This was expected, as there is no DNA-RNA heterodimer present in the regular nanocage design, and RNAse H does not cleave DNA-DNA or RNA-RNA duplexes. In contrast, RNAse H nanocages exhibited a remarkably different PAGE profile after being incubated with the enzyme (lane 7), with a band of lower molecular weight being present along with a slight smear pattern. This suggests that RNAse H recognized and cleaved the heteroduplex present in the newly designed nanocages, although the resulting structures are not clearly defined.

Since RNAse H nanocages were shown to be processed by RNAse H, their gene silencing properties might be improved. The recognition by intracellular RNAse H should help to disassemble the structure, and this could possibly release functional siRNA duplexes to induce a RNAi response, as intended. This would provide an advantage over regular nanocages, as their Dicer-mediated release of siRNAs could not be verified. To evaluate this, U2OS-GFPLuc cells were transfected with RNAse H and regular anti-GFP nanocages, and the luciferase expression was evaluated with a luciferase reporter gene assay (Figure 33).

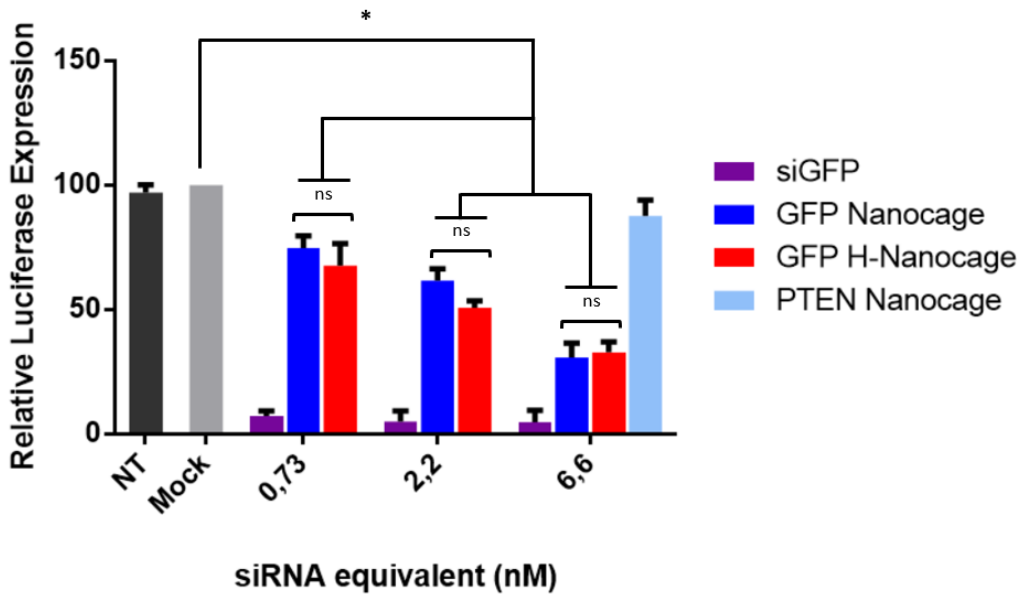

Fig.33 – Relative expression of luciferase 96 hours after transfection with nanocages. GFP-Luc U2OS-GFPLUC cells were transfected with siGFP, RNAse H and regular nanocages targeting GFP, as well as a control anti-PTEN nanocage. 96 hours after transfection, luciferase expression was evaluated by a luciferase reporter assay and normalized by microBCA protein assay. Concentration is expressed as siRNA equivalent (1 nanocage=3 siRNAs). Anti-GFP nanocages and H-nanocages were compared through a two-way Anova, with Sidak's multiple comparison tests, and were both compared to Mock through t-test. Results are expressed as mean + standard deviation of relative luciferase expression normalized to the mock control. N=3 independent experiments. *ns=non-significant; *p<0,0001, except for 0,73 nM GFP Nanocage (p=0,0002)*

As expected, anti-PTEN nanocages did not cause a significant downregulation of luciferase expression, suggesting that the silencing observed in the other nanocages was solely due to the functional siRNAs in their structure.

Both RNAse H and regular nanocages exhibited a dose-dependent response and achieved maximum silencing (≈70%) at 6,6 nM. However, no significant differences were observed between them across all concentrations, indicating that the proposed design for RNAse H seems not to contribute to increase the silencing activity in this assay.

When considering the similar downregulation properties of both types of nanocages, it may be concluded that the disassembly mediated by RNAse H did not play a key role in their silencing pathway. Hence, the previously stated non-specific degradation hypothesis might justify this. Nanocages could undergo non-specific degradation during or after the transfection, promoting the release of many heterogeneous RNA duplexes (with less active sequence patterns) and single strands. This non-specific degradation can be occurring with a faster kinetics than what could be achieved by the specific RNAse H and Dicer enzymes. In fact, several different nuclease enzyme types exist both extra and intracellularly [194,195].

The result is then the formation of heterogeneous and less active RNA duplexes at a much faster rate than which the more specific RNAse H and Dicer-mediated cleavage products could be formed. This would explain the similarities between the activity of RNAse H nanocages and regular nanocages.

Nonetheless, it is worth noting that, when transfected, siRNA nanocages elicited a significant RNAi effect against both an endogenous (PTEN in HT22 cells) and an overly expressed exogenous gene (GFP-Luc in U2OS cells). This demonstrates that, despite the still uncharacterized mechanism of action, siRNA nanocages could be applicable as an effective gene silencing agent.

Despite the apparent inability of Dicer to recognize and cleave the arms of the nanocage, other strategies could be employed with the goal of releasing the active siRNAs present in the structure. As mentioned earlier, the use of cleavable linkers to facilitate siRNA release from molecular bioconjugates is a well-established technique. For example, utilizing a trebler with disulfide bonds as linkers would lead to the release of the RNA arms in the intracellular reductive environment, possibly facilitating Dicer recognition and RISC incorporation. However, chemical synthesis of oligonucleotides with disulfide modifications is a complex process with low yields. Still, owing to its modular structure, the fine-tuning of siRNA nanocage properties can be made without greatly affecting the overall structural design.

Another approach for the optimization of the nanocages activity could encompass the introduction of more chemical modifications in order to increase their stability. As there is the possibility that non-specific degradation is occurring, the introduction of modifications in susceptible cleavage sites might contribute to boost nanocages resistance against nucleases. Nanocages are probably more susceptible to exonuclease degradation in the area around the nicks in the 3´ ends of D-R strands. As such, the inclusion of modifications such as phosphorothioates at these termini could promote more stability against degradation, as phosphorothioates have proved to be effective when incorporated in duplex terminals [152]. Furthermore, the inclusion of LNAs, 2'-F or 2'-O-Me along the sequence could also enhance nuclease resistance. In fact, fully modified siRNAs with alternating 2'-F and 2'-O-Me modifications, as well as with phosphorothioates at the terminals, are effectively used with conjugates [196]. As nanocages might depend on Dicer recognition, fully modified strands would hamper their activity; however, more moderate patterns could be studied, avoiding the area of recognition by the Dicer PAZ domain (represented in Figure 7). Additionally, adjusting nanocages assembly by including a step for closing the existing nicks would also be a strategy worth studying. Possibly, this could be made by employing ligases or by covalently linking the two nucleotides encompassing the nick through thymine dimers [197].

This could all be important considerations in order to redirect their mechanism of action towards the proposed RNAse H cleavage method, thus increasing their biological activity.

4.5 Cellular Uptake Evaluation

Molecular bioconjugates are one of the main approaches to promote targeted delivery of siRNA. By covalently or non-covalently linking a functional biomolecule to siRNA, cellular internalization can be promoted through receptor-mediated endocytosis. As the main goal of this work was to develop a bioconjugate that could primarily target neuronal cells, conjugation of nanocages with Tet1 was attempted.

Tet1 is a small peptide derived from phage display that binds to GT1b gangliosides, highly expressed on neuronal cell types [198]. As such, the development of nanocage-Tet1 conjugates could promote their internalization by neuronal cell types through receptor-mediated endocytosis.

It was previously demonstrated that siRNA nanocages can be functionalized with ssDNA-biotin conjugates through a hybridization-driven self-assembly process. A similar approach was tested, incubating ssDNA-Tet1 conjugates (Figure S.6) with purified siRNA nanocages at 25°C for 30 min to promote the hybridization. The efficacy of the assembly was assessed through PAGE (Figure 34).

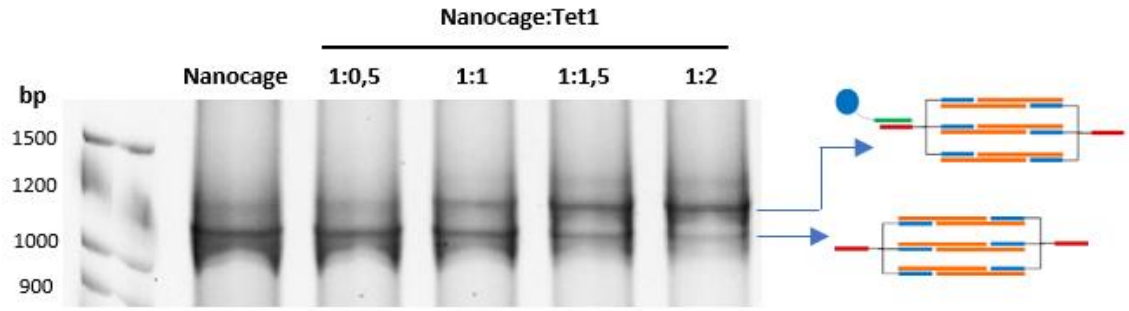

Fig.34 – PAGE analysis of the functionalization of anti-GFP nanocages with Tet1-ssDNA. Different ratios of nanocage:Tet1 were tested, as shown in the figure. DNA ladder is shown at the leftmost lane, with the base-pairs of corresponding bands.

It can be observed that a new band starts to appear when higher molar ratios of nanocage:Tet1 were used, while the band corresponding to the non-functionalized nanocage starts to fade away. This band shift indicates that a structure of a higher molecular weight is being formed as more Tet1 is added in solution, similar to what was observed with the biotin-nanocage conjugate. Hence, these observations suggest that the assembly of the Tet1-nanocage is occurring as predicted. It is worth noting that despite the theoretical nanocage:Tet1 ratio for complete functionalization being 1:1 (as Tet1 should only hybridize with one overhang), the observed ratio was about 1:2. This is probably due to errors associated with the concentration measurements of Tet1, as this peptide presents low solubility and could induce some variation if not properly solubilized.

After the assembly of the Tet1-nanocage conjugates, a study was conducted in order to evaluate if the conjugation with Tet1 would improve the cellular uptake of the nanocages in primary neuronal cells. Primary cortical neurons of mouse embryos were incubated or transfected with siRNAs and nanocages containing Cy5 fluorophores, and after 3 hours the cells were lysed, and the fluorescence levels were measured (Figure 35).

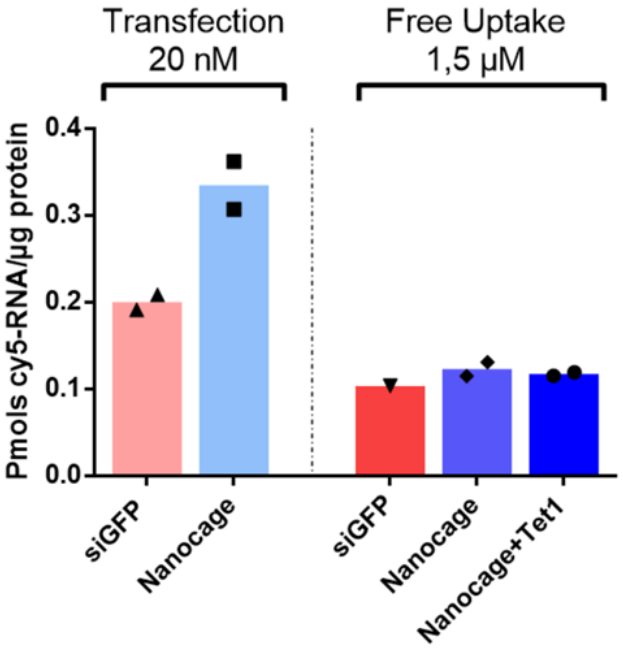

Fig.35 – Intracellular quantity of Cy.5-labeled RNA after transfection or incubation of primary cortical neurons with Cy.5 labeled anti-GFP siRNAs and nanocages. After 3 hours, the cells were treated with heparin to remove membrane-bound oligonucleotides, then lysed and fluorescence intensity was measured. Cy5-RNA quantity was assessed through a calibration curve (Figure S.7). Concentrations expressed as siRNA equivalents (1 nanocage=3 siRNAs). Results are expressed as mean of replicates. N=1 independent experiment

One positive control was introduced in the form of transfected siRNA and nanocages. When comparing these two conditions it appears that nanocages displayed a slightly higher uptake, as higher fluorescence levels were observed. In fact, this can be explained due to nanocages having a significantly higher density of negative charges, given their bigger nucleic acid structure. This may promote a higher association with the cationic transfection reagent and increase the formation of lipoplexes, promoting a slightly higher efficiency of transfection.

No significant differences were observed between either siRNA, functionalized and non-functionalized cages. It was expected that functionalization with Tet1 would promote receptor-mediated endocytosis, thus leading to a higher internalization of nanocages; however, further tests are needed to access this hypothesis.

Obvious justifications would be that either Tet1 was not correctly functionalized with the nanocages or that its mechanism of internalization does not support the transport of nanocages, albeit it has been used to successfully promote neuronal internalization of other molecules and nanocomplexes [199]. In addition, non-specific internalization might be occurring, promoting the uptake of siRNA and nanocages to such a higher extent that it would conceal the effect of Tet1-mediated endocytosis. Indeed, it has been reported that scavenger receptors, that have affinity to anionic molecules like nucleic acids, might be widely expressed in cortical neurons [18], supporting the non-specific internalization hypothesis. One way to verify this hypothesis would be through the blocking of these non-specific receptors with inert nucleic acids, thus only evaluating the internalization due to Tet1 specific receptor-ligand interactions.

Nonetheless, these were preliminary studies, as only 1 independent experiment was conducted. It is only possible to draw precise conclusions with further independent experiments.

Besides quantitatively analyzing the cellular uptake of Tet1-nanocage conjugates, preliminary microscopy studies were also conducted. Primary cortical neurons of mouse embryos were incubated with both Tet1-nanocage conjugates and regular nanocages for 1 hour at 4°C, and then for 2 hours at 37°C after replacing the medium. Cells were then stained and analyzed with confocal microscopy (Figure 36).

It can be observed that the functionalized nanocages show higher association with cellular bodies when compared to the non-functionalized nanocages, although it is worth noting that some of these observations may correspond to aggregates in cells with decreased viability, as seen by the condensation of the nucleus. Overall, these images seem to indicate that Tet1 did promote internalization to a certain degree, contrasting with the observations of the previous fluorescence assay.

Nevertheless, some facts should be taken into account before comparing these results. The nature of these two methods is different, as confocal microscopy offers a qualitative analysis and may have improved sensitivity, while the spectrofluorometer offers a less sensible quantitative reading of an entire well. As such, a reading with the fluorometer might also detect “unwanted” fluorescence levels in the form of aggregates inside less viable cells, for example. In addition, the protocols for cell treatment had some changes that might be meaningful. Cells analyzed by confocal imaging did not underwent a heparin treatment for the removal of membrane-bound oligos, possibly explaining the apparent cellular association of Tet1-nanocages. The times and temperatures of incubation were also different, introducing some variables that could prevent the comparation of both results. In fact, the incubation at 4ºC can allow for structures to bind to cell membranes without being internalized. Hence, after washing, weakly bound structures would dissociate from cell membranes, and only strongly

associated structures through receptor-ligand interactions would proceed to be internalized at 37ºC, possibly explaining these observations.

The fact that these were preliminary studies should be considered, as the protocols might not be fully optimized. Additionally, the experimental design could be further optimized, as the employment of fluorescent-labeled nanocages can be introducing a bias on the observed results. Indeed, it has been recently reported that the use of hydrophobic fluorophores like Cy5 can enhance the intracellular accumulation of siRNA conjugates by promoting interactions with the cellular membrane [200], and as such, other methods should be tested before drawing precise conclusions.

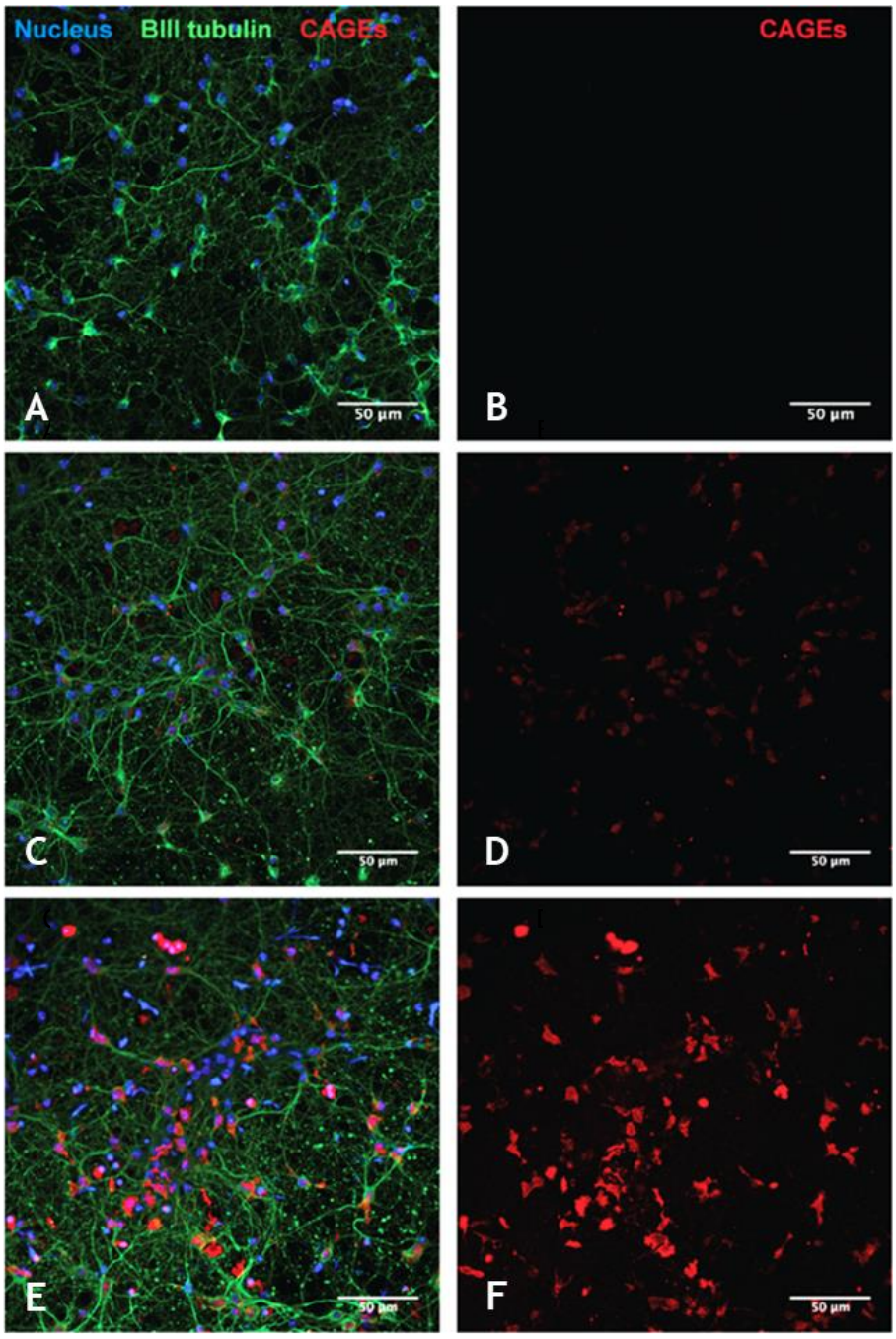

Fig.36 – Confocal microscopy of primary cortical neurons of mouse embryos after incubation with either non-functionalized or Tet-1 functionalized nanocages, both fluorescently labeled with Cy5 (red). Cells were stained for ßIII-tubulin (green) and for the nucleus with Hoechst (blue). Images **A)** and **B)** correspond to the non-treated control; **C)** and **D)** to cells treated with nanocages; **E)** and **F)** to cells treated with Tet1-nanocage conjugates. Images **A)**, **C)** and **E)** represent the 3 merged channels, and **B)**, **D)** and **D)** represent the respective Cy.5 channel. Scale bar: 50 µm.

Chapter 5: Conclusions and Future Perspectives

Over the last 2 decades, siRNA therapeutics have steadily been developing into a clinical reality, showing great promise for the treatment of many diseases that cannot be addressed presently. Nevertheless, there is still much work to be done, as siRNAs still face some major hurdles against their effective employment in vivo such as poor biodistribution, susceptibility do degradation or unwanted off-target effects. Thus, they suffer an overall lack of therapeutically efficiency, and several strategies are being developed in order to overcome these issues. Namely, the employment of molecular bioconjugates is a promising strategy in order to improve siRNA targeted delivery and cellular uptake, with siRNA-GalNAc conjugates already in late-stage clinical trials. Nonetheless, GalNAc success is largely due to the unique properties of its target receptor, including considerably high expression levels in hepatocytes and fast recycling time. Extra-hepatic targeting with molecular conjugates remains a challenge as no targets with similar therapeutic potential have been reported. Branched siRNAs and other structural variants present compelling alternatives, as they can increase the activity and number of siRNAs delivered in a bioconjugate while maintaining a small and well-defined structure.

Herein, we developed siRNA nanocages, a novel and multivalent branched siRNA nanoarchitecture that allowed for the conjugation with multiple functional biomolecules through a simple hybridization-based mechanism. Their successful production was seemingly accomplished through a two-step self-assembly process, although more characterization tests should be required, as structural characterization studies conducted through TEM were still at a preliminary phase. Higher-resolution techniques like cryogenic TEM or atomic force microscopy could help in this structural characterization.

Due to their modular nature, the production of siRNA nanocages targeting different genes was possible, and they displayed the ability to elicit a significant RNAi response against both endogenous and exogenous genes in vitro following transfections in two different cell lines. This indicates compatibility with the RNAi mechanism, and thus potential applicability for gene

silencing purposes. Despite their somewhat reduced silencing potency when compared to canonical siRNAs, this may serve as a starting point for further development.

In fact, we also demonstrated proof-of-concept for a method based on RNAse H cleavage to facilitate the release mechanism of siRNA from their structure. Although further work is required to translate this method into significant improvements in gene silencing properties, it paves the way for the development of new approaches to enhance siRNA nanocages functional properties. By exploring the chemical space of nucleotide chemistry and adapting it to the design of siRNA nanocages, some other options for optimization arise: the introduction of site-specific chemical modifications like 2'-O-Me or phosphorothioates could enhance nanocage resistance against non-specific degradation; the employment of other types of linkers like intracellular-cleavable disulfide bonds could facilitate siRNA release; and the fine tuning of the design could increase structural stability, for example, by bridging existing nicks in their sequence. Moreover, the modification of the original nanocage design to incorporate more branching units would increase its multivalence, allowing for the delivery of more than 3 siRNAs per structure; however, current constraints in the synthesis and purification of highly branched oligonucleotides limit the feasibility of this approach. Alternatively, they could also be designed as a multi-target drug, incorporating different siRNA sequences in the same structure, thus possibly improving their therapeutic properties in the treatment of more complex conditions.

In an attempt to confer targeting properties against neuronal cells, siRNA nanocages were also functionalized with the Tet1 peptide in order to promote uptake through receptor-mediated endocytosis. Despite the fact that only some preliminary tests were conducted, this conjugation showed signs of promoting neuronal association, although it seems that it did not enhance uptake. Further studies with optimized protocols should be conducted in order to clarify the effect of Tet1 conjugation. If nanocages are to be employed as molecular conjugates for neuronal cell targeting, other targeting conjugates could also be screened, like neurotensin [199], to give an example . Other functional moieties that grant increased pharmacokinetics or promote endosomal escape, for example, could also be interesting alternatives. In addition, fundamental tests like resistance to serum degradation and immune system activation should also be conducted before considering overall applicability as therapeutic molecular bioconjugates.

In conclusion, the results of this work suggest that siRNA nanocages can act as a potential scaffold for easy functionalization with multiple biomolecules through a simple hybridization-based process. Their modular nature also allows for the personalization and fine-tuning of several properties while maintaining a significant gene silencing activity. Owning to their versatility and customizable design, and with further development, siRNA nanocages could

conceivably be applied as therapeutic conjugates targeting not only the CNS, but also many other tissues.

Appendix

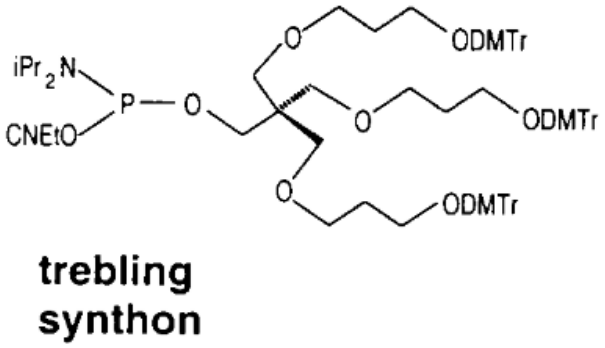

Fig. S.1 – Chemical strucuture of the trebler unit. Adapted from Shchepinov et al., 1997

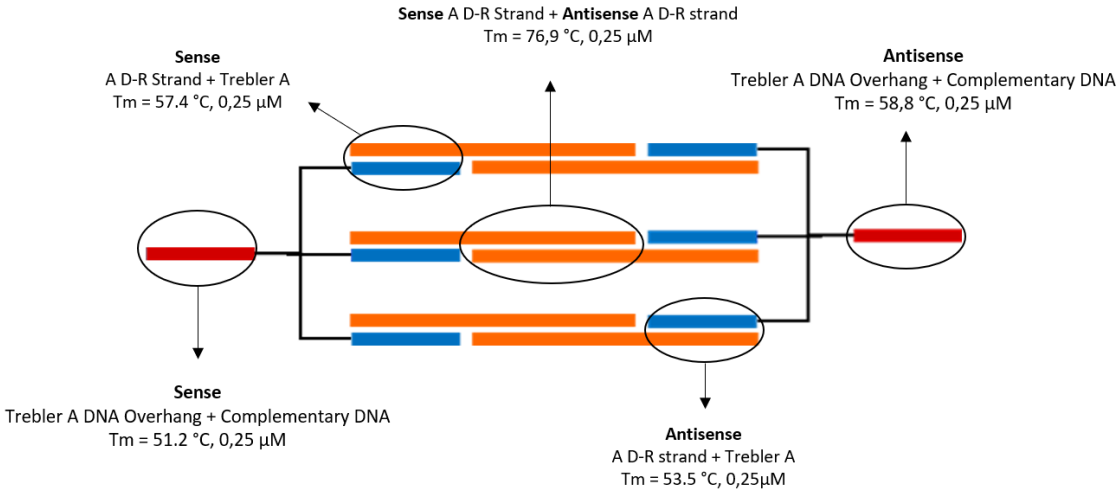

Fig. S.2 – Theroretical melting temperatures of the different sequences that encompass an anti-GFP nanocage. Values were calculated with OligoAnalyzer software (Integrated DNA Technologies) considering 150 mM NaCl and a concentration of 0,25 µM.

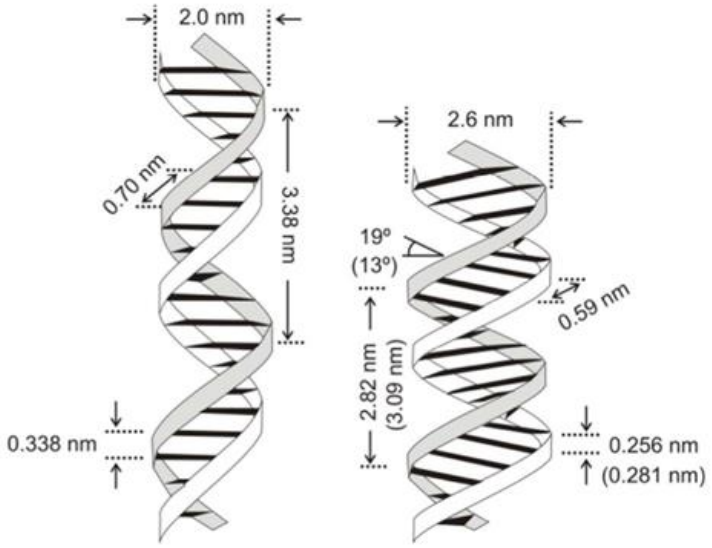

Fig. S.3 - Schematic view of B (left) and A (right) double-helix forms of DNA, along with estimated structural parameters. Values for the A-form of dsRNA are presented in brackets. Adapted from Arias-Gonzalez et al., 2014.

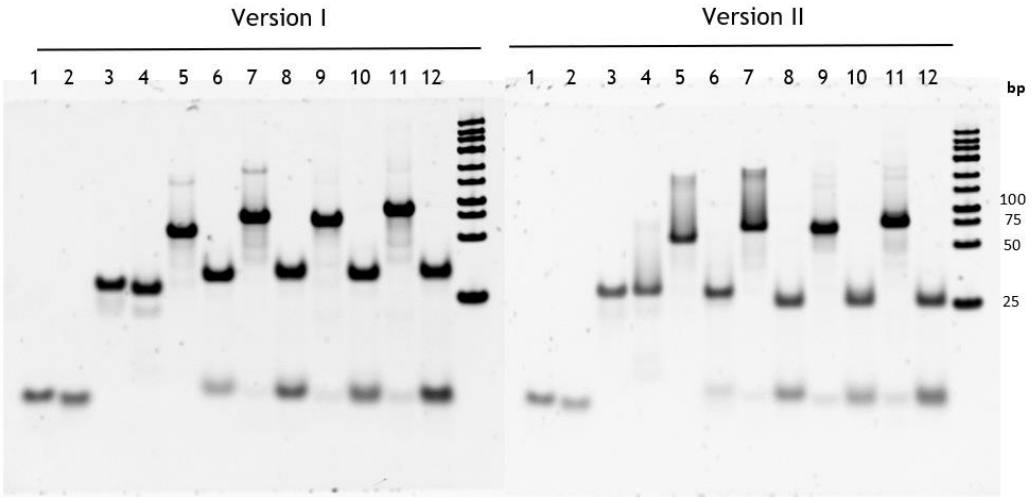

Fig. S.4 – PAGE analysis of RNAse cleavage of version I and II D-R strand duplexes blocked with DNA arms. The formation of two single well-defined bands after incubating the duplexes with RNAse H clearly indicates that RNAse H is recognizing and cleaving the structure. Lane correspondence: **1)** DNA arm sense; **2)** DNA arm antisense; **3)** Sense D-R strand; **4)** Antisense D-R strand; **5)** D-R duplex; **6)** D-R duplex+RNAseH; **7)** D-R duplex+DNA Arm sense; **8)** D-R duplex+DNA arm sense+RNAse H; **9)** D-R duplex+DNA arm antisense; **10)** D-R duplex+DNA arm antisense+RNAse H; **11)** D-R duplex+DNA arms sense/antisense; **12)** D-R duplex+DNA arms sense/antisense+RNAse H. DNA ladder is presented in the leftmost lanes, with the corresponding base-pairs.

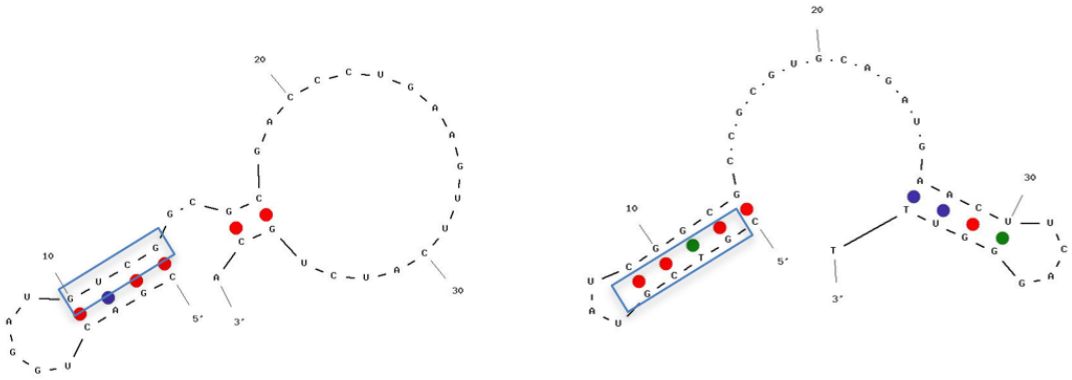

Sense D-R strand version I (DNA folding = 45.3°C)

Antisense D-R strand version I (DNA folding = 43.2°C)

Fig. S.5 – Analysis of self-dimer conformations of version I D-R strands. It is observable that these strands self-dimers include a RNA-DNA hybrid in the overhang region that may induce RNAse cleavage. This may explain the recognition and cleavage of D-R strand duplexes observed in Figure S.4, even when the DNA arms are not blocking the overhangs and promoting the cleavage.

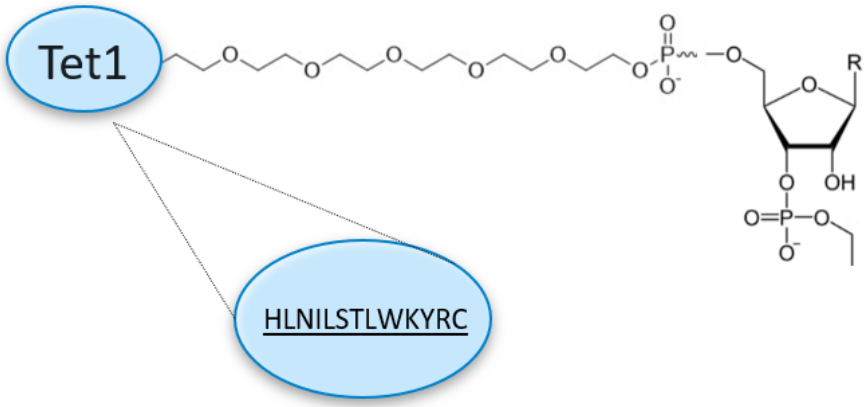

Fig. S.6 – Representation of the molecular structure of Tet1-DNA conjugate

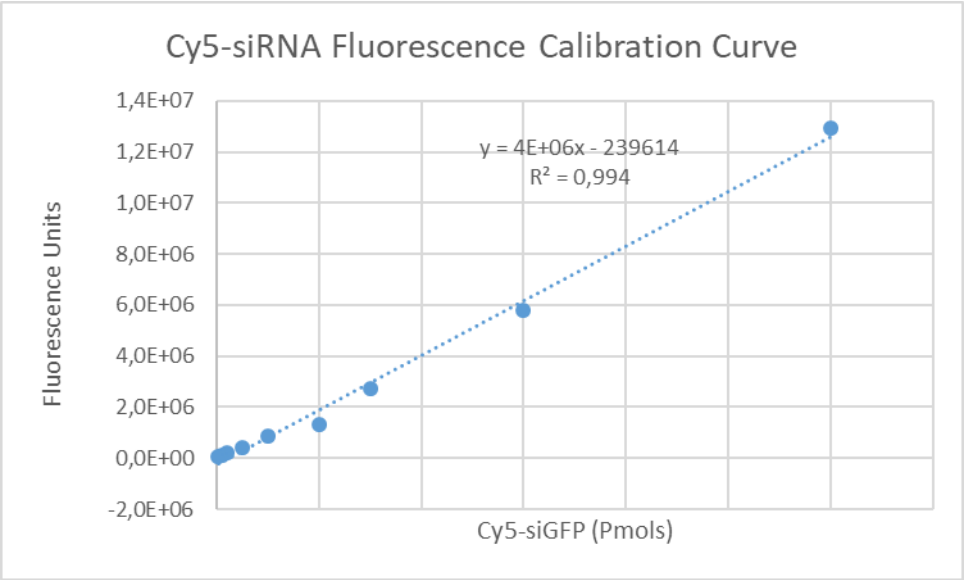

Fig. S.7 – Calibration curve used to determine the molar quantity of internalized Cy5-labeled molecules in the fluorometer cellular uptake experiments.

References

1. Feigin, V. L. *et al*. Global, regional, and national burden of neurological disorders, 1990–2016: a systematic analysis for the Global Burden of Disease Study 2016. *Lancet Neurol.* **18**, 459–480 (2019).
2. WHO. Neurological disorders: a public health approach. *Neurol. Disord. public Heal. challenges* 40–110 (2006). doi:10.1037/e521482010-002
3. Kim, Y., Kim, Y., Hwang, O. & Jin, D. Pathology of Neurodegenerative Diseases. *Brain Damage - Bridg. Between Basic Res. Clin.* 1–22 (2012). doi:10.5772/38028
4. Gilmore, J. L., Yi, X., Quan, L. & Kabanov, A. V. Novel nanomaterials for clinical neuroscience. *J. Neuroimmune Pharmacol.* **3**, 83–94 (2008).
5. Gustincich, S., Zucchelli, S. & Mallamaci, A. *The Yin and Yang of nucleic acid-based therapy in the brain. Progress in Neurobiology* **155**, (Elsevier Ltd, 2017).
6. Silva, G. A. Nanotechnology approaches for the regeneration and neuroprotection of the central nervous system. *Surg. Neurol.* **63**, 301–306 (2005).
7. Canter, R. G., Penney, J. & Tsai, L. H. The road to restoring neural circuits for the treatment of Alzheimer's disease. *Nature* **539**, 187–196 (2016).
8. Taylor, J. P., Brown, R. H., Cleveland, D. W. & Cleveland, D. W. Decoding ALS: from genes to mechanism. *Nature* **539**, 197–206 (2016).
9. Abeliovich, A. & Gitler, A. D. Defects in trafficking bridge Parkinson's disease pathology and genetics. *Nature* **539**, 207–216 (2016).
10. de Boer, A. . & Gaillard, P. J. Drug targeting to the brain. *Pharm. Res.* **24**, 1733–1744 (2007).
11. Cordon-Cardo, C. *et al*. Multidrug-resistance gene (P-glycoprotein) is expressed by endothelial cells at blood-brain barrier sites. *Proc. Natl. Acad. Sci.* **86**, 695–698 (1989).
12. Mahringer, A., Ott, M., Reimold, I., Reichel, V. & Fricker, G. The ABC of the blood-brain barrier - regulation of drug efflux pumps. *Curr. Pharm. Des.* **17**, 2762–70 (2011).
13. Ueno, M. *et al*. Transporters in the brain endothelial barrier. *Curr. Med. Chem.* **17**, 1125–38 (2010).
14. Fornaguera, C. *et al*. PLGA nanoparticles prepared by nano-emulsion templating using low-energy methods as efficient nanocarriers for drug delivery across the blood–brain barrier. *J. Control. Release* **211**, 134–143 (2015).
15. Singh, I. *et al*. Lactoferrin bioconjugated solid lipid nanoparticles: a new drug delivery system for potential brain targeting. *J. Drug Target.* **24**, 212–223 (2016).
16. Misra, S., Chopra, K., Sinha, V. R. & Medhi, B. Galantamine-loaded solid–lipid nanoparticles for enhanced brain delivery: preparation, characterization, *in vitro* and *in vivo* evaluations. *Drug Deliv.* **23**, 1434–1443 (2016).
17. Vinogradov, S. V., Batrakova, E. V. & Kabanov, A. V. Nanogels for Oligonucleotide Delivery to the Brain. *Bioconjug. Chem.* **15**, 50–60 (2004).
18. Labieniec-Watala, M. & Watala, C. PAMAM dendrimers: Destined for success or doomed to fail? Plain and modified PAMAM dendrimers in the context of biomedical applications. *J. Pharm. Sci.* **104**, 2–14 (2015).
19. Patel, M. M. & Patel, B. M. Crossing the Blood–Brain Barrier: Recent Advances in Drug Delivery to the Brain. *CNS Drugs* **31**, 109–133 (2017).

20. Evers, M. M., Toonen, L. J. A. & van Roon-Mom, W. M. C. Antisense oligonucleotides in therapy for neurodegenerative disorders. *Adv. Drug Deliv. Rev.* **87**, 90–103 (2015).

21. Margetis, K. *et al.* Intrathecal baclofen therapy for the symptomatic treatment of hereditary spastic paraplegia. *Clin. Neurol. Neurosurg.* **123**, 142–145 (2014).

22. Al-Zaidy, S. A. & Mendell, J. R. From Clinical Trials to Clinical Practice: Practical Considerations for Gene Replacement Therapy in SMA Type 1. *Pediatr. Neurol.* (2019). doi:10.1016/j.pediatrneurol.2019.06.007

23. Ver Donck, A. *et al.* Intrathecal Drug Administration in Chronic Pain Syndromes. *Pain Pract.* **14**, n/a-n/a (2013).

24. Bailey, A. M. *et al.* Review of Intranasally Administered Medications for Use in the Emergency Department. *J. Emerg. Med.* **53**, 38–48 (2017).

25. Thorne, R. G., Emory, C. R., Ala, T. A. & Frey, W. H. Quantitative analysis of the olfactory pathway for drug delivery to the brain. *Brain Res.* **692**, 278–282 (1995).

26. Lochhead, J. J. & Thorne, R. G. Intranasal delivery of biologics to the central nervous system. *Adv. Drug Deliv. Rev.* **64**, 614–628 (2012).

27. Khan, A. R., Liu, M., Khan, M. W. & Zhai, G. Progress in brain targeting drug delivery system by nasal route. *J. Control. Release* **268**, 364–389 (2017).

28. Zhang, F., Lin, Y.-A., Kannan, S. & Kannan, R. M. Targeting specific cells in the brain with nanomedicines for CNS therapies. *J. Control. Release* **240**, 212–226 (2016).

29. Rungta, R. L. *et al.* Lipid Nanoparticle Delivery of siRNA to Silence Neuronal Gene Expression in the Brain. *Mol. Ther. Acids* **2**, e136 (2013).

30. Haney, M. J. *et al.* Exosomes as drug delivery vehicles for Parkinson's disease therapy. *J. Control. Release* **207**, 18–30 (2015).

31. Chu, D. S. H., Schellinger, J. G., Bocek, M. J., Johnson, R. N. & Pun, S. H. Optimization of Tet1 ligand density in HPMA-co-oligolysine copolymers for targeted neuronal gene delivery. *Biomaterials* **34**, 9632–9637 (2013).

32. Zhang, H. *et al.* Selective neuronal targeting, protection and signaling network analysis via dopamine-mediated mesoporous silica nanoparticles. *Medchemcomm* **6**, 1117–1129 (2015).

33. Fire, A. *et al.* Potent and specific genetic interference by double-stranded RNA in caenorhabditis elegans. *Nature* **391**, 806–811 (1998).

34. Jorgensen, R. Altered gene expression in plants due to trans interactions between homologous genes. *Trends Biotechnol.* **8**, 345–348 (1990).

35. System, C. C. *et al.* Mechanisms of gene silencing by double-stranded RNA. *Nature* **10**, 1–7 (2016).

36. Lewis, B. P., Burge, C. B. & Bartel, D. P. Conserved seed pairing, often flanked by adenosines, indicates that thousands of human genes are microRNA targets. *Cell* **120**, 15–20 (2005).

37. Bartel, D. P. MicroRNAs: Genomics, Biogenesis, Mechanism, and Function. *Cell* **116**, 281–297 (2004).

38. Zamore, P. D., Tuschl, T., Sharp, P. A. & Bartel, D. P. RNAi: double-stranded RNA directs the ATP-dependent cleavage of mRNA at 21 to 23 nucleotide intervals. *Cell* **101**, 25–33 (2000).

39. Pratt, A. J. & MacRae, I. J. The RNA-induced silencing complex: A versatile gene-silencing machine. *J. Biol. Chem.* **284**, 17897–17901 (2009).

40. Ozcan, G., Ozpolat, B., Coleman, R. L., Sood, A. K. & Lopez-Berestein, G. Preclinical and clinical development of siRNA-based therapeutics. *Adv. Drug Deliv. Rev.* **87**, 108–119 (2015).

41. Wang, Q. & Carmichael, G. G. Effects of Length and Location on the Cellular Response to Double-Stranded RNA. *Microbiol. Mol. Biol. Rev.* **68**, 432–452 (2004).

42. Elbashir, S. M. *et al.* Duplexes of 21 ± nucleotide RNAs mediate RNA interference in cultured mammalian cells. *Nature* **411**, 494–498 (2001).

43. Reynolds, A. *et al.* Rational siRNA design for RNA interference. *Nat. Biotechnol.* **22**, 326–330 (2004).

44. Fakhr, E., Zare, F. & Teimoori-Toolabi, L. Precise and efficient siRNA design: A key point in competent gene silencing. *Cancer Gene Ther.* **23**, 73–82 (2016).

45. LAYZER, J. M. *et al.* In vivo activity of nuclease-resistant siRNAs. *RNA* **10**, 766–771 (2004).

46. Turner, J. J., Jones, S. W., Moschos, S. A., Lindsay, M. A. & Gait, M. J. MALDI-TOF mass spectral analysis of siRNA degradation in serum confirms an RNAse A-like activity. *Mol. BioSyst.* **3**, 43–50 (2007).

47. Terrazas, M., Alagia, A., Faustino, I., Orozco, M. & Eritja, R. Functionalization of the 3′-Ends of DNA and RNA Strands with N-ethyl-N-coupled Nucleosides: A Promising Approach To Avoid 3′-Exonuclease-Catalyzed Hydrolysis of Therapeutic Oligonucleotides. *ChemBioChem* **14**, 510–520 (2013).

48. van de Water, F. M. *et al.* INTRAVENOUSLY ADMINISTERED SHORT INTERFERING RNA ACCUMULATES IN THE KIDNEY AND SELECTIVELY SUPPRESSES GENE FUNCTION IN RENAL PROXIMAL TUBULES. *Drug Metab. Dispos.* **34**, 1393–1397 (2006).

49. Juliano, R. L. The delivery of therapeutic oligonucleotides. *Nucleic Acids Res.* **44**, 6518–6548 (2016).

50. Kang, L. *et al.* Noninvasive Visualization of RNA Delivery with 99mTc-Radiolabeled Small-Interference RNA in Tumor Xenografts. *J. Nucl. Med.* **51**, 978–986 (2010).

51. Nielsen, C., Kjems, J., Sørensen, K. R., Engelholm, L. H. & Behrendt, N. Advances in targeted delivery of small interfering RNA using simple bioconjugates. *Expert Opin. Drug Deliv.* **11**, 791–822 (2014).

52. Whitehead, K. A., Dahlman, J. E., Langer, R. S. & Anderson, D. G. Silencing or Stimulation? siRNA Delivery and the Immune System. *Annu. Rev. Chem. Biomol. Eng.* **2**, 77–96 (2011).

53. Alexopoulou, L., Holt, A. C., Medzhitov, R. & Flavell, R. A. Recognition of double-stranded RNA and activation of NF-kappaB by Toll-like receptor 3. *Nature* **413**, 732–8 (2001).

54. Judge, A. D. *et al.* Sequence-dependent stimulation of the mammalian innate immune response by synthetic siRNA. *Nat. Biotechnol.* **23**, 457–462 (2005).

55. Zhang, Z., Weinschenk, T., Guo, K. & Schluesener, H. J. siRNA binding proteins of microglial cells: PKR is an unanticipated ligand. *J. Cell. Biochem.* **97**, 1217–1229 (2006).

56. Marques, J. T. *et al.* A structural basis for discriminating between self and nonself double-stranded RNAs in mammalian cells. *Nat. Biotechnol.* **24**, 559–565 (2006).

57. Dowdy, S. F. Overcoming cellular barriers for RNA therapeutics. *Nat. Biotechnol.* **35**, 222–229 (2017).

58. Lipinski, C. A., Lombardo, F., Dominy, B. W. & Feeney, P. J. Experimental and Computational Approaches to Estimate Solubility and Permeability in Drug Discovery and Develop ment Settings. *Adv. Drug Deliv. Rev.* **23**, 3–25 (1997).

59. Juliano, R. L., Ming, X., Carver, K. & Laing, B. Cellular Uptake and Intracellular Trafficking of Oligonucleotides: Implications for Oligonucleotide Pharmacology. *Nucleic Acid Ther.* **24**, 101–113 (2014).

60. Chen, C., Yang, Z. & Tang, X. Chemical modifications of nucleic acid drugs and their

delivery systems for gene-based therapy. *Med. Res. Rev.* 1–41 (2018). doi:10.1002/med.21479

61. Deleavey, G. F. & Damha, M. J. Designing chemically modified oligonucleotides for targeted gene silencing. *Chem. Biol.* **19**, 937–954 (2012).

62. Wang, Y. *et al.* Nucleation, propagation and cleavage of target RNAs in Ago silencing complexes. *Nature* **461**, 754–761 (2009).

63. Breslow, R. & Chapman, W. H. On the mechanism of action of ribonuclease A: relevance of enzymatic studies with a p-nitrophenylphosphate ester and a thiophosphate ester. *Proc. Natl. Acad. Sci. U. S. A.* **93**, 10018–21 (1996).

64. FINDLY, D., HERRIES, D. G., MATHIAS, A. P., RABIN, B. R. & ROSS, C. A. The Active Site and Mechanism of Action of Bovine Pancreatic Ribonuclease. *Nature* **190**, 781–784 (1961).

65. Mole, L. D. B. & Sabatier, P. NEW EMBO MEMBER'S REVIEW Small nucleolar RNA-guided post-transcriptional modi®cation of cellular RNAs. *EMBO J.* **20**, 3617–3622 (2001).

66. Volkov, A. A. *et al.* Selective Protection of Nuclease-Sensitive Sites in siRNA Prolongs Silencing Effect. *Oligonucleotides* **19**, 191–202 (2009).

67. Manoharan, M. RNA interference and chemically modified small interfering RNAs. *Curr. Opin. Chem. Biol.* **8**, 570–579 (2004).

68. Judge, A. D., Bola, G., Lee, A. C. H. & MacLachlan, I. Design of Noninflammatory Synthetic siRNA Mediating Potent Gene Silencing in Vivo. *Mol. Ther.* **13**, 494–505 (2006).

69. Cummins, L. L. *et al.* Characterization of fully 2'-modified oligoribonucleotide hetero- and homoduplex hybridization and nuclease sensitivity. *Nucleic Acids Res.* **23**, 2019–2024 (1995).

70. Dorn, G. *et al.* siRNA relieves chronic neuropathic pain. *Nucleic Acids Res.* **32**, e49–e49 (2004).

71. Prakash, T. P. *et al.* Positional Effect of Chemical Modifications on Short Interference RNA Activity in Mammalian Cells. *J. Med. Chem.* **48**, 4247–4253 (2005).

72. Braasch, D. a & Corey, D. R. Locked nucleic acid (LNA): fine-tuning the recognition of DNA and RNA. *Chem. Biol.* **8**, 1–7 (2001).

73. Elmén, J. *et al.* Locked nucleic acid (LNA) mediated improvements in siRNA stability and functionality. *Nucleic Acids Res.* **33**, 439–447 (2005).

74. Hornung, V. *et al.* Sequence-specific potent induction of IFN-α by short interfering RNA in plasmacytoid dendritic cells through TLR7. *Nat. Med.* **11**, 263–270 (2005).

75. Czauderna, F. *et al.* Structural variations and stabilising modifications of synthetic siRNAs in mammalian cells. *Nucleic Acids Res.* **31**, 2705–2716 (2003).

76. Shen, W., Liang, X.-H., Sun, H. & Crooke, S. T. 2'-Fluoro-modified phosphorothioate oligonucleotide can cause rapid degradation of P54nrb and PSF. *Nucleic Acids Res.* **43**, 4569–78 (2015).

77. Shen, W. *et al.* Acute hepatotoxicity of 2′ fluoro-modified 5–10–5 gapmer phosphorothioate oligonucleotides in mice correlates with intracellular protein binding and the loss of DBHS proteins. *Nucleic Acids Res.* **46**, 2204–2217 (2018).

78. Ohrt, T. & Schwille, P. siRNA Modifications and Sub-Cellular Localization: A Question of Intracellular Transport? *Curr. Pharm. Des.* **14**, 3674–3685 (2008).

79. Janas, M. M. *et al.* Safety evaluation of 2′-deoxy-2′-fluoro nucleotides in GalNAc-siRNA conjugates. *Nucleic Acids Res.* **47**, 3306–3320 (2019).

80. Alagia, A. & Eritja, R. siRNA and RNAi optimization. *Wiley Interdiscip. Rev. RNA* **7**, 316–329 (2016).

81. Eckstein, F. Nucleoside Phosphorothionates. *J. Am. Chem. Soc*. 4292–4294 (1969).

82. Eckstein, F. Phosphorothioates, Essential Components of Therapeutic Oligonucleotides. *Nucleic Acid Ther*. **24**, 374–387 (2014).

83. Wang, S. *et al*. Cellular uptake mediated by epidermal growth factor receptor facilitates the intracellular activity of phosphorothioate-modified antisense oligonucleotides. *Nucleic Acids Res.* **46**, 3579–3594 (2018).

84. Meade, B. R. *et al*. Efficient delivery of RNAi prodrugs containing reversible charge-neutralizing phosphotriester backbone modifications. *Nat. Biotechnol*. **32**, 1256–1261 (2014).

85. Trubetskoy, V. S. *et al*. Phosphorylation-specific status of RNAi triggers in pharmacokinetic and biodistribution analyses. *Nucleic Acids Res.* **45**, 1469–1478 (2017).

86. Elkayam, E. *et al*. SiRNA carrying an (E)-vinylphosphonate moiety at the 5' end of the guide strand augments gene silencing by enhanced binding to human Argonaute-2. *Nucleic Acids Res.* **45**, 3528–3536 (2016).

87. Jackson, A. L. & Linsley, P. S. Recognizing and avoiding siRNA off-target effects for target identification and therapeutic application. *Nat. Rev. Drug Discov*. **9**, 57–67 (2010).

88. Khvorova, A., Reynolds, A. & Jayasena, S. D. Functional siRNAs and miRNAs Exhibit Strand Bias. *Cell* **115**, 209–216 (2003).

89. Schwarz, D. S. *et al*. Asymmetry in the Assembly of the RNAi Enzyme Complex. *Cell* **115**, 199–208 (2003).

90. Hohjoh, H. Enhancement of RNAi activity by improved siRNA duplexes. *FEBS Lett*. **557**, 193–8 (2004).

91. Bramsen, J. B. *et al*. Improved silencing properties using small internally segmented interfering RNAs. *Nucleic Acids Res.* **35**, 5886–5897 (2007).

92. Kim, D.-H. *et al*. Synthetic dsRNA Dicer substrates enhance RNAi potency and efficacy. *Nat. Biotechnol*. **23**, 222–226 (2005).

93. Rose, S. D. *et al*. Functional polarity is introduced by Dicer processing of short substrate RNAs. *Nucleic Acids Res.* **33**, 4140–4156 (2005).

94. Collingwood, M. A. *et al*. Chemical Modification Patterns Compatible with High Potency Dicer-Substrate Small Interfering RNAs. *Oligonucleotides* **18**, 187–200 (2008).

95. Siolas, D. *et al*. Synthetic shRNAs as potent RNAi triggers. *Nat. Biotechnol*. **23**, 227–231 (2005).

96. Abe, N., Abe, H. & Ito, Y. Dumbbell-Shaped Nanocircular RNAs for RNA Interference. *J. Am. Chem. Soc.* **129**, 15108–15109 (2007).

97. Ku, S. H., Jo, S. D., Lee, Y. K., Kim, K. & Kim, S. H. Chemical and structural modifications of RNAi therapeutics. *Adv. Drug Deliv. Rev*. **104**, 16–28 (2016).

98. Gvozdeva, O. V. *et al*. 42- and 63-bp anti-MDR1-siRNAs bearing 2'-OMe modifications in nuclease-sensitive sites induce specific and potent gene silencing. *FEBS Lett*. **588**, 1037–1043 (2014).

99. Gvozdeva, O. V. *et al*. Nuclease-resistant 63-bp trimeric siRNAs simultaneously silence three different genes in tumor cells. *FEBS Lett*. **592**, 122–129 (2018).

100. Nakashima, Y., Abe, H., Abe, N., Aikawa, K. & Ito, Y. Branched RNA nanostructures for RNA interference. *Chem. Commun.* **47**, 8367 (2011).

101. Nair, B. G. *et al*. Enhancement of synergistic gene silencing by RNA interference using branched "3-in-1" trimer siRNA. *J. Mater. Chem. B* **5**, 4044–4051 (2017).

102. Shchepinov, M. S., Udalova, I. A., Bridgman, A. J. & Southern, E. M. Oligonucleotide

dendrimers: synthesis and use as polylabelled DNA probes. *Nucleic Acids Res.* **25**, 4447–54 (1997).

103. Shchepinov, M. S., Mir, K. U., Elder, J. K., Frank-Kamenetskii, M. D. & Southern, E. M. Oligonucleotide dendrimers: Stable nano-structures. *Nucleic Acids Res.* **27**, 3035–3041 (1999).

104. Grimau, M. G. *et al.* Synthesis of Branched Oligonucleotides as Templates for the Assembly of Nanomaterials. *Helv. Chim. Acta* **86**, 2814–2826 (2003).

105. Aviñó, A., Ocampo, S. M., Perales, J. C. & Eritja, R. Branched RNA: A New Architecture for RNA Interference. *J. Nucleic Acids* **2011**, 1–7 (2011).

106. Chang, C. Il *et al.* Enhanced intracellular delivery and multi-target gene silencing triggered by tripodal RNA structures. *J. Gene Med.* **14**, 138–146 (2012).

107. Gvozdeva, O. V. & Chernolovskaya, E. L. Noncanonical Synthetic RNAi Inducers. *RNA Interf.* (2016). doi:10.5772/61685

108. Zelphati, O. & Szoka, F. C. Mechanism of oligonucleotide release from cationic liposomes. *Proc. Natl. Acad. Sci. U. S. A.* **93**, 11493–11498 (1996).

109. Sato, Y. *et al.* A pH-sensitive cationic lipid facilitates the delivery of liposomal siRNA and gene silencing activity in vitro and in vivo. *J. Control. Release* **163**, 267–276 (2012).

110. Kanasty, R., Dorkin, J. R., Vegas, A. & Anderson, D. Delivery materials for siRNA therapeutics. *Nat. Mater.* **12**, 967–977 (2013).

111. Hoy, S. M. Patisiran: First Global Approval. *Drugs* **78**, 1625–1631 (2018).

112. Merkel, O. M. & Kissel, T. Quo vadis polyplex? *J. Control. Release* **190**, 415–423 (2014).

113. Khan, A. *et al.* Sustained polymeric delivery of gene silencing antisense ODNs, siRNA, DNAzymes and ribozymes: In vitro and in vivo studies. *J. Drug Target.* **12**, 393–404 (2004).

114. Amjad, M. W., Kesharwani, P., Mohd Amin, M. C. I. & Iyer, A. K. Recent advances in the design, development, and targeting mechanisms of polymeric micelles for delivery of siRNA in cancer therapy. *Prog. Polym. Sci.* **64**, 154–181 (2017).

115. Biswas, S. & Torchilin, V. P. Dendrimers for siRNA delivery. *Pharmaceuticals* **6**, 161–183 (2013).

116. Huang, Y. Preclinical and Clinical Advances of GalNAc-Decorated Nucleic Acid Therapeutics. *Mol. Ther. - Nucleic Acids* **6**, 116–132 (2017).

117. Zatsepin, T. S., Kotelevtsev, Y. V & Koteliansky, V. Lipid nanoparticles for targeted siRNA delivery - going from bench to bedside. *Int. J. Nanomedicine* **11**, 3077–86 (2016).

118. Song, E. *et al.* Antibody mediated in vivo delivery of small interfering RNAs via cell-surface receptors. *Nat. Biotechnol.* **23**, 709–717 (2005).

119. Turner, J. J. *et al.* Cell-penetrating peptide conjugates of peptide nucleic acids (PNA) as inhibitors of HIV-1 Tat-dependent trans-activation in cells. *Nucleic Acids Res.* **33**, 6837–49 (2005).

120. Meade, B. R. *et al.* Efficient delivery of RNAi prodrugs containing reversible charge-neutralizing phosphotriester backbone modifications. *Nat. Biotechnol.* **32**, 1256–1261 (2014).

121. Dovydenko, I., Tarassov, I., Venyaminova, A. & Entelis, N. Method of carrier-free delivery of therapeutic RNA importable into human mitochondria: Lipophilic conjugates with cleavable bonds. *Biomaterials* **76**, 408–417 (2016).

122. Yang, J., Chen, C. & Tang, X. Cholesterol-Modified Caged siRNAs for Photoregulating Exogenous and Endogenous Gene Expression. *Bioconjug. Chem.* **29**, 1010–1015 (2018).

123. Satake, N. *et al.* Novel Targeted Therapy for Precursor B Cell Acute Lymphoblastic

Leukemia: anti-CD22 Antibody-MXD3 Antisense Oligonucleotide Conjugate. *Mol. Med.* **22**, 632–642 (2016).

124. Lorenz, C., Hadwiger, P., John, M., Vornlocher, H.-P. & Unverzagt, C. Steroid and lipid conjugates of siRNAs to enhance cellular uptake and gene silencing in liver cells. *Bioorg. Med. Chem. Lett.* **14**, 4975–4977 (2004).

125. Craig, K., Abrams, M. & Amiji, M. Recent Preclinical and Clinical Advances in Oligonucleotide Conjugates Recent Preclinical and Clinical Advances in Oligonucleotide Conjugates. *Expert Opin. Drug Deliv.* **0**, (2018).

126. Bijsterbosch, M. K. *et al.* Modulation of plasma protein binding and in vivo liver cell uptake of phosphorothioate oligodeoxynucleotides by cholesterol conjugation. *Nucleic Acids Res.* **28**, 2717–25 (2000).

127. Bijsterbosch, M. K. *et al.* Delivery of cholesteryl-conjugated phosphorothioate oligodeoxynucleotides to Kupffer cells by lactosylated low-density lipoprotein. *Biochem. Pharmacol.* **62**, 627–633 (2001).

128. Soutschek, J. *et al.* Therapeutic silencing of an endogenous gene by systemic administration of modified siRNAs. *Nature* **432**, 173–178 (2004).

129. Biscans, A. *et al.* Diverse lipid conjugates for functional extra-hepatic siRNA delivery in vivo . *Nucleic Acids Res.* **47**, 1082–1096 (2018).

130. Gvozdeva, O. V. *et al.* Modified siRNA effectively silence inducible immunoproteasome subunits in NSO cells. *Biochimie* **125**, 75–82 (2016).

131. Chernikov, I. V. *et al.* Cholesterol-Containing Nuclease-Resistant siRNA Accumulates in Tumors in a Carrier-free Mode and Silences MDR1 Gene. *Mol. Ther. - Nucleic Acids* **6**, 209–220 (2017).

132. DiFiglia, M. *et al.* Therapeutic silencing of mutant huntingtin with siRNA attenuates striatal and cortical neuropathology and behavioral deficits. *Proc. Natl. Acad. Sci. U. S. A.* **104**, 17204–9 (2007).

133. Alterman, J. F. *et al.* Hydrophobically Modified siRNAs Silence Huntingtin mRNA in Primary Neurons and Mouse Brain. *Mol. Ther. Nucleic Acids* **4**, e266 (2015).

134. Soutschek, J., Akinc, A., Bramlage, B., Nature, K. C.- & 2004, undefined. Therapeutic silencing of an endogenous gene by systemic administration of modified siRNAs. *Nature.Com* 173–178 doi:10.1038/nature03121

135. Khan, T. *et al.* Silencing Myostatin Using Cholesterol-conjugated siRNAs Induces Muscle Growth. *Mol. Ther. - Nucleic Acids* **5**, (2016).

136. Dyall, S. C. Long-chain omega-3 fatty acids and the brain: a review of the independent and shared effects of EPA, DPA and DHA. *Front. Aging Neurosci.* **7**, 52 (2015).

137. Nikan, M. *et al.* Docosahexaenoic Acid Conjugation Enhances Distribution and Safety of siRNA upon Local Administration in Mouse Brain. *Mol. Ther. Nucleic Acids* **5**, e344 (2016).

138. Nishina, K. *et al.* Efficient in vivo delivery of siRNA to the liver by conjugation of α-tocopherol. *Mol. Ther.* **16**, 734–740 (2008).

139. Raouane, M. *et al.* Synthesis, characterization, and in vivo delivery of siRNA-squalene nanoparticles targeting fusion oncogene in papillary thyroid carcinoma. *J. Med. Chem.* **54**, 4067–4076 (2011).

140. Petrova, N. S. *et al.* Carrier-free cellular uptake and the gene-silencing activity of the lipophilic siRNAs is strongly affected by the length of the linker between siRNA and lipophilic group. *Nucleic Acids Res.* **40**, 2330–44 (2012).

141. Midoux, P., Pichon, C., Yaouanc, J. J. & Jaffrès, P. A. Chemical vectors for gene delivery: A current review on polymers, peptides and lipids containing histidine or imidazole as nucleic acids carriers. *Br. J. Pharmacol.* **157**, 166–178 (2009).

142. Muratovska, A. & Eccles, M. R. Conjugate for efficient delivery of short interfering RNA (siRNA) into mammalian cells. *FEBS Lett.* **558**, 63–68 (2004).

143. Midoux, P. & Monsigny, M. Efficient Gene Transfer by Histidylated Polylysine / pDNA Complexes. *Bioconjug. Chem.* **10**, 406–411 (1999).

144. Okuda, T., Sugiyama, A., Niidome, T. & Aoyagi, H. Characters of dendritic poly(L-lysine) analogues with the terminal lysines replaced with arginines and histidines as gene carriers in vitro. *Biomaterials* **25**, 537–544 (2004).

145. Lo, S. L. & Wang, S. An endosomolytic Tat peptide produced by incorporation of histidine and cysteine residues as a nonviral vector for DNA transfection. *Biomaterials* **29**, 2408–2414 (2008).

146. Wong, S. C. *et al.* Co-injection of a targeted, reversibly masked endosomolytic polymer dramatically improves the efficacy of cholesterol-conjugated small interfering RNAs in vivo. *Nucleic Acid Ther.* **22**, 380–90 (2012).

147. Hsu, T. & Mitragotri, S. Delivery of siRNA and other macromolecules into skin and cells using a peptide enhancer. *Proc. Natl. Acad. Sci. U. S. A.* **108**, 15816–21 (2011).

148. Moschos, S. A. *et al.* Lung Delivery Studies Using siRNA Conjugated to TAT(48−60) and Penetratin Reveal Peptide Induced Reduction in Gene Expression and Induction of Innate Immunity. *Bioconjug. Chem.* **18**, 1450–1459 (2007).

149. El-Andaloussi, S., Järver, P., Johansson, H. J. & Langel, Ü. Cargo-dependent cytotoxicity and delivery efficacy of cell-penetrating peptides: a comparative study. *Biochem. J.* **407**, 285–292 (2007).

150. Chernikov, I. V., Vlassov, V. V. & Chernolovskaya, E. L. Current Development of siRNA Bioconjugates: From Research to the Clinic. *Front. Pharmacol.* **10**, (2019).

151. D'Souza, A. A. & Devarajan, P. V. Asialoglycoprotein receptor mediated hepatocyte targeting - Strategies and applications. *J. Control. Release* **203**, 126–139 (2015).

152. Nair, J. K. *et al.* Impact of enhanced metabolic stability on pharmacokinetics and pharmacodynamics of GalNAc-siRNA conjugates. *Nucleic Acids Res.* **45**, 10969–10977 (2017).

153. Nair, J. K. *et al.* Multivalent *N* -Acetylgalactosamine-Conjugated siRNA Localizes in Hepatocytes and Elicits Robust RNAi-Mediated Gene Silencing. *J. Am. Chem. Soc.* **136**, 16958–16961 (2014).

154. Garber, K. Alnylam terminates revusiran program, stock plunges. *Nat. Biotechnol.* **34**, 1213–1214 (2016).

155. Matsuda, S. *et al.* siRNA Conjugates Carrying Sequentially Assembled Trivalent N-Acetylgalactosamine Linked Through Nucleosides Elicit Robust Gene Silencing In Vivo in Hepatocytes. *ACS Chem. Biol.* **10**, 1181–1187 (2015).

156. Liu, X. *et al.* Tumor-targeted in vivo gene silencing via systemic delivery of cRGD-conjugated siRNA. *Nucleic Acids Res.* **42**, 11805–11817 (2014).

157. Parker, N. *et al.* Folate receptor expression in carcinomas and normal tissues determined by a quantitative radioligand binding assay. *Anal. Biochem.* **338**, 284–293 (2005).

158. Thomas, M. *et al.* Ligand-Targeted Delivery of Small Interfering RNAs to Malignant Cells and Tissues. *Ann. N. Y. Acad. Sci.* **1175**, 32–39 (2009).

159. Kumar, P. *et al.* Transvascular delivery of small interfering RNA to the central nervous system. *Nature* **448**, 39–43 (2007).

160. Ferrés-Coy, A. *et al.* Therapeutic antidepressant potential of a conjugated siRNA silencing the serotonin transporter after intranasal administration. *Mol. Psychiatry* **21**, 328–338 (2016).

161. Willibald, J., Harder, J., Sparrer, K., Conzelmann, K. K. & Carell, T. Click-modified anandamide siRNA enables delivery and gene silencing in neuronal and immune cells. *J. Am. Chem. Soc.* **134**, 12330–12333 (2012).

162. Sugo, T. *et al.* Development of antibody-siRNA conjugate targeted to cardiac and skeletal muscles. *J. Control. Release* **237**, 1–13 (2016).

163. Nygren, P.-Å. Alternative binding proteins: Affibody binding proteins developed from a small three-helix bundle scaffold. *FEBS J.* **275**, 2668–2676 (2008).

164. Dar, G. H., Gopal, V. & Rao, M. Conformation-dependent binding and tumor-targeted delivery of siRNA by a designed TRBP2: Affibody fusion protein. *Nanomedicine Nanotechnology, Biol. Med.* **11**, 1455–1466 (2015).

165. Stumpp, M. T., Binz, H. K. & Amstutz, P. DARPins: A new generation of protein therapeutics. *Drug Discov. Today* **13**, 695–701 (2008).

166. Lorenzer, C. *et al.* Targeted delivery and endosomal cellular uptake of DARPin-siRNA bioconjugates: Influence of linker stability on gene silencing. *Eur. J. Pharm. Biopharm.* **141**, 37–50 (2019).

167. Nimjee, S. M., Rusconi, C. P. & Sullenger, B. A. Aptamers: An Emerging Class of Therapeutics. *Annu. Rev. Med.* **56**, 555–583 (2005).

168. Neff, C. P. *et al.* An Aptamer-siRNA Chimera Suppresses HIV-1 Viral Loads and Protects from Helper CD4 + T Cell Decline in Humanized Mice. **3**, 1–20 (2011).

169. Zhou, J. *et al.* Functional in vivo delivery of multiplexed anti-HIV-1 siRNAs via a chemically synthesized aptamer with a sticky bridge. *Mol. Ther.* **21**, 192–200 (2013).

170. McNamara, J. O. *et al.* Cell type-specific delivery of siRNAs with aptamer-siRNA chimeras. *Nat. Biotechnol.* **24**, 1005–1015 (2006).

171. Esposito, C. L. *et al.* A combined microRNA-based targeted therapeutic approach to eradicate glioblastoma stem-like cells. *J. Control. Release* **238**, 43–57 (2016).

172. Esposito, C. L. *et al.* STAT3 Gene Silencing by Aptamer-siRNA Chimera as Selective Therapeutic for Glioblastoma. *Mol. Ther. Nucleic Acids* **10**, 398–411 (2018).

173. Liu, H. Y. & Gao, X. A universal protein tag for delivery of SiRNA-aptamer chimeras. *Sci. Rep.* **3**, 3129 (2013).

174. Rozema, D. B. *et al.* Dynamic PolyConjugates for targeted in vivo delivery of siRNA to hepatocytes. *Proc. Natl. Acad. Sci. U. S. A.* **104**, 12982–7 (2007).

175. Rozema, D. B. *et al.* Protease-triggered siRNA delivery vehicles. *J. Control. Release* **209**, 57–66 (2015).

176. Wooddell, C. I. *et al.* Hepatocyte-targeted RNAi therapeutics for the treatment of chronic hepatitis B virus infection. *Mol. Ther.* **21**, 973–85 (2013).

177. Turner, A. M. *et al.* Hepatic-targeted RNA interference provides robust and persistent knockdown of alpha-1 antitrypsin levels in ZZ patients. *J. Hepatol.* **69**, 378–384 (2018).

178. Wang, L. *et al.* A Novel Family of Small Molecules that Enhance the Intracellular Delivery and Pharmacological Effectiveness of Antisense and Splice Switching Oligonucleotides. *ACS Chem. Biol.* **12**, 1999–2007 (2017).

179. Le, T. D., Nakagawa, O., Fisher, M., Juliano, R. L. & Yoo, H. RGD Conjugated Dendritic Polylysine for Cellular Delivery of Antisense Oligonucleotide. *J. Nanosci. Nanotechnol.* **17**, 2353–2357 (2017).

180. Iversen, F. *et al.* Optimized siRNA-PEG conjugates for extended blood circulation and reduced urine excretion in mice. *Theranostics* **3**, 201–9 (2013).

181. Lorenzer, C., Dirin, M., Winkler, A. M., Baumann, V. & Winkler, J. Going beyond the liver: Progress and challenges of targeted delivery of siRNA therapeutics. *J. Control. Release* **203**, 1–15 (2015).

182. Zadeh, J. N. *et al*. NUPACK: Analysis and design of nucleic acid systems. *J. Comput. Chem.* **32**, 170–173 (2011).

183. Kwok, C. K. & Merrick, C. J. G-Quadruplexes: Prediction, Characterization, and Biological Application. *Trends Biotechnol.* **35**, 997–1013 (2017).

184. Liu, K. *et al*. PTEN deletion enhances the regenerative ability of adult corticospinal neurons. *Nat. Neurosci.* **13**, 1075–81 (2010).

185. Lopez-Gomollon, S. & Nicolas, F. E. Purification of DNA Oligos by Denaturing Polyacrylamide Gel Electrophoresis (PAGE). in *Methods in enzymology* **529**, 65–83 (2013).

186. McDonell, M. W., Simon, M. N. & Studier, F. W. Analysis of restriction fragments of T7 DNA and determination of molecular weights by electrophoresis in neutral and alkaline gels. *J. Mol. Biol.* **110**, 119–146 (1977).

187. Høiberg, H. C., Sparvath, S. M., Andersen, V. L., Kjems, J. & Andersen, E. S. An RNA Origami Octahedron with Intrinsic siRNAs for Potent Gene Knockdown. *Biotechnol. J.* **14**, 1700634 (2019).

188. Arias-Gonzalez, J. R. Single-molecule portrait of DNA and RNA double helices. *Integr. Biol. (Camb).* **6**, 904–25 (2014).

189. Lou, C. *et al*. Peptide–oligonucleotide conjugates as nanoscale building blocks for assembly of an artificial three-helix protein mimic. *Nat. Commun.* **7**, 12294 (2016).

190. MacRae, I. J. *et al*. Structural Basis for Double-Stranded RNA Processing by Dicer. *Science (80-.).* **311**, 195–198 (2006).

191. Chang, C. Il *et al*. Branched, Tripartite-Interfering RNAs Silence Multiple Target Genes with Long Guide Strands. *Nucleic Acid Ther.* **22**, 30–39 (2012).

192. Donis-Keller, H. Site specific enzymatic cleavage of RNA. *Nucleic Acids Res.* **7**, 179–92 (1979).

193. Lundin, K. E., Gissberg, O. & Smith, C. I. E. Oligonucleotide Therapies: The Past and the Present. *Hum. Gene Ther.* **26**, 475–85 (2015).

194. Fisher, T. L., Terhorst, T., Cao, X. & Wagner, R. W. Intracellular disposition and metabolism of fluorescently-labeled unmodified and modified oligonucleotides microinjected into mammalian cells. *Nucleic Acids Res.* **21**, 3857–65 (1993).

195. Monia, B. P., Johnston, J. F., Sasmor, H. & Cummins, L. L. Nuclease resistance and antisense activity of modified oligonucleotides targeted to Ha-ras. *J. Biol. Chem.* **271**, 14533–40 (1996).

196. Khvorova, A. & Watts, J. K. The chemical evolution of oligonucleotide therapies of clinical utility. *Nat. Biotechnol.* **35**, 238–248 (2017).

197. Gerling, T., Kube, M., Kick, B. & Dietz, H. Sequence-programmable covalent bonding of designed DNA assemblies. *Sci. Adv.* **4**, eaau1157 (2018).

198. Liu, J. K. *et al*. A novel peptide defined through phage display for therapeutic protein and vector neuronal targeting. *Neurobiol. Dis.* **19**, 407–418 (2005).

199. Park, I.-K., Lasiene, J., Chou, S.-H., Horner, P. J. & Pun, S. H. Neuron-specific delivery of nucleic acids mediated by Tet1-modified poly(ethylenimine). *J. Gene Med.* **9**, 691–702 (2007).

200. Chernikov, I. V. *et al*. Fluorophore Labeling Affects the Cellular Accumulation and Gene Silencing Activity of Cholesterol-Modified siRNAs *In Vitro*. *Nucleic Acid Ther.* **29**, 33–43 (2019).